

UC Irvine

UC Irvine Electronic Theses and Dissertations

Title

Epithelial mechanisms in digit separation and cutaneous wound healing

Permalink

<https://escholarship.org/uc/item/96s3x0dz>

Author

Kashgari, Ghaidaa Yacoub

Publication Date

2019

Peer reviewed|Thesis/dissertation

UNIVERSITY OF CALIFORNIA,
IRVINE

Epithelial Mechanisms in Digit Separation and Cutaneous Wound Healing

DISSERTATION

Submitted in partial satisfaction of the requirements
for the degree of

DOCTOR OF PHILOSOPHY

in Biomedical Sciences

by

Ghaidaa Yacoub Kashgari

Dissertation Committee:

Professor Bogi Andersen, Chair

Associate Professor Maksim Plikus

Assistant Professor Kai Kessenbrock

2019

© 2018 Elsevier Inc.

DEDICATION

To

My daughter Sereen

You are my sunshine, my best friend and my joy,
without you this journey would not have been possible

TABLE OF CONTENTS

	Page
LIST OF FIGURES	vi
LIST OF TABLES	viii
ACKNOWLEDGMENTS	ix
CURRICULUM VITAE	x
ABSTRACT OF THE DISSERTATION	xv
CHAPTER 1: INTRODUCTION	
CHAPTER 2: EPITHELIAL MECHANISMS IN DIGIT SEPARATION DURING DEVELOPMENT	
Introduction	
Materials and Methods	
Results	
Discussion	
CHAPTER 3: TRANSCRIPTIONAL REGULATION OF EPITHELIAL CELL ADHESION REQUIRED FOR COLLECTIVE CELL MIGRATION DURING CUTANEOUS WOUND HEALING	
Introduction	
Materials and Methods	
Results	
Discussion	
CHAPTER 4: GRHL3-MEDIATED VASODILATION DURING WOUND HEALING	
Introduction	
Materials and Methods	
Results	
Discussion	
REFERENCES	

LIST OF FIGURES

	Pages
Figure 1.1 Surface ectoderm specification	33
Figure 2.1 Stages of epidermal stratification	34
Figure 1.3. Non-epithelial cells of the epidermis.	35
Figure 2.1 Grhl3 is required for normal digit separation	59
Figure 2. 2 Mesenchymal interdigital cell death progresses normally in <i>Grhl3</i> ^{-/-} mice	60
Figure 2.3 Digits in <i>Grhl3</i> ^{-/-} embryos are joined by an epithelial sheet	61
Figure 2.4 Formation of an interdigital epithelial tongue in normal digit separation	63
Figure 2.5 Modeling suggests that directed cell migration plays a role in the formation of the IET	65
Figure 2.6 Collective cell migration of the IET during digit separation	67
Figure 2.7 Grhl3 is required for normal periderm development	69
Figure 2-S1 Grhl3 is required for normal digit separation	71
Figure 2-S2 Interdigital fusion of the epithelial results in unseparated digits in <i>Grhl3</i> ^{-/-}	72
Figure 2-S3 Modeling suggests that directed cell migration plays a role in the formation of the IET	73
Figure 2-S4 Collective cell migration of the IET during digit separation	74
Figure 2-S5 Grhl3 is required for normal periderm development	75
Figure 2.S6 Grhl3 is required for normal periderm development	76
Figure 3.1 Spatiotemporal expression of GRHL3 during stages of wound healing	98
Figure 3.2 Delayed healing of full-thickness wounds in mice lacking epidermal <i>Grhl3</i>	99
Figure 3.3 Increased cellular-adhesion between follower cells in <i>K14Cre-Grhl3</i> ^{-/-} migrating wound tongue	101
Figure 3.4 Isolation of wound-edge keratinocytes during wound re-epithelialization	103

Figure 3.5 Transcriptional and chromatin landscape in wound-front keratinocytes during re-epithelization	104
Figure 3.6 Grhl3 promote collective cell migration via direct regulation of FSCN1 expression in follower cells	106
Figure 3.7 Grhl3-Fscn1 mechanism in human acute wounds	108
Figure 3.8 Proposed model of Grhl3-Fscn1 signaling pathway during collective cell migration in	109
Figure 4-1 Defective vasodilation in mice lacking epidermal Grhl3	128
Figure 4-2 Decreased relative blood flow in K14Cre-Grhl3 ^{-/-} mice during wound healing	129
Figure 4-3 Unaltered inflammatory response in K14Cre-Grhl3 ^{-/-} mice	130
Figure 4-4 Grhl3 mediates Prostaglandin E2 production in the epidermis during wound healing	131
Figure 4-5 Grhl3-mediated Vasodilation in cutaneous wound healing	132

LIST OF TABLES

	Pages
Table 3.1 Top up-regulated genes in WT wounded-keratinocytes 3 days post wounding	110
Table 3.2 Top down-regulated genes in WT wounded-keratinocytes 3 days post wounding	112
Table 3.3 Top up-regulated genes in K14Cre-Grhl3 ^{-/-} wounded-keratinocytes 3 days post wounding	114
Table 3.4 Top down-regulated genes in K14Cre-Grhl3 ^{-/-} wounded-keratinocytes 3 days post wounding	116
Table 4.1 Top differentially expressed genes in K14Cre-Grhl3 ^{-/-} wounded-keratinocytes 24 hrs post wounding	133

ACKNOWLEDGMENTS

Words cannot express how grateful I am to have so many great people in my life that showed me nothing but support and love....

To my parents, Yacoub and Safiya, without whom I would not be here. I want to you to know how much I love you. No words can express how thankful I am to have you as my parents. I have missed you all these years. Your love and support made this happen. I hope I made you proud

To my husband, Sahal, who had to live all these years away from his own daughter and wife. Thank you for all your love and support.

To my siblings, Seham, Suzan, Nisreen, Eman, Amal, Dhai, Mohammed (RIP) and Ahmad. Thank you for being the best siblings I could ever ask for. Thank you for your love and support.

To my mentor, Bogi, thank you for making me become the scientist I am today. My journey with you has greatly changed me as a scientist and as a person. I couldn't not be more grateful for having you as a mentor. Looking forward for future collaborations.

To my special friends, I am so grateful to have you and my life. Thank you for all the love and support

CURRICULUM VITAE

Ghaidaa Yacoub Kashgari

Depts. of Biological Chemistry

School of medicine

University of California, Irvine

845 Health Sciences Road, Irvine, CA 92697-4716, USA

E-mail: gkashgar@uci.edu

EDUCATION AND TRAINING

2014- 2019 **Doctor of Philosophy, Biomedical sciences**

University of California, Irvine CA

2014-2016 **Master of Science, Biomedical Science**

University of California, Irvine CA

2011-2012 **Master of Science, Biotechnology**

Florida Institute of Technology, Melbourne, FL

2004-2008 **Bachelor of Biomedical Science, Medical Laboratory Technology**

King Abdulaziz University, Saudi Arabia

RESEARCH AND TRAINEE FELLOWSHIP

01/14-present **Graduate Research Assistant-** Lab advisor: Dr. Bogi Andersen

Department of Biological chemistry, School of medicine,

University of California, Irvine

01/13-04/13 **Graduate Research Assistant-** Lab advisor: Dr. Michael Kemp.

Department of Cell and Molecular Biology, Florida institute of Technology

08/12- 12/12 **Applied biotech intern**

Department of Cell and Molecular Biology, Florida institute of technology

01/12-04/12 **Biological researcher**

Department of biochemistry/biophysics, Florida institute of technology

05/09-10/09 **Medical Laboratory Technologist**

Department of Microbiology, King Fahad Armed Forces Hospital,
Jeddah, Saudi Arabia

02/09-04/09 **Medical Laboratory Technologist**

Department of Hematology, King Fahad Armed Forces Hospital,
Jeddah, Saudi Arabia

11/08-01/09 **Medical Laboratory Technologist**

Department of Clinical Chemistry, King Fahad Armed Forces Hospital,
Jeddah, Saudi Arabia

TEACHING AND LEADERSHIP EXPERINECE

01/19-03/19 **Teaching Assistant**

School of Biological Sciences (Bio100-Scientific Writing)

08/18-09/19 **Teaching Assistant**

School of Biological Sciences (Bio100-Scientific Writing)

01/15-present **Research Mentor**

School of Biological Sciences (Bio199-Undergraduate Research)

BIBLIOGRAPHY – PEER-REVIEWED PUBLICATIONS AND ABSTRACTS

- **Kashgari G**, Lina Meinecke, William Gordon, Hsiang Ho, Bryan Ruiz, Jady Yang, Yilu Xie, Qing Nie, James Jester and Andersen B. “Epithelium-mediated mechanisms for digit separation during limb development”. Manuscript. *Expected 2019*
- **Kashgari G**, Sanan Venkatesh, Anita Bayat, Rachel Klein, Maksim Plikus and Andersen B. “Transcriptional regulation of epithelial cell adhesion required for collective cell migration during cutaneous wound healing”. Manuscript. *Expected 2019*
- **Kashgari G**, Alexander Ethan, Sanan Venkatesh, Pai, Bernard Choi and Andersen B. “Grhl3-mediated vasodilation in cutaneous wound healing”. Manuscript. *Expected 2019*
- **Kashgari G**, Yanzhi H, Andersen B. “Embryonic development of the epidermis”. Reference Module in Biomedical Sciences. 2018 Mar 16
- Klein RH, Hu W, **Kashgari G**, Lin Z, Nguyen T, Doan M, Andersen B. “Characterization of enhancers and the role of the transcription factor KLF7 in regulating corneal epithelial differentiation”. *J Biol Chem* 2017 Sep 15
- **Kashgari G**, Seim al Dahar, M et.al. Assessment of Physical Exercise and Diet on Different Blood. *Abstract* 2008 June

PRESENTATIONS, SEMINARS AND POSTER SESSIONS

- **Ghaidaa Kashgari** – (2019). Clinical and Translational science Research Day. UC Irvine, CA, USA (Oral presentation).
- **Ghaidaa Kashgari** – (2019). UCI System Biology annual retreat. Los Angeles, CA, USA (poster presentation).
- **Ghaidaa Kashgari** – (2019). SoCal Rare Genetic Diseases meeting. UC Irvine, CA, USA (Oral presentation).
- **Ghaidaa Kashgari** – (2018). School of medicine Grad Day. UC Irvine, CA, USA (poster presentation).
- **Ghaidaa Kashgari** – (2018). UCI skin club. UC Irvine, CA, USA (Oral presentation).
- **Ghaidaa Kashgari** – (2018). Biological chemistry department seminar series. UC Irvine, CA, USA (Oral presentation).

- **Ghaidaa Kashgari**, Andersen B. (2017). Dermatology Skin Symposium. *UC Irvine, Irvine, CA, USA* (Poster presentation).
- **Ghaidaa Kashgari**, Andersen B. (2008). 4th Applied Medical Science Annual Student Meeting. *KAU, Jeddah, Saudi Arabia* (Oral presentation).

CORE COMPETENCIES

Transferable: Experimental design and conceptualization, Data analysis, Scientific writing (grants, technical reports, protocols, SOPs), Laboratory and project management, Public speaking, Teaching, Training, Laboratory safety.

Technical: Mouse genetics, Models of skin disease, Models of cutaneous wound healing and regeneration, Non-model organisms, Non-invasive mouse surgical procedures, Tissue and cell culture, Basic bioinformatics, Standard molecular biology techniques, Viral vectors, Transfection, Transduction, Fluorescence and bright field microscopy, Bulk RNA-sequencing (SMART-seq2), PCR/qPCR, FACS, Histology/Immunocytochemistry/Immunofluorescence staining, Chromatin/DNA/RNA/Protein purification, Western Blot, single cell Western Blot, UCSC Genome Browser, Transmission electron microscopy, Animal handling and husbandry (rodents).

Computer: Mac and Windows operating systems, Microsoft Office Suite, FlowJo, ImageJ, GraphPad Prism, Adobe Photoshop, RStudio.

ACCOLADES AND HONORABLE MENTIONS

- PhD student Travel Stipend Award (2019)
- Saudi Arabia Cultural mission scholarship for higher-education (2010- 2017).
- Best scientific oral presentation award in 4th Applied Medical Science Annual Student Meeting, Saudi Arabia (2008)

INTERSTS AND HOBBIES

Music, singing and dancing

ACADEMIC REFERENCES

Bogi Andersen, MD

Professor

Departments of Medicine and Biological Chemistry

University of California, Irvine

Phone: +1 (949) 824-9093 | E-mail: bogi@uci.edu

By

Peter Myrmev Anteater

Doctor of Philosophy in Social Ecology University of California, Irvine, 2015 Professor Godfrey-Sykes
Irvine, Chair

ABSTRACT OF THE DISSERTATION

Epithelial Mechanisms in digit separation and cutaneous wound healing

By

Ghaidaa Yacoub Kashgari

Doctor of Philosophy in Biomedical Sciences

University of California, Irvine, 2019

Professor Bogi Andersen, Chair

The epidermis, the outermost layer of the skin, continuously develops to form a tight epidermal barrier that is required for animal hydration and survival. Epidermal development occurs during embryogenesis via the mechanism of epidermal differentiation. We have previously described the role of the epidermal transcription factor Grainyhead like-3 (GRHL3) in epidermal differentiation and barrier formation. Additionally, we observed that mice lacking *Grhl3* in the epidermis exhibit soft-tissue syndactyly between their digits, this phenomenon was also detected in *Grhl3* germline knockouts (*Grhl3*KO). Through our work, we identified epithelial mechanisms required for normal digit separation during development. We discovered the formation of a multi-layered epithelial structure between the digits. In *Grhl3*KO embryos, the interdigital epithelia is fused, resulting in syndactyly. The separation of the epithelial structure depends on the anti-adhesive properties of the periderm, a transient layer located at the uppermost surface of the embryonic epidermis. We found that periderm cells in *Grhl3* KO are hyper-adhesive with abnormal expression

of adhesion molecules on their surfaces. Our findings reveal novel epithelial mechanisms required for digit separation; they also uncover a crucial role of Grhl3 in normal periderm development.

Adult skin is normally maintained in the absence of Grhl3. Our previous work indicated that Grhl3 is required for epidermal recovery after injury. Adult mice lacking Grhl3 in the epidermis exhibit impaired full-thickness wound healing and delayed keratinocyte migration. We observed an increase in cell-cell adhesion between follower cells at the wound-edge in Grhl3 cKO, concomitant with an increase expression of the adherens junction's protein, E-cadherin. Gene expression analysis of Grhl3 cKO wounded-keratinocytes 3 days post wounding shows a significant downregulation of F-actin protein Fscn1, a protein known to negatively regulate the expression of E-cadherin. These data indicate a novel Grhl3-Fscn1 mechanism required for cell-cell loosening in follower cells during keratinocyte migration in wounding. In addition, we observed that early after wounding, Grhl3 cKO mice exhibit a defect in dermal vasodilation and decreased blood flow. Gene expression analysis of wounded-keratinocytes 24 hrs post wounding suggest that Grhl3 regulate the expression of enzymes required for the biosynthesis of vasodilator factor prostaglandin E2. These observations are intriguing and suggest a Grhl3-mediated vasodilation during cutaneous wound healing.

CHAPTER 1: INTRODUCTION

Embryonic development of the epidermis

The mammalian skin regulates body temperature, prevents dehydration, protects the organism from external pathogens and UV damage, and mediates sensation. These functions rely on the formation of an intact skin composed of epidermis, dermis, and subcutaneous fat. The epidermis, the outermost layer of skin, comprises the interfollicular epidermis, a stratified squamous epithelium, and hair follicles.

The multilayered interfollicular epidermis built during the later stages of embryogenesis is mainly composed of keratinocytes. Maintenance of epidermal stem cells and the development of the epidermal barrier depend on tightly regulated layer-specific gene expression programs. But non-keratinocyte cell types are also incorporated into the epidermis, thus forming a highly heterogeneous tissue with complex cell–cell interactions conferring the multiple functions of the epidermis. Melanin produced by epidermal melanocytes protects the skin from UV-induced DNA damage. In addition, the epidermis contains immune cells and sensory Merkel cells that act, respectively, in the immune response and as mechanosensors.

Over 100 genetic diseases affecting the control and execution of epidermal differentiation highlight the health importance of normal epidermal development (Lopez-Pajares et al., 2013). Abnormalities in late differentiation and epidermal barrier formation lead to diseases

referred to as ichthyoses, some of which exhibit such severe barrier defects that they are lethal soon after birth (Elias et al., 2008).

Surface Ectoderm Specification

After gastrulation, the embryo consists of three primary germ layers: endoderm, mesoderm, and ectoderm (Fig. 1). The ectoderm, the exterior layer, gives rise to two main organs, the nervous system and the epidermis (Grubb, 2006). The separation of the two organs is mediated by the process of neurulation involving multiple steps. First, cells in the middle of the ectoderm start to thicken, forming a flat neural plate with a pseudo-stratified epithelium, while the surface ectodermal cells lateral to the neural plate are maintained as a simple squamous epithelium (Fig. 1) (Rolo et al., 2016). Second, the lateral edges of the neural plate bend dorsally toward the midline of the embryo. Cells at the plate border, located between the neural ectoderm and the surface ectoderm, form the neural crest (Fig. 1). Third, midline fusion of the two borders completes the closure of the neural tube and disconnects the neural tube from the surface ectoderm, the future epidermis (Fig. 1) (Grubb, 2006; Nikolopoulou et al., 2017).

Surface ectoderm specification and its distinction from neuroectoderm is controlled by autocrine and mesodermal paracrine factors whose expression is regulated in time and space. One of the autocrine factors secreted by the ectodermal cells is bone morphogenic protein 4 (Bmp4), a TGF- β family member (Wilson and Hemmati-Brivanlou, 1995). At the same time, paracrine fibroblast growth factors, including Fgf3, are secreted by the underlying mesodermal cells (Fig. 1) (Anderson et al., 2016; Cohen et al., 2010). The fate of

ectodermal cells is then determined by the relative concentrations of Bmp and Fgf, which in turn are regulated by Wnt signaling. Bmp4 is expressed in a gradient across the ectodermal sheet with the highest expression at the lateral sides and the lowest expression at the middle, the future neuroectoderm. In the middle region of the ectodermal sheet where Bmp4 expression is low, Fgf expression is high; this results in neuronal ectodermal commitment and formation of the neural plate. In contrast, in the future surface ectoderm, high expression of Bmp4 and low expression of Fgf from the underlying mesoderm results in epidermal cell fate (Fig. 1) (Grubb, 2006; Litsiou et al., 2005) with Bmp/Smad signaling activating the transcription of early surface ectoderm markers (Aberdam et al., 2007).

For years, researchers believed that neuronal cells at the neural plate borders mediated midline epithelial fusion. Recent studies, however, show evidence that surface ectodermal cells, not neuronal cells, mediate midline fusion and neural tube closure (De Castro et al., 2018; Kimura-Yoshida et al., 2015; Pyrgaki et al., 2010). Uncommitted progenitor cells are located at the neural plate border between the surface ectoderm and the neural plate prior to midline fusion and neural tube closure (Fig. 1) (Kimura- Yoshida et al., 2015). These uncommitted progenitor cells, which express embryonic stem cell markers Oct4, Klf5, and Ssea4, are specified by canonical Wnt signaling and can commit to either neuronal or epidermal fate. Misexpression of the Wnt antagonist Dkk1 in embryos promotes specification of neural ectoderm fate and inhibits the epidermal fate in the neural plate border. In contrast, misexpression of the Wnt ligand Wnt8a causes epidermal specification of uncommitted progenitor cells and down- regulation of neural fate markers. Thus, the

balance between Wnt inhibition and Wnt activation at the neuro-ectodermal border is essential for neural tube closure and epithelial fusion.

The evolutionarily conserved transcription factor Grainyhead like-3 (Grhl3) is induced by Wnt signaling and highly expressed in the uncommitted progenitor cells at the neural plate borders (Fig. 1). Germline deletion of Grhl3 in mice results in neural tube defects, principally spina bifida, but also exencephaly in some embryos. Thus, GRHL3-positive cells (uncommitted progenitors) mediate the epidermal fusion while GRHL3-negative cells (neural plate border) close the neural tube (Kimura-Yoshida et al., 2015). In addition to its expression in the surface ectoderm, Grhl3 is also expressed in the endoderm during neural tube closure (De Castro et al., 2018). Yet, it is the function of GRHL3 in the surface ectoderm that is primarily required for neural tube closure and midline fusion (De Castro et al., 2018). The molecular mechanism and downstream target genes of GRHL3 in surface ectoderm epithelial midline fusion are still unknown.

By E7.5, the embryo is uniformly covered by the single layered surface ectoderm expressing the simple epithelial intermediate filaments Krt8 and Krt18 (Fig. 1). These keratins will later be replaced by the basal specific intermediate filaments Krt5 and Krt14, marking the specification of the epidermis (Fig. 2).

Epidermal Stratification and Differentiation

After completion of neuroectoderm specification, the surface ectoderm develops into the embryonic epidermis with a switch in keratin expression and subsequently stratification.

Starting around E8.5, the simple squamous epithelial Krt8/Krt18-expressing cells of the surface ectoderm undergo morphological changes associated with expression of epidermal-specific keratins Krt5 and Krt14. Epidermal development starts at the dorsal surface and then spreads laterally to the ventral surface of the embryo. During embryogenesis, epidermal development on the dorsal side of the embryo is 1 day ahead of the ventral side.

The first epidermal cells that are generated from the surface ectoderm are the future basal cell layer, a single layer of stem cells capable of self-renewing, stratifying, and maintaining the epidermis throughout life. During epidermal stratification, basal cells divide asymmetrically perpendicular to the basal lamina, giving rise to one daughter cell that stays in the basal layer and maintains stemness and another cell that moves upward to differentiate. Cells above the basal layer form the spinous layer. Those cells continue their differentiation, forming first the granular layer and later the cornified layer, a layer of dead cells. By E18.5, the embryonic epidermis comprises four main layers: basal, spinous, granular, and cornified (Fig. 2).

Cytokeratins are abundantly expressed in the multilayered epidermis with layer-specific expression of keratin types. The expression and organization of cytokeratins are essential for the structural integrity and function of the epidermis. Epidermal cells are also held together by epithelial cell junctions: desmosomes, adherens junctions, and tight junctions (Sumigay and Lechler, 2015). Desmosomes link cells together and bundle with the intermediate filaments to provide mechanical strength, whereas adherens junctions, such as E-cadherin, link the F-actin cytoskeleton to the plasma membrane (Fujita et al., 1992;

Sumigray and Lechler, 2015). Lastly, tight junctions join cells of the granular layer to provide a permeability barrier.

Cell junctions are expressed throughout the multilayered epidermis with differences in localization and subtypes. In the basal layer, desmosomes and E-cadherin are expressed on the lateral and apical sides of the cell membrane giving basal cells a unique cuboidal cell shape, whereas in the suprabasal layers, they are expressed throughout the entire cell membrane (Peltonen et al., 2010; Sumigray and Lechler, 2015). In contrast, tight junctions are restricted to the granular layer where they localize at the apico-lateral side of the cell membrane giving these cells a diamond-shape. In addition, hemidesmosomes, a cell junction complex only formed in the basal layer, connects the basal cells to the basement membrane, a thin layer of transmembrane receptors and collagen fibers, thus firmly attaching the epidermis to the underlying dermis.

The epidermal differentiation gene expression program is controlled by signaling molecules including calcium, Notch and Wnt, and transcription factors that interact with epigenetic mechanism in a layer-specific manner (Klein and Andersen, 2015).

During embryogenesis, epidermal basal cells also give rise to cells that are not normally formed during homeostasis in adult epidermal stratification. These are Merkel cells, responsible for touch sensation, and the periderm, a transient anti-adhesive barrier that protects the embryo during epidermal stratification.

Basal Layer Formation

Downregulation of surface ectoderm keratins Krt8 and Krt18, and the induction of epidermal-specific keratins Krt14 and Krt5 mark the initiation of epidermis formation around E8.5 (Fig. 2) (Byrne et al., 1994). At E8.5, p63, a member of the p53 family of transcription factors, is detected in Krt18-positive cells of the surface ectoderm. The expression of p63 is higher in the mesenchymal-related surface ectoderm than the neural tube-related surface ectoderm, suggesting that signals from the underlying mesenchyme induce p63 in the surface ectoderm during development (Zhao et al., 2015). The persistence of the surface ectoderm layer and complete absence of the epidermis in p63^{-/-} mice identifies p63 as a master transcription factor required for the conversion of surface ectodermal cells to basal epidermal cells (Koster et al., 2004; Koster and Roop, 2004; Senoo et al., 2007; Yang et al., 1999).

There are two major isoforms of p63: one with an N-terminal transactivation domain (TAp63) and another without it (DNp63) (Candi et al., 2006). While it has been controversial whether TAp63 or DNp63 is first expressed in the surface ectoderm, both isoforms can induce Krt14 expression during epidermal development. DNp63 directly binds to the Krt14 gene and induces its expression, whereas TAp63 indirectly induces Krt14 expression through the transcription factor AP2g, another key transcription factor in epidermal development (Koster et al., 2006). While mice lacking AP2g can still form the epidermis, they exhibit a delay in the expression of epidermal markers, including p63, Krt14, and Krt1 (Guttormsen et al., 2008), suggesting a positive feedback loop between p63 and AP2g.

Cells of the single-layered embryonic epidermis proliferate to keep up with the enlarging embryo (Fig. 2). Epidermal progenitor cells can undergo two types of cell division: symmetric and asymmetric (Kulukian and Fuchs, 2013). Symmetric division of epidermal basal cells generates two daughter cells parallel to the basement membrane with equivalent cell polarity whereas asymmetric division generates one progenitor cell and one differentiated cell. Prior to stratification, active proliferation with symmetric cell division is required to prevent premature differentiation of the rapidly expanding embryonic epidermis (Blanpain and Fuchs, 2009; Williams et al., 2011). Localization of proteins controlling mitotic-spindle orientation and basal cell polarity is highly regulated in epithelial cells to control the balance between symmetric and asymmetric cell division. The mitotic activity of epidermal basal cells during development is maintained in part by p63 repressing the expression of cell-cycle inhibitors such as p21 and 14-3-3 (Sumigray and Lechler, 2015).

By E9.5, the embryonic epidermis is composed of a single layer of Krt14/Krt5-positive, proliferating basal cells. The next step in epidermal development is the formation of the multilayered epidermis through stratification.

The Periderm

At E9.5, the single cell layer of basal cells first stratifies, forming a transient single cell layer called the periderm, which is sloughed off prior to birth (Fig. 2) (M'Boneko and Merker, 1988). Periderm forms as cells of the basal layer lose their basement membrane attachment and migrate upward as they lose their basal cuboidal shape, acquiring a flat, endothelial-like

shape. Unlike later epidermal stratification, the periderm does not form through asymmetric division of basal cells perpendicular to the basal lamina (Hammond et al., 2017; M'Boneko and Merker, 1988). Periderm formation matches the patterned formation of the embryonic epidermis, starting in the tail and limb regions, and then spreading to the trunk and facial area. In the facial area, the periderm is first formed at the maxillary prominence, and then in the oral cavity, over the palate and the developing tooth germs. By E14.5 the periderm covers the entire mouse embryo (Richardson et al., 2014).

Periderm cells proliferate as a separate cell lineage to keep up with the expanding embryo surface; between E14.5 and birth the underlying epidermis stratifies below the periderm cells with no contribution from periderm cells. Periderm cells, however, express specific keratin filaments, initially Krt17 and later Krt6, that are not expressed by basal cells. The expression of Krt6 persists in the periderm until epidermal stratification is completed and the periderm is sloughed off (Hammond et al., 2017; McGowan and Coulombe, 1998) (Fig. 2).

The highly polarized endothelial-like shape of the periderm cells results from the site-specific expression of adhesion molecules such as Desmoplakin, E-cadherin and ZO-1 which are found only on the basolateral side of the periderm cells. This is in contrast to suprabasal epidermal cells which express adhesion molecules on all surfaces. Consequently, when periderm cells are lost, the underlying epidermal cells are exposed with superficial adhesion molecules which causes hyperadhesion (Sumigray and Lechler, 2015). Such hyperadhesion can lead to fusion of adjacent skin surfaces in the embryo. Thus, an essential role of the

periderm is to act as an antiadhesive coat preventing pathological adhesion between adjacent regions of embryonic surfaces.

By E18.5, when the epidermal cornified layer has formed, the periderm has disappeared (Hammond et al., 2017; M'Boneko and Merker, 1988), apparently having been shed from the fully developed epidermis (M'Boneko and Merker, 1988). Epidermal stratification and barrier formation seems to be required for periderm shedding as periderm is retained in mutant mice that fail to complete epidermal differentiation (De Groote et al., 2015). The loss of periderm progresses in a region-specific manner, starting at the back and moving forward across the embryo's body with the eyelids and neck region losing periderm last. The region-specific loss of periderm cells recapitulates the patterned barrier formation (Hardman et al., 1999).

A key transcriptional regulator of periderm formation is interferon regulatory factor 6 (IRF6), which is highly expressed in the periderm. Mouse models with either deleted *Irf6* or expression of a mutant *Irf6* fail to develop normal periderm and exhibit oral intraepithelial adhesion (Richardson et al., 2006). The pathological oral adhesion in *Irf6* mutant mice were detected before the initiation of epidermal differentiation. Periderm cells in *Irf6* mutant mice show loss of periderm marker expression (Krt17 and Krt6) and an increase in p63-positive cells (Kousa et al., 2017; Richardson et al., 2014). The expression of adhesion molecules is also altered in the absence of *Irf6*. Desmosomes and adherent junction proteins are found on the apical surface of the periderm layer in *Irf6* mutant epidermis and oral epithelia, resulting in interepithelial adhesion between opposing oral epithelial cells.

Irf6 acts in part by increasing the expression of epidermal differentiation transcription factor Grhl3 (de la Garza et al., 2013). Grhl3 is highly expressed in normal periderm cells but absent in the abnormal periderm of Irf6 / mice, suggesting a role for Grhl3 in the expression of adhesion proteins in periderm cells (de la Garza et al., 2013; Kousa et al., 2017). Mice lacking Grhl3 exhibit a similar phenotype as Irf6/ mice in that they fail to form a functional periderm (Peyrard-Janvid et al., 2014). The similarities between the Irf6 and Grhl3 mutant mice phenotypes suggest that the two genes function in the same molecular pathway during periderm development. The exact molecular mechanism and downstream targets of Grhl3 during periderm formation have not been identified.

Mice lacking the enzyme Ikb kinase-a (IKKa), the Notch ligand Jagged-2 (Jag2), the enzyme Receptor-interacting Serine/ threonine-Protein Kinase 4 (RIPK4), and the cell-cycle Regulator Protein Stratifin (SFN) have periderm phenotypes similar to that of Irf6 knockout mice (Casey et al., 2006; De Groote et al., 2015; Li et al., 1999). The mechanisms by which these regulators promote periderm development are not fully clear. Currently, there is no evidence for biochemical interactions between Irf6, IKKa, and Sfn. Phenotypes in Irf6^b/R84C Sfn^b/Er double knockout mice, however, suggest genetic interactions between these Irf6 and Sfn in periderm formation (Richardson et al., 2014).

Mutant mice lacking Fgf10 and Fgfr2 exhibit oral adhesion suggesting a role of Fgf signaling in periderm development. Consistent with this finding, studies on oral periderm

development indicate that *Irf6* and *Sprouty-4* (*Spry4*), an inhibitor of *Fgf* signaling, act in the same pathway in periderm development (Kousa et al., 2017).

The transcription factor p63 seems to be a master transcriptional regulator of oral periderm development (Thomason et al., 2010). p63 binds genomic regions that are assumed to regulate the expression of *Irf6*, *Sfn*, *Grhl3*, *Jag2*, and other genes involved in cell adhesion and periderm formation (Richardson et al., 2017). Consistently, mice lacking p63 fail to form periderm (Bakkers et al., 2002; Romano et al., 2012).

Malformations of periderm cause congenital disorders such as Popliteal Pterygium Syndrome and Van der Woude syndrome. These disorders are characterized by pathological adhesion between adjacent regions of the skin and within the oral cavity resulting in skin webs and palate abnormalities (Kondo et al., 2002; Richardson et al., 2014). *IRF6* mutations are the main cause of popliteal pterygium syndrome and also account for 70% of Van der Woude cases (Kondo et al., 2002). Some of the remaining cases are caused by dominant-negative mutations in *GRHL3* (de la Garza et al., 2013; Peyrard-Janvid et al., 2014). In addition, a coding variant of *GRHL3* is associated with risk for nonsyndromic cleft palate only (Mangold et al., 2016).

In sum, the periderm is a single layer of large flat cells that cover the embryo from mid-gestation until the epidermal barrier is formed at the end of gestation. While the periderm may act as transient permeability barrier for the embryo (M'Boneko and Merker, 1988), the evidence is stronger that its main role is to prevent abnormal adhesions between adjacent

regions of the embryo surface. Interestingly, some of the key regulators of periderm formation later play important roles in epidermal differentiation.

Early Epidermal Differentiation—Formation of the Spinous Layer

Asymmetric cell division of a basal cell is the first event promoting the basal-suprabasal transition in epidermal development (Poulson and Lechler, 2012; Ray and Lechler, 2011). At E12.5, a small number of basal cells divide asymmetrically perpendicular to the basal lamina, thereby generating daughter cells that are free from the basement membrane (Fig. 2). These cells form the first suprabasal layer of cells (Lechler and Fuchs, 2005). The number of asymmetrically dividing basal cells markedly increases between E12.5 and E15.5, concomitant with epidermal stratification.

Asymmetric cell division is tightly regulated by a network of cell polarity proteins such as Par3, Par6 and aPKC, and spindle orientation proteins such as LGN, mInS and NuMa. The localization of the evolutionary conserved LGN/NuMa complex on the apical surface of basal cells is required for asymmetric cell division and suprabasal layer formation (Bergstralh et al., 2013; Seldin et al., 2016; Williams et al., 2011; Zheng et al., 2010). Phosphoinositide-dependent kinase 1 (PDK1) regulates the activation and cellular localization of Akt and aPKC, two of the key signaling molecules promoting asymmetric cell division during epidermal differentiation. In addition, upon mitotic entry, the adherens junction E-cadherin recruits LGN/NuMa complex at cell–cell contacts, mediating the formation of stable cortical attachments of mitotic microtubules to the cell’s junctions (Gloerich et al., 2017).

An early hallmark of epidermal differentiation is the switch from basal-specific Krt14/Krt5 expression to early differentiation-specific Krt1/Krt10 expression (Fig. 2) (Dale et al., 1985; Weiss and Zelicson, 1975). Krt1 is the first marker expressed in the suprabasal layer during development. Similar to basal specific keratins, Krt1 and Krt10 are expressed in a regional pattern and their mRNA is detected as early as E13.5 in the developing epidermis (Byrne et al., 1994). The formation of the spinous layer depends on signaling pathways and transcription factors that orchestrate the activation of differentiation genes and suppress basal specific and cell-cycle genes.

Krt1/Krt10 expression is induced by evolutionarily conserved Notch signaling acting in parallel with the LGN/NuMa complex (Williams et al., 2011). Loss of epidermal notch signaling results in hyperproliferation of the basal layer and loss of spinous and granular layer formation (Blanpain et al., 2006). The maintenance of spinous cells and inhibition of premature terminal differentiation is mediated by the transcription factor Hairy and enhancer of split-1 (Hes1), a downstream target of Notch. Loss of Hes1 in the epidermis leads to premature terminal differentiation of spinous cells into granular cells, resulting in the absence of the spinous layer during epidermal development (Blanpain et al., 2006). Notch signaling therefore has multiple roles in the developing epidermis: it represses basal proliferation, induces early differentiation and prevents premature terminal differentiation (Massi and Panelos, 2012; Moriyama et al., 2008). Activation of Notch depends on layer-specific ligand-receptor binding and expression. Once activated, the Notch receptor undergoes proteolysis to release NICD that enters the nucleus and associates with the DNA-binding protein RBP-J and mastermind-like MAML to activate the transcription of

downstream target genes. Notch promotes differentiation by activating the cell cycle-inhibitor p21, suppressing proliferation, and by directly inducing the expression of differentiation genes such as Krt1.

In addition, Notch signaling acts in parallel with AP-2 to regulate the expression of the transcription factor CCAAT-enhancer-binding proteins (C/EBPa and C/EBPb). During epidermal development, C/EBPa and C/EBPb are expressed in basal-suprabasal transitioning keratinocytes where they induce the expression of Krt10 and repress the expression of DNp63, thus mediating cell-cycle arrest and epidermal differentiation (Lopez et al., 2009; Maytin et al., 1999). Other transcription factors such as IRF6, IKKa, 14-3-3delta and Ovol1 also regulate early epidermal differentiation (Blanpain and Fuchs, 2009; Descargues et al., 2008; Hammond et al., 2012; Ingraham et al., 2006; Koster and Roop, 2007; Nair et al., 2006). A common phenotype in IRF6, IKKa, 14-3-3delta and Ovol1 mutant mice is failure of cell-cycle withdrawal and impaired epidermal differentiation. The repression of the transcription factor c-Myc, a direct target of Ovol1, is required for cell-cycle arrest in the formation of suprabasal cells (Gandarillas and Watt, 1997; Nair et al., 2006).

Exclusively during a short period of epidermal development (E13.5–E15.5), differentiated suprabasal cells exhibit an intermediate state when they are mitotically active while expressing differentiation markers (Hardman et al., 1999; Lechler and Fuchs, 2005) (Fig. 2). The absence of the intermediate layer during epidermal homeostasis suggests that during embryogenesis, the mitotically active intermediate layer expedites the process of epidermal stratification to cover the large surface area of the embryo in less than 10 days before birth.

The molecular machinery that controls gene expression in the intermediate layer during epidermal differentiation is still poorly understood. At E14.5, intermediate cells start to withdraw from the cell cycle, while still maintaining the expression of the early differentiation markers Krt1 and Krt10, thus forming the Spinous layer. Next, the non-proliferating cells at the spinous layer that express Krt10 at high levels undergo terminal differentiation (Fig. 2).

Terminal Differentiation and Barrier Formation—Development of the Granular and Cornified Layers

At E15.5, Krt10-positive spinous cells undergo terminal differentiation, forming the granular layer (Fig. 2). Granular cells produce structural proteins (keratins, loricrin, profilaggrin, and others) and lipids (ceramides, free fatty acids, and others) that get used in the formation of the cornified layer. Around E16.5, the upward-moving granular cells undergo cell death, degrade their DNA and lose their nuclei, forming the cornified layer, a layer of dead, metabolically inactive cells. The cell walls of corneocytes are formed by the heavily crosslinked cornified envelope that is surrounded by lipids, thus forming a tough, impermeable skin surface (Costanzo et al., 2015; Fischer et al., 2011). At E18.5, all four layers of the interfollicular epidermis have formed.

Corneocytes will later be constantly shed in a regulated process known as epidermal desquamation which is balanced by cell production in the basal layer. Mutations in genes that interfere with proper desquamation of the cornified layer, such as serine protease inhibitor SPINK5 and ATP-binding cassette transporter 12 ABCA12, are associated with

severe barrier defects and skin abnormalities in Netherton syndrome (NS) and harlequin ichthyosis (HI), respectively (Chan et al., 2015; Simon et al., 2008).

Within granular cells pro-filaggrin and loricrin aggregate to form keratohyalin granules that give the granular layer its name. Within these granules, pro-filaggrin is processed to a mature filaggrin and released to bundle keratin filaments (Candi et al., 2005; Dale et al., 1985; Kumar et al., 2015; Steven et al., 1990). A group of enzymes called Transglutaminases cross-link cornified envelope proteins such as envoplakin, loricrin, small proline-rich proteins (SPRs), and involucrin underneath the cell plasma membrane, forming a scaffold for cornified envelope assembly (Długosz and Yuspa, 1994; Matsuki et al., 1998; Bickenbach et al., 1995; Candi et al., 2005; Steven et al., 1990).

In the upper spinous layer, lipid molecules are synthesized and packaged into lamellar bodies that later accumulate in the granular layer (Elias et al., 2014). During terminal differentiation, lamellar bodies in the upper granular layer fuse to the plasma membrane and empty their lipid contents into the extracellular space between the top of the granular layer and the lowest part of the cornified layer. Transglutaminases link the extracellular lipids, including ceramides, to the cornified envelope proteins by ester bonds. This linkage builds hard blocks of corneocytes that are stacked on top of each other and filled with lipids in between. This brick and mortar structure of the cornified layer is a major component of the epidermal barrier (Kumar et al., 2015).

Intercellular adhesion also plays an integral role in the formation and integrity of the epidermal barrier. In addition to desmosomes and adherens junctions, tight junctions are

exclusively formed in the granular layer where they locate at the apico- lateral side of the granular cell (Bäsler and Brandner, 2017; Sumigray and Lechler, 2015). Tight junctions regulate the paracellular transport of water and solutes, thus acting as a permeability barrier. Claudins and Occludins are two of the main components of epidermal tight junctions with Claudins found in all epidermal layers, whereas Occludins are found only in the upper granular layer and in the transient periderm. During cornification, desmosomal complexes in the upper granular layer get cross-linked with adhesion proteins corneodesmosin, envoplakin, and periplakin. These modified desmosomes, also known as corneodesmosomes, mediate corneocyte–corneocyte adhesion; they are later degraded during desquamation (Kalinin et al., 2001; Mack et al., 2005).

An increase in extracellular Ca^{2+} is a key driver of terminal differentiation (Bikle et al., 2012). A gradient of extracellular Ca^{2+} is present through the cell layers of the epidermis with the innermost layer (basal) having the lowest concentration and the upper granular layer having the highest concentration. Extracellular Ca^{2+} modulates the corresponding intracellular Ca^{2+} sensing machinery, activating protein kinase C and tyrosine kinases. While several isoforms of PKC are expressed in the epidermis, PKC- α is the best known Ca^{2+} -dependent PKC in terminal differentiation (Denning, 2010; Yuspa et al., 1989). In response to high extracellular Ca^{2+} , activated PKC- α regulates keratinocytes gene expression, increasing the expression of late-differentiation markers loricrin, pro-filaggrin, SPR-1, involucrin, and transglutaminase while repressing the expression of early-differentiation markers Krt1 and Krt10 (Długosz and Yuspa, 1994; Yuspa et al., 1989).

The induction of late-differentiation markers in response to calcium is mediated by AP1 transcription factors, a family of proteins, including c-jun, c-fos, and Fra-1, that dimerize and bind to late-differentiation genes such as involucrin (Eckert et al., 2013; Welter et al., 1995). Another downstream target of PKC- α during epidermal differentiation is the transcription factor Distal-less homeodomain-3 (DLX3). Dlx3 is highly expressed in the granular layer of the developing epidermis where it directly binds and induces the expression of genes encoding structural proteins, including pro-filaggrin. In addition, the zinc-finger COUP-TF-interacting protein 1 (CTIP1/BCL11a), which is highly expressed in the developing epidermis, regulates genes required for pro-filaggrin processing and lipid metabolism (Li et al., 2017).

Mammalian target of rapamycin complexes mTORC1 and mTORC2 were recently found to be required during epidermal development. mTORC1-dependent phosphorylation of its downstream targets (S6K, S6, and 4E-BP1) in the basal and suprabasal layers regulates cell proliferation and translation of differentiation markers, whereas mTORC2-dependent phosphorylation of its downstream targets (Akt-pS473) mediates late terminal differentiation and barrier formation (Ding et al., 2016).

The transcription factor Kruppel-like factor-4 (KLF4) is highly expressed in the suprabasal layers of the epidermis where it directly binds and regulates the expression of genes encoding for barrier proteins (Ivl and Sprr2a) and lipid biosynthesis enzymes (Far2) (Chew et al., 2013; Jaubert et al., 2003; Patel et al., 2006; Segre et al., 1999). During terminal differentiation, KLF4 expression is indirectly induced by p63 via the zinc finger protein ZNF750 (Sen et al., 2012).

The POU domain factors Skn-1 (POU2F3) and Tst-1/Oct6 (POU3F1) collaborate to turn on differentiation factors such as Sprr2a and to repress basally-expressed genes in the suprabasal layers (Andersen et al., 1993, 1997a,b). In addition to its roles in surface ectoderm specification and periderm formation, Grhl3 is a key regulator of epidermal terminal differentiation (Ting et al., 2005; Yu et al., 2006). Grhl3 directly binds and activates the expression of multiple genes that encode for adhesion molecules, lipid-producing enzymes, transglutaminases and structural proteins—all required for the integrity of the epidermal barrier. In addition, transcriptional repressor Blimp-1, also known as PRDM1, represses the expression of cornified envelope and lipid metabolism genes in the granular layer, thus regulating granular cell maturation to cornocytes (Magnúsdóttir et al., 2007).

The gene expression profiles of the most undifferentiated basal epidermal stem cell and the most differentiated granular cells are markedly different. Yet, both cells contain the same genetic information. Hence, it is not surprising that epigenetic regulators, including DNA/histone modifying enzymes, Polycomb repressor complexes (PRC1 and PRC2), chromatic remodeling factors and long noncoding RNAs, have been found to play major roles in the development of the epidermis (Botchkarev, 2015; Cangkrama et al., 2013; Ghosh et al., 2018; Klein and Andersen, 2015).

The epidermal differentiation complex (EDC) comprises a cluster of genes encoding proteins involved in cornified envelope formation (Marenholz et al., 2001; Oh and de Guzman Strong, 2017). During epidermal development, the master regulator p63 directly induces the

expression of chromatin regulators such as Stab1 and Brg1 in basal progenitor cells. Stab1 regulates the chromatin organization of the epidermal differentiation complex (EDC) whereas Brg1 remodels its nuclear localization; both factors regulate the expression of genes at the EDC locus (Fessing et al., 2011; Mardaryev et al., 2014). In addition, the balance between proliferation and differentiation in epidermal progenitor cells is controlled by PRC1 and PRC2. Ezh2 and Jarid2, subunits of the PRC2 complex, promote proliferation and inhibit the expression of differentiation genes in epidermal progenitor cells (Ezhkova et al., 2009; Mejetta et al., 2011; Perdigoto et al., 2014b)

Long noncoding RNAs (LncRNAs) also act in conjunction with a MAF:MAFB transcription factors network to regulate epidermal differentiation (Klein and Andersen, 2015; Lopez-Pajares et al., 2015). The antidifferentiation lncRNA (ANCR), maintains the undifferentiated state of progenitor cells by inhibiting MAF:MAFB expression, whereas the pro-differentiation lncRNA (TINCR) promotes differentiation by activating MAF:MAFB expression (Labott and Lopez-Pajares, 2016; Miyai et al., 2016).

Region-Specific Epidermal Differentiation and Transition Zones

While the basic interfollicular epidermal structure is maintained over the whole body surface, there are regional differences in the thickness and other features of the epidermis. Prominently, volar regions (palmoplantar) develop thick epidermis that confers greater mechanical strength than nonvolar epidermis. In addition to thicker suprabasal epidermal layers, volar skin has less pigmentation and no hair follicles (Holbrook and Odland, 1980).

Volar epidermis uniquely expresses Krt9 which is thought to be important for its mechanical integrity (Fu et al., 2014).

The volar-specific differentiation of keratinocytes is controlled by HOX-specified regional differences in the underlying fibro- blasts (Chang et al., 2002). HOXA13 in fibroblasts induces expression of the Wnt ligand Wnt5a, which acts on volar keratinocytes to induce expression of Krt9. Although Wnt5a is reduced in HoxA13 knockout limbs, it is not completely absent, suggesting other upstream transcription factors induce Wnt5a expression during volar-specific differentiation. In addition, canonical Wnt inhibitor DKK1, a known suppressor of hair follicle formation and melanocytes proliferation, is also expressed in volar fibroblasts (Yamaguchi et al., 2004). Therefore, the combination of Wnt5a and Dkk1 expression in volar fibroblasts result in the formation of Krt9 positive epidermis that lacks hair follicles and pigmentation (Yamaguchi et al., 2008).

The nipple is another specialized skin region where underlying mesenchyme influences epidermal differentiation. While the nipple epidermis shares many features with volar epidermis, nipple keratinocytes express Krt2e rather than Krt9 (Foley et al., 2001; Mahler et al., 2004). The parathyroid hormone-related protein (PTHrP) and its receptor PTHR1 are required for mammary gland and nipple-skin development. During embryogenesis, PTHrP-positive mammary epithelial buds derived from the surface epider- mis, invade the underlying dermal mesenchyme, and induce local mammary-specific mesenchyme differentiation. The mammary- specific mesenchyme then induces the overlying epidermis to become the nipple epidermis. Therefore, loss of PTHrP results in failure of mammary and

nipple development, whereas PTHrP overexpression in the epidermis transforms the whole epidermis into nipple-epidermis (Foley et al., 2001).

In contrast to volar skin, the lip epidermis has a thin cornified layer that makes a transition to the oral mucosa (Kim et al., 2016). The epidermis also transitions to mucosal surfaces of the lower gastrointestinal tract, the genitourinary tract and in the eyelids. Such transitions between keratinized epidermis and nonkeratinized mucosal surfaces are referred to as mucocutaneous junctions, a form of transition zones (Kobayashi and Tagami, 2004). Cells at the mucocutaneous junctions express epithelial markers that are shared between the keratinized and mucosal epithelia such as Krt14, Krt5, but they also express markers that are exclusively found only in differentiated epidermis such as Krt1/Krt10 and mucosal epithelia Krt4 krt13, Krt19, and mucin1 (Knop et al., 2011; Riau et al., 2008). The molecular mechanisms that allow the formation of precise borders at mucocutaneous junctions are poorly understood.

Non-epithelial Cells of the Epidermis

Although the majority of cells comprising the epidermis are epithelial keratinocytes, during development specialized non-epithelial cell populations enter the epidermis (Fig. 3). These non-epithelial cells interact with keratinocytes to carry out distinct epidermal functions in the adult. Thus, the epidermis develops a specialized system whereby melanocytes interact with keratinocytes to protect the organism against ultraviolet (UV) light and DNA damage. The epidermis also develops a mechanosensory complex connected to the nervous system

to sense the environment, and an immunogenic barrier with immune cells that sense and responds to microorganisms and damage.

Melanocytes

Epidermal melanocytes produce UV radiation-absorbing melanin, preventing DNA damage and protecting the skin from solar radiation damage (Cichorek et al., 2013). The melanin produced by activated melanocytes is packed into melanosomes that are transferred to neighboring keratinocytes, forming the epidermal melanin unit composed of one melanocyte and over 25 keratinocytes.

Epidermal melanocytes form during embryogenesis. Around E8.5, neural crest cells detach from the neural tube and undergo epithelial-to-mesenchymal transition (Ernfors, 2010; Mayor and Theveneau, 2013; Mort et al., 2015) (Fig. 1). Delamination of the multipotent neural crest cells from the neural tube generates different types of cells including melanoblasts, the melanocytes precursors. Around E14.5, at the beginning of epidermal stratification, migrating melanoblasts invade the basement membrane and take up residence in the basal layer of the epidermis where they differentiate to mature melanocytes upon stimulation from keratinocytes (Fig. 3). In the mouse, around E15.5, epidermal melanoblasts leave the interfollicular epidermis and migrate to the developing hair follicle as their final destination where they differentiate into melanocytes. The location of mature melanocytes differs between adult human and mouse skin. In human skin, melanocytes reside along the basal layer of the epidermis and hair follicles in the dermis, whereas in mouse skin they are located in hair follicles except in ears and tails (Cichorek et al., 2013; Holbrook et al., 1988).

Wnt/beta-catenin signaling is a key pathway in neural crest induction and melanocyte development (Hari et al., 2012). Persistent Wnt signaling in neural crest cells and decreased concentration of Bmp induce the expression of selected genes that are required for the melanocyte lineage fate. Transcription factors Sox10 and Pax3 activate the expression of the melanocyte master regulator Microphthalmia-associated transcription factor (MITF) in melnaoblasts (Aoki et al., 2003; Levy et al., 2006). In addition, activated endothelin Edn3/Ednrb and tyrosine kinase-kit signaling in migratory neural crest cells are required for melanocytes fate specification (Karafiat et al., 2007; Saldana-Caboverde and Kos, 2010).

Activated Wnt signaling in melanoblasts directly induces Mitf expression through beta-catenin/LEF-1/TCF (Cichorek et al., 2013; Ernfors, 2010). Melanoblast-activated MITF then binds to and activates the expression of several target genes required for melanoblast migration to the epidermis (Levy et al., 2006); changes in the actin cytoskeleton promote melanoblast migration to the epidermis and hair follicle. Dorsolateral melanoblasts, located between the surface ectoderm and somite, move to the interfollicular epidermis whereas ventrolateral melanoblasts, located between the neural tube and somite, move to hair follicles (Ernfors, 2010; Mort et al., 2015). Neural crest-derived Schwann cell precursors (SCPs) are also a source of epidermal melanoblasts (Adameyko et al., 2009).

Migrating melanoblasts in the dermis express adhesion molecules such as E-cadherin and P-cadherin (Nishimura et al., 1999). At E12.5, the expression of E-cadherin in dermal melanoblasts increases, mediating their migration toward the epidermis. In addition, the

expression of E-cadherin in epidermal melanoblasts is required for keratinocyte-melanocyte interactions (Hsu et al., 2000) and keratinocyte-mediated growth regulation of melanoblasts/melanocytes.

Keratinocytes play a major role in melanoblast migration, proliferation, and differentiation. Keratinocyte-derived factors, including stem cell factor (SCF, a c-kit ligand), basic fibroblast growth factor (bFGF), endothelin (ET-1), nerve growth factors (NGF), and melanocyte-stimulating hormone (α -MSH), bind to their receptors on the melanoblast/melanocyte plasma membrane (Hirobe, 2014; White and Zon, 2008). Ligand-receptor binding induces signaling pathways protein kinase A (PKA), protein kinase C (PKC) and Mitogen-activated protein kinases (MAPK) that activate melanocyte-specific transcription factors, promoting melanoblast proliferation. MITF directly regulates the expression of genes involved in many processes in melanocyte pigmentation, proliferation, and survival (Cichorek et al., 2013; Levy et al., 2006). In addition, MITF interacts with chromatin remodeling factors such as Brg1 to regulate melanocyte proliferation (Laurette et al., 2015).

Merkel Cells

Merkel cell-neurite complexes mediate the mechanosensing function of the epidermis—the discrimination of touch, shape and texture of objects. Merkel cells are named after Friedrich S. Merkel who discovered them back in 1875. These cells cluster and physically contact intra-epidermal sensory nerve endings in a structure referred to as the touch-dome (Niu et al., 2014).

Their close association with nerve endings and production of neurotransmitters led researchers to believe that Merkel cells originated from neural crest cells, migrating to the epidermis during embryogenesis as melanoblasts do (Szeder et al., 2003). But we now know that Merkel cells appear in the epidermis before nerve endings innervate the epidermis. And, recent studies using lineage tracing and conditional knockout mouse models show that Merkel cells originate from basal stem cells in the developing epidermis (Van Keymeulen et al., 2009). Thus, in addition to periderm and differentiated keratinocytes, basal stem cells give rise to a distinct cell population, Merkel cells.

Transcriptome analysis of epidermal Merkel cells indicate the expression of Merkel-specific genes that are not found in differentiated keratinocytes (Perdigoto et al., 2014a). *Atoh1*, a basic helix-loop-helix transcription factor and a unique marker of Merkel cells, is required for Merkel cell specification (Ostrowski et al., 2015). Conditional deletion of *Atoh1* in *Krt14*-expressing epidermal cells resulted in the loss of epidermal Merkel cells (Van Keymeulen et al., 2009). *Atoh1*-positive cells are first detected in the developing epidermis at E15.5 (Fig. 3B).

Mature Merkel cells found in the neonatal epidermis express Merkel-specific differentiation markers such as *Krt8*, *Krt18*, and *Krt20* that are not found in differentiated epidermal keratinocytes (Moll and Moll, 1992). Maturation of *Atoh1*-positive Merkel cells is induced by *Sox2* that is expressed in all *Atoh1*-positive Merkel cells at E15.5; *Sox2* is an upstream regulator of *Atoh1*, sustaining *Atoh1* expression in differentiated Merkel cells. Loss of

epidermal Sox2 results in complete absence of mature Merkel cells in the newborn epidermis with loss of Krt18 and Krt20 expression (Perdigoto et al., 2014a). The LIM-homeodomain transcription factor Isl1 is also expressed during mid-stage of Merkel cells maturation; it physically interact with Sox2 to sustain the transcription of Atoh1 during Merkel cells differentiation (Perdigoto et al., 2014a).

Sox2 expression in basal stem cells is regulated by PRC2 subunits Ezh1 and Ezh2 (Bardot et al., 2013). Ezh1/2 null mice exhibit an increase in epidermal Merkel cells, a phenotype that is attenuated by ablation of Sox2, indicating that PRC2 represses Sox2 expression in epidermal basal stem cells to maintain their epidermal fate.

Mature Merkel cells are detected within the basal layer of the epidermis at E17. They account for 2%–5% of total epidermal cells although their abundance varies between anatomical locations. They are mainly located at touch-sensitive areas of the skin such as human fingertips, and mouse whiskers and paw pads (Maksimovic et al., 2014). Merkel cell–neurite complexes are formed when Merkel cells are innervated by sensory neurons. At the epidermal-dermal junction, Merkel cells physically contact Ab sensory neurons, specifically the slowly adapting I (SAI) mechanoreceptors, which express neural filament heavy chain (NFH) (Niu et al., 2014). Neurogenic factors such as neurotrophins (NTF3) and nerve growth factors (NRG) secreted by Merkel cells and epidermal keratinocytes bind to tyrosine kinase receptors found on the sensory nerve fibers. These interactions are required for epidermal innervation and formation of Merkel cell–neurite complexes.

Epidermal Innervation

Sensory nerves found in the epidermis mediate touch reception, pain, and thermal sensation. The skin is innervated by two types of nerve fibers, sensory and autonomic. Nerve fibers innervating the skin originate from dorsal root ganglia nerve cell bodies of sensory nerves (Hsieh et al., 1997). At E13–E14 the sensory nerves elongate from the dorsal root ganglion and migrate toward the skin. At E15.5, nerve fibers are detected in the dermis (Peters et al., 2002). A day later, at E16.5, sensory nerves penetrate the basement membrane and innervate the epidermis by moving vertically, terminating at the granular layer of the epidermis. Nerve fibers migrate toward secreted factors released by their targeted-tissue. Both epithelial and nonepithelial cells in the epidermis release neurotrophins such as nerve growth factor (NGF), brain-derived neurotrophic factor (BDNF), neurotrophin-3 (NT-3), and neurotrophin4/5 (NT-4/5) that mediate nerve fibers innervation and outgrowth. Sensory nerve fibers that are not associated with epidermal Merkel cells invade the upper layers of the epidermis and remain as free endings.

Immune Cells

The epidermis is an active immune organ, equipped with immune-competent cells that execute immune responses against pathogenic organisms, environmental toxins and injury. While keratinocytes are important actors in the epidermal immune response, the ability of the epidermis to respond immediately to an insult depends on epidermal immune cells. Epidermal immune cells also play a major role in autoimmune diseases of the skin such as

psoriasis and atopic dermatitis. There is extensive cross-talk between keratinocytes and immune cells of the epidermis.

The two types of dendritic leukocytes found in the epidermis are Langerhans cells and epidermal T-cells. Langerhans cells are antigen-presenting cells expressing MHC-class II molecules; they are believed to be involved in both the innate and adaptive immune responses of the epidermis. Langerhans cells are located in the suprabasal layer of the epidermis, hugging the neighboring keratinocytes with their dendritic cytoplasmic protrusions that extend to the stratum corneum (Fig. 3A). Specific intracellular structures referred as Birbeck granules are found exclusively in mature Langerhans cells. These granules express a lectin receptor called Langerin (CD207), which is expressed in other nonepidermal dendritic cells types (Romani et al., 2010, 2012).

Since their discovery by Paul Langerhans in 1868, the origin of epidermal Langerhans cells has been debated. Earlier biochemical studies argued that Langerhans cells originate from the neural crest while others suggested a mesenchymal origin. Recent studies using human transplantation and mouse models indicated that Langerhans cells originate, at least in part, from bone-marrow stem cells (Fig. 3B).

Langerhans cells are first detected at a relatively low density in the developing epidermis at E16–E17, and at this stage they do not express all surface markers that are found in the adult mature Langerhans cells. These immature Langerhans cell precursors express CD45, CD115, CD11b, and CX3CR1 but not MHC class II. Between the day of birth to postnatal day 5, these

precursors differentiate and start expressing markers of mature Langerhans cells (MHC-class II, Langerin, and CD11c). Concomitant with this differentiation, mature Langerhans cells proliferate, dramatically increase in number, forming a Langerhans cell epidermal network.

Dendritic epidermal T cells (DETCs), are the second type of leukocytes found in mouse epidermis (Nielsen et al., 2017) (Fig. 3A). They are believed to originate from the thymus, and then migrate into the epidermis (Fig. 3B). DETCs are first detected in the developing epidermis at E16–E17, then expressing only CD45 but not Thy-1. They are smaller and rounder in shape than Langerhans cells, but the density of both cell types is similar in the embryonic epidermis. Postnatal differentiation of dendritic epidermal T cells results in CD3-TCR Vg3/Vd1 membrane-expression. Differentiated DETCs then undergo extensive proliferation and reactivity peaking weeks after birth. The expression of T cell-specific markers CD3 and Thy-1 and epidermal T cells specific receptors Vg3/Vd1 distinguishes DETCs from epidermal Langerhans cells and other nonepithelial dendritic T cells. Other types of epidermal T cells such as memory CD8 β T-cells accumulate in the epidermis after being recruited as part of adaptive immune response to infections or inflammations (Gebhardt et al., 2011; Zaid et al., 2014).

DETCs start to migrate toward chemokines secreted from epidermal keratinocytes. These keratinocyte-produced chemokines also regulate dendritic T cell migration, proliferation and function. Interleukin-7 (IL-7) is one of the key cytokines secreted by keratinocytes and DETCs themselves early during epidermal DETC recruitments. Other cytokines and factors

such as IL-2, IL-15, and tumor necrosis factor alpha (TNF α) are also secreted by keratinocytes to promote DETC proliferation and immunogenic function. DETCs are also known to secrete factors that regulate the immune function of both keratinocytes and Langerhan cells (West and Bennett, 2017).

Conclusion

Studies of genetic mouse mutants have led to the identification of signaling pathways, transcription factors and epigenetic mechanisms in epidermal development. In addition, advances in human genetics have identified the cause of multiple diseases of epidermal development. We draw from these studies to highlight some of the molecular mechanisms that regulate the developmental stages of epidermal development, including surface ectoderm specification, periderm formation, and epidermal stratification. Studies on periderm formation and function have been mainly done in the context of oral epithelial development. Thus, the molecular control and function of skin periderm is still poorly understood.

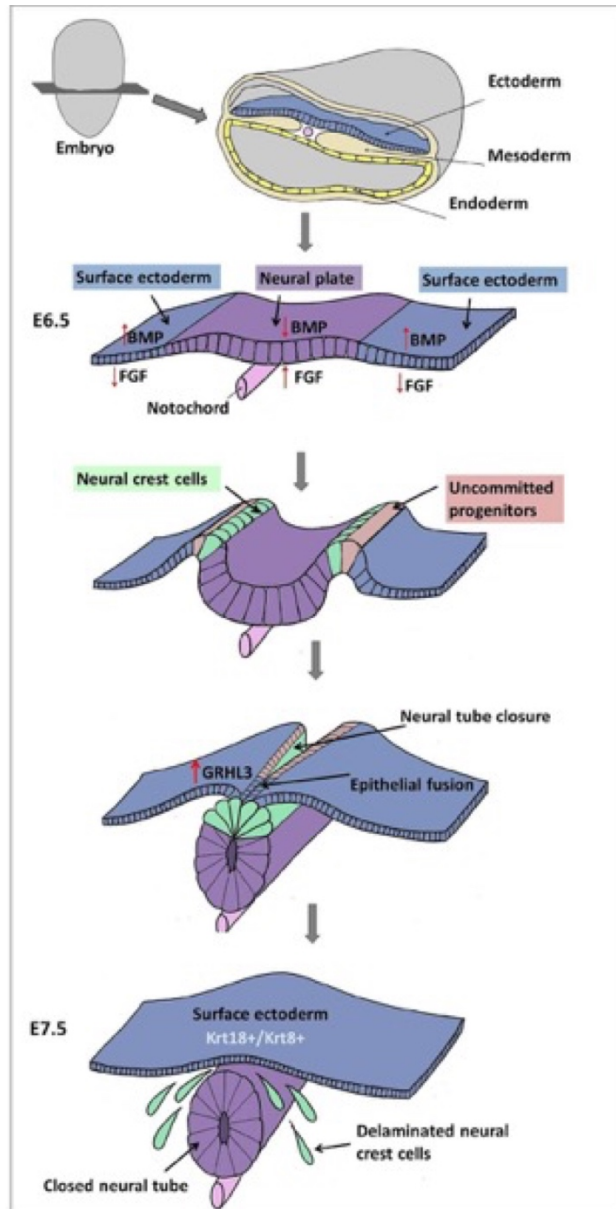


Figure 1. Surface ectoderm specification.

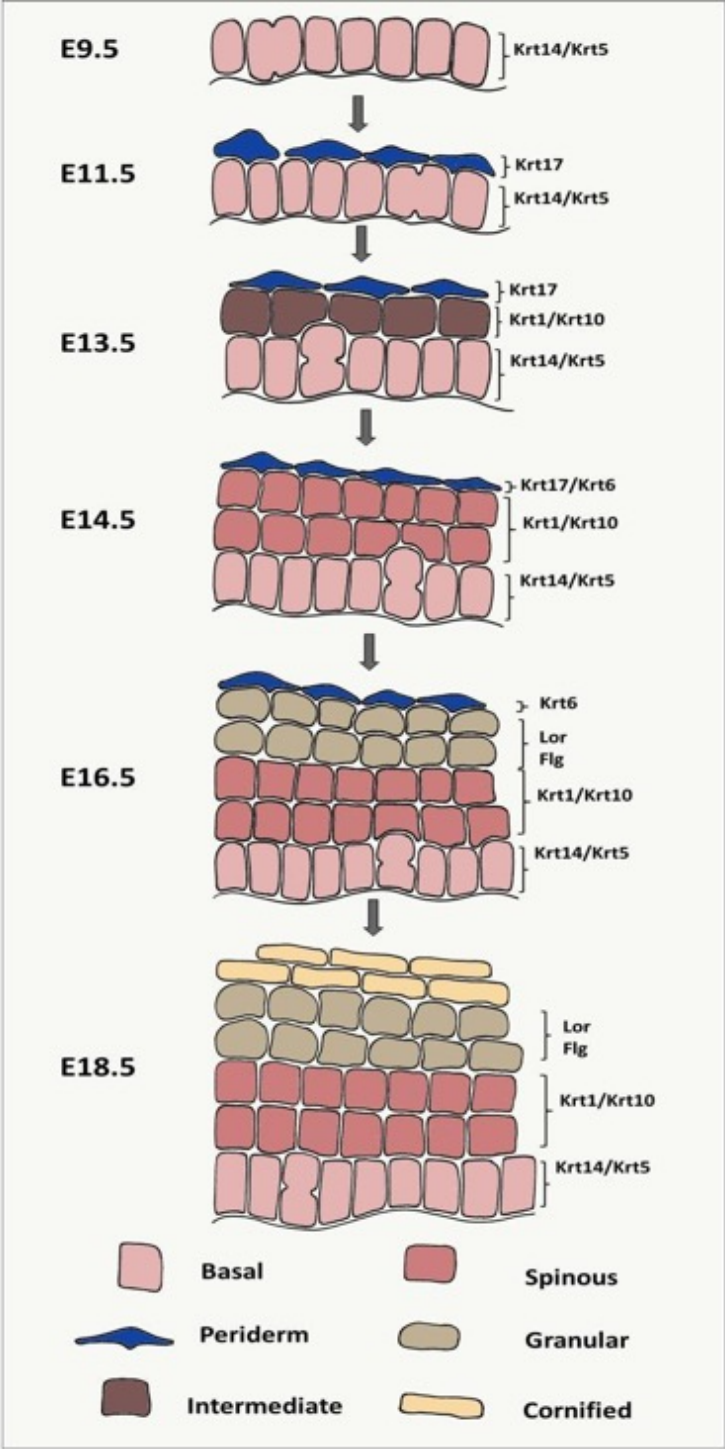


Figure 2. Stages of epidermal stratification.

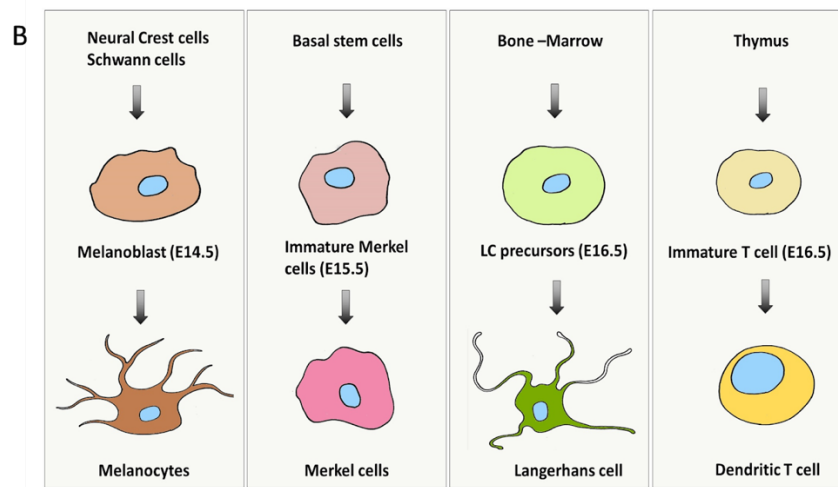
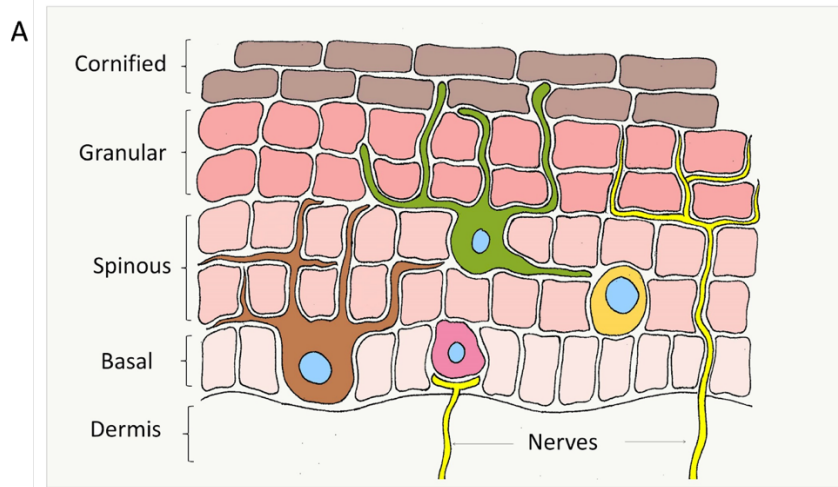


Figure 3. Non-epithelial cells of the epidermis.

CHAPTER 2: EPITHELIAL MECHANISM IN DIGIT SEPARATION DURING MOUSE LIMB DEVELOPMENT

ABSTRACT

Syndactyly, the fusion of digits or toes, is the most common congenital limb malformation. It can be inherited as an isolated abnormality or as part of complex syndromes, including Van der Woude syndrome where it is associated with cleft lip and/or palate. While Van der Woude syndrome is most commonly caused by mutations in the transcription factor IRF6, a subset of cases is caused by dominant negative mutations in the epithelial transcription factor Grainyhead like-3 (GRHL3). Interestingly, mice deleted for *Grhl3* exhibit soft tissue syndactyly, similar to that in Van der Woude patients. Previous studies in multiple different genetic mutants have found that syndactyly is caused by impaired interdigital cell death of mesenchymal cells between the forming digits. Surprisingly, mice deleted for *Grhl3* had normal mesenchymal interdigital cell death, suggesting alternative mechanisms for abnormal digit separation in Van der Woude syndrome. Using 3D reconstructions of multiple tissue sections from embryonic mouse forelimbs, we found that during digit separation, the overlying epidermis forms an interdigital epithelial tongue (IET) at the leading edge as the epithelium moves in between the separating digits. The anti-adhesive property of the surface periderm cells allows the IET to bifurcate as the digits separate. In *Grhl3*^{-/-} mice the IET moves normally between the digits but fails to bifurcate because of hyperadhesion of the periderm. Morphological analysis indicates that *Grhl3* is required for normal polarity of periderm cells such that adhesion factors are limited to the basolateral surfaces. Our data

identify a novel epidermal developmental process that is required for digit separation and explain mechanistically why patients with Van der Woude syndrome develop syndactyly.

INTRODUCTION

Syndactyly, fusion of the digits and or the toes, can be an isolated birth defect or part of a complex syndrome with multiple developmental abnormalities. It is the most common limb malformation in humans, occurring in 1 in 2000 live births.(Ahmed, Akbari, Emami, & Akbari, 2017).

Classical studies in model organisms showed that cell death in the interdigital mesenchyme is required for digit separation ((Fallon & Cameron, 1977; Hernández-Martínez & Covarrubias, 2011; Montero & Hurlé, 2010).ICD starts at the distal mesenchyme, underneath the apical ectodermal ridge around E12.5. The diffusion of Bone morphogenic proteins (Bmp's) and inhibition of fibroblasts growth factors (Fgf's) in the ectodermal ridge activate and control the underlying ICD (Kaltcheva, Anderson, Harfe, & Lewandoski, 2016). ICD occurs via apoptosis and involves the activation of pro-apoptotic factors such as the Bcl2 family proteins, activation of caspase enzymes and reactive oxygen species (ROS)(Salas-Vidal et al., 1998). Clearance of apoptotic cells by phagocytosis results in interdigital tissue regression, ultimately separating the digits (Lorda-Diez, Montero, Garcia-Porrero, & Hurle, 2015).

Work on mouse mutants with soft tissue syndactyly has attributed the digit fusion to impaired interdigital cell death. Even developmental regulators that are selectively expressed in the digit epithelium are thought to signal to the underlying mesenchyme to effect digit separation (Pajni-Underwood, Wilson, Elder, Mishina, & Lewandoski, 2007; Salas-

Vidal, Valencia, & Covarrubias, 2001). But whether mechanisms intrinsic to the digit epidermis play a role in digit separation is unknown.

Van der Woude syndrome is characterized by cleft lip and or cleft palate. In addition, 7-8% of Van der Woude patients have limb defects, most commonly soft tissue syndactyly, suggesting shared developmental mechanisms in oral-clefting and digit separation. Whereas mutations in the transcription factor gene Interferon Regulatory Factor 6 (IRF6) cause most Van der Woude cases, dominant-negative mutations in the transcription factor gene Grainyhead-like 3 (GRHL3) cause up to 30% of cases (Kondo et al., 2002; Peyrard-Janvid et al., 2014). Oral clefting in Van der Woude syndrome is thought to be caused by hyperadhesion of oral periderm cells, but the cause of syndactyly in these patients is unknown (Richardson et al., 2014).

Similar to Van der Woude patients, mice deleted for *Grhl3* have syndactyly, leading us to investigate epithelial mechanisms in digit separation. We found that despite normal interdigital cell death, *Grhl3*^{-/-}embryos exhibit syndactyly, suggesting that mechanisms in addition to interdigital cell death are required for digit separation. We show that a specialized epithelial structure, the interdigital epithelial tongue (IET), forms at leading edge of the epithelium invaginating between the digits. At the same time, the overlying periderm is required to prevent the extension of the IET and epithelial fusion of opposing digits.

MATERIALS AND METHOD

Mice

All mice were housed and maintained in accordance with protocols approved by the University Laboratory Animal Resources (ULAR) in a C57BL/6 background. Transgenic

mouse strains used in these studies are Grhl3 floxed mice, K14-Cre/Grhl3^{-/-} mice, and Grhl3-Cre/LacZ reporter mice. Grhl3 floxed mice were previously generated and used by the Andersen lab (). Skin-specific deletion of Grhl3 in C57BL/6J/ mice was generated by crossing Grhl3 floxed mice with Tg(KRT14-cre)1Amc/J (stock# 004782). Offsprings were bred to produce Wild type, heterozygous and homozygous-Grhl3-flox Cre-positive mice (*Krt14-Cre Grhl3^{-/-}*, *Krt14-Cre Grhl3^{fl/-}* and *Krt14-CreGrhl3^{fl/fl}*, respectively. *Grhl3-Cre/LacZ* reporter mice were purchased from MMRRC.

Scanning and Transmission Electron Microscopy

Mouse embryos were collected at several developmental stages, indicated by timed-pregnancy breeding. Forelimbs were harvested and fixed with 0.25% Glutaraldehyde for 24 hrs in 4C, followed dehydration by series of ethanol and acetone 30%, 50%, 70%, 80%, 90% and 100% at 20 min each. Samples were incubated in 100% acetone and then loaded into CPD (CO₂ critical point dryer). After gold coating, tissues were observed with scanning electron microscope using Quanta 3D SEM. The background of the collected images was modified using imageJ.

For EM, embryonic limbs were fixed in 0.25% Glutaraldehyde for 1-2 days followed by post-fixation with 1% osmium tetroxide. Limbs were dehydrated through several ethanol series and embedded in resin. One nanometer of transverse limb sections was processed for imaging.

Plastic-embedded limbs for 3D reconstructions

Embryonic limbs were collected at the indicated time points then fixed in 4% PFA at 4C, overnight. The next day, limbs were then embedded in low melting point agarose (3%). All tissues were dehydrated in 50%, 70%, then 95% ethanol for 30 mins each at room temperature before a final rotation in 100% ethanol for a further 30 mins. After dehydration, tissues were infiltrated with BMMA resin (Polyscience, Warrington PA) at 4C, over three days, displacing the ethanol in an ascending BMMA concentration gradient from 25% to 75% BMMA in ethanol. The tissue was then submerged and rotated in a 100% BMMA for 24 hrs at 4C before the polymerization stage. Each limb was then placed in a BEEM gelatin capsule with fresh BMMA and sealed tightly. For polymerization, the capsules were placed under the UV light for 20 hrs in Pelco UCV2 cryo chamber (Ted Pella, Redding CA) set at 4C. Sections were serially cut (2 um) using a diamond knife (DiAtome, Hatfield, PA) on a Leica EM UC7 ultramicrotome.

immunofluorescence staining of plastic sections and 3D reconstructions

Slides of plastic thin sections were permeabilized with permeabilization buffer (triton-X in PBS) for 10-15 mins and blocked with blocking buffer (). Sections were incubated with the primary antibody (table) overnight at 4C. The next day, slides were washed with 1XPBS three times, followed by incubation with anti-goat-Alexa Fluor 488, donkey-anti-rabbit- Alexa Fluor 555, donkey-anti-Armenian for 1 hour in room temperature. For nuclear staining, slides were incubated with dapi solution for 1 min, then mounted with 50% glycerol. For re-staining plastic slides, mounting solution was removed by 1XPBS, and slides were incubated in stripping buffer (glycerine) for 1-2 hrs in 60C incubators, followed by several 1x PBS washes. For 3D reconstructions, a continuous series of stained slides were imaged using

Leica DMI6000B fully automated inverted fluorescent microscope (Leica Microsystems Inc., Buffalo Grove, IL). Images were aligned and 3d constructs were generated using AMIRA software.

Whole-mount staining and immunohistochemistry of embryonic mouse limbs

Whole limbs were collected at the indicated time points and fixed with 4% PFA overnight at 4C. Post fixation, limbs were washed with 1XPBS several times 20 mins each and permeabilized with permeabilization buffer (triton-X in PBS) for 30-45 mins and blocked with blocking buffer for 2-3 hrs. Limbs were then incubated with primary Antibody 1-2 days. On day3, limbs were washed with 1XPBS for 20-30 mins each and then incubated with secondary antibody 3-4 hrs at RT or 1 day at 4c in the dark. Limbs were mounted with Glycerol and confocal imaging of the whole limb was processed using Zeiss LSM 510 (Carl Zeiss, Jena, Germany) and femtosecond laser (Chameleon, Coherent Inc., Santa Clara, CA).

For Immunofluorescence staining, cryosections (8 um thick) of limbs and dorsal skin were collected on microplus glass slides. Immunostaining was performed according to previous methods (). Slides were fixed with cold Acetone for 13 mins, followed by 3 washed with 1XPBS, then fixed again with 4% PFA for 10 mins at RT. after fixation, slides were permeabilized with permeabilization buffer (triton-X in PBS) for 10-15 mins and blocked with blocking buffer for 1 hr at RT. slides were incubated with primary antibody for 2 hrs at RT or overnight at 4C. The next day, slides were washed three times with 1XPBS then incubated with secondary antibody for 1 hr at RT in the dark. Slides were mounted with DAPI mount and imaged using Leica DMI6000B fully automated inverted fluorescent microscope (Leica Microsystems Inc., Buffalo Grove, IL)

For Edu staining, pregnant female mouse was injected with 0.5 mg/ml of Edu and sacrificed after 3 hrs post injection. Embryos were collected and limbs were dissected and embedded in plastic. Edu staining was performed on plastic section using Click-iT EdU Alexa Fluor 488 Imaging Kit - Thermo Fisher Scientific. For tunnel assay, embryonic limbs at E13.5 were dissected and embedded in OCT. Frozen sections (8 um) thick were stained using (Click-iT™ Plus TUNEL Assay for In Situ Apoptosis Detection, Alexa Fluor™ 488 dye, ThermoFisher, Cat#C10617) as described by the manufacturer.

LysoTracker assay

Embryonic limbs at E13.5 were dissected and processed as previously described [1] for lysosomal staining.

Mathematical Modeling

We construct a two-dimensional multiscale model of the developing limb along the dorsal-ventral axis to simulate the limb separation over time. In the cell-centered and Voronoi models each cell is represented by a single point [1, 2, 6, 8, 9]. To model the biomechanical forces inside a tissue these nodes are connected by generalized Morse potentials that exercise forces on nearby nodes such that the cells move (Fig S3). We modeled the mesenchymal cells by a single point and visualized them as ellipsoids (gray in Fig. 3). Epithelial cells were also represented by a single point but visualized as the Voronoi tessellation (red in Fig. 3) of the point cloud. Periderm cells we modeled with a modified subcellular element method [4, 5, 10, 11, 13]. Each periderm cell is represented by a central

node surrounded by 11 surface molecules along the sides and basal surface of an elongated hexagon. The modification from the traditional subcellular element method is that the nodes representing a cell have constant positions relative to each other, modeling a rigid body. The central node and surface molecules are connected to all other nodes in the model by different Morse potentials. The sum of all the forces leads to a lateral translation and rotation of each periderm cell. The mesenchymal cells surrounding the bones are inactive and immobile but pose reflective boundary conditions on the moving cells. To model a directed cell migration, an attractive potential for all cells is placed in the middle between the two bones. At constant time intervals one epithelial cell divides randomly. To model the apoptosis of the mesenchymal cells we randomly remove a mesenchymal node at constant time intervals. The digit development over time is then simulated by solving the differential equations resulting from the force equations numerically.

Measurements of nucleus orientation

The orientation of epidermal daughter cells located at the IET and surface epithelia was determined by measuring the angular plane of the nucleus relative to the basement membrane as described by Fuchs and Lechler 2005. Cells were categorized as either perpendicular or non-perpendicular, wherein perpendicular cells possessed an angular measurement of 90 ± 30 degrees relative to the basement membrane and non-perpendicular cells possessed angles between 0 ± 60 degrees and above 120 degrees relative to the basement membrane (n=90). Angular measurements were processed using IMAGEJ 1.51r. Normalized epidermal cell angles were then plotted as radial histograms using Origin 2019b (OriginLab) from data binned into 15° increments.

Measurements of Periderm cell size

Images (40X) of whole-mount immunofluorescence staining of the limb skin with keratin-17 were used to measure the size of periderm cells. Images were calibrated with a micrometer scale bar taken at the same magnification. The cells were processed through IMAGEJ 1.51r with a conversion factor of 5.26 pixels/ μM . Cell area measurements (μM^2) were collected by circumscribing each cell membrane using the segmented line tool (n=118). The collected measurements were then processed in Microsoft Excel. For each genotype, 3-4 embryos were analyzed. Statistical analysis was performed using student's T-test.

RESULTS

***Grhl3* is required for normal digit separation**

Although mice germline-deleted for *Grhl3* (*Grhl3*^{-/-}) die at birth with an open neural tube and epidermal barrier defects, mice deleted for *Grhl3* in the epidermis (*Krt14Cre-Grhl3*^{flox/flox}) survive into adulthood. Up to a quarter of these mice have soft tissue syndactyly (Fig. 1a) similar to that found in 7% of VWS patients with *GRHL3* mutations, indicating that epithelial expression of *Grhl3* is required for normal digit separation and that *Grhl3* deletion can model syndactyly in VWS.

To understand the role of *Grhl3* in digit separation, we studied digit development in *Grhl3*^{-/-} mouse embryos at key developmental stages: E12.5, E13.5, E14.5, and E15.5 (Fig. 1b,c, S1a). We limited our analyses to the developmental stages before the re-fusion of the digits that starts around E16 in mice.

As a consequence of cell death in the interdigital zone, WT hand pads form an interdigital indentation between E12.5 and E13.5 (Fig. 1b, c; upper rows). A similar interdigital indentation was detected in *Grhl3*^{-/-}-embryos (Fig. 1b, c; lower rows), suggesting that *Grhl3* loss does not affect interdigital cell death. In WT mice, digit separation proceeds progressively from E13.5 to E15.5 (Fig. 1b, c; upper panels) as previously described (). By contrast, in *Grhl3*^{-/-}-embryos, digit separation proceeds more slowly between E13.5 and E14.5, and there is beginning re-fusion of the digits at E15.5 (Fig. 1b, c; lower panels). We found a similar digit separation delay in the foot pads of *Grhl3*^{-/-}-embryos (Fig. S1b). These phenotypes are highly consistent; syndactyly was found in 100% of fore- and hind limbs of *Grhl3*^{-/-}-embryos. Together, these data indicate that *Grhl3* is required for digit separation during limb development.

Interdigital cell death progresses normally in *Grhl3*^{-/-}-mice

Research with mouse mutants indicates that defective programmed cell death in the interdigital mesenchyme underlies most cases of soft tissue syndactyly. This is even true for regulators restricted to the overlying epidermis; those are proposed to signal to the interdigital mesenchyme to control cell death. Hence, we initially hypothesized that *Grhl3*, which is expressed in the epidermis, regulates cell death signals sent from the overlying epidermis to the underlying interdigital mesenchyme.

Immunofluorescence staining of E13.5 forelimbs with an antibody against cleaved caspase-3, a common marker for caspase-dependent apoptosis, shows a mild decrease in casp3a-positive cells in the interdigital zone of *Grhl3*^{-/-}-mice (Fig. 2a,b). In contrast, overall interdigital cell death as indicated by lysosomal activation (Fig. 2c) and DNA fragmentation

(Fig. 2d) is unaffected in *Grhl3*^{-/-}-mice. These findings are consistent with the normal interdigital indentation in *Grhl3*^{-/-}-hand pads at E13.5 (Fig. 1b,c,S1). Together, these results indicate that death of the interdigital mesenchyme occurs normally in the absence of Grhl3, despite the mild decrease in caspase-3 cleavage; the mechanisms that induce death of the interdigital mesenchyme are highly redundant and partially caspase-independent.

As our data suggest that mechanisms independent of interdigital cell death cause defective digit separation in *Grhl3*^{-/-}-embryos, we next investigated the nature of the interdigital fusion in E15.5 *Grhl3*^{-/-}-embryos. To obtain a complete picture of the syndactyly, we embedded WT and *Grhl3*^{-/-}-E15.5 forelimbs in plastic, followed by serial thin sectioning (2 μm) and staining with the epithelial marker keratin 5. Serial sections were then tiled scanned and mosaic images digitally assembled followed by 3D reconstruction—this allowed large scale imaging of the entire limb (Fig. 3a). Using imaging software, we could then slice the 3D reconstructs along two different planes: YZ axis, dorsal-ventral; and YX axis, proximal-distal (Fig. 3b).

Using this method, we discovered that the digits in *Grhl3*^{-/-}-embryos are primarily joined by an epithelial fusion rather than by interdigital mesenchyme that failed to undergo cell death (Fig. 3c). The two ortho-slice views indicate that the epithelial fusion of the digits in *Grhl3*^{-/-}-embryos is observed in both directions, dorsal-ventral and proximal-distal (Fig. 3d). No interdigital epithelial fusion was detected at E13.5 in *Grhl3*^{-/-}-embryos (Fig. S2a), consistent with normal digit appearance at this time-point (Fig. 1b). Beginning interdigital epithelial fusion was detected at E14.5 in *Grhl3*^{-/-}-mice (Figure S2b), consistent with the onset of defective digit separation as observed by scanning electron microscopy (Fig. 1b). Based on

these data, we hypothesize that in addition to interdigital cell death, mechanisms intrinsic to the epidermis are required for digit separation.

Formation of an interdigital epithelial tongue in normal digit separation

Investigating potential epidermal mechanisms in digit separation, we noticed the formation of a multi-layered interdigital epithelial tongue (IET) in the WT E15.5 forelimb 3D reconstructs (Fig. 4a). The IET forms between the digits at the leading edge of the epidermis as it invaginates from the ventral and the dorsal side (Fig. 4a). The IETs from the dorsal and ventral side eventually meet, fuse, and then bifurcate, allowing separation of the digits; these events progress in a distal-to-proximal direction (Fig. 4a,b). The IET has not formed at E13.5 (Figure S2), but is clearly observed at E14.5, concurrent with the active phase of digit separation in normal mice (Fig. 4b).

Despite being multilayered, the IET is composed of basal keratinocytes as indicated by the expression of Krt14 and the lack of expression of the differentiated keratinocyte markers Krt1 and Krt10 and the periderm marker Krt17 (Fig 4c). The differentiated keratinocyte layer and the periderm cover the surface of the skin, including the IET, but do not extend into the IET's leading edge. Edu staining of forelimb sections shows active cell proliferation along the basal epidermis, including in (although not preferentially) the IET (Fig. 4d). The IET is reminiscent of other developmental structures involved in collective migration of epithelia, suggesting that it may play an active role in digit separation.

Modeling suggests that directed cell migration plays a role in the formation of the IET

Next, we modeled the processes required for IET formation, testing the influence of cell proliferation and active migration—processes that are important in the early formation of epithelial appendages such as hair follicles and the mammary gland. Thus, we considered two possible cellular models driving IET formation (Fig. 5a). Model 1 posits that epidermal cell proliferation along with cell death in the underlying interdigital mesenchyme is sufficient for forming a multi-layered epithelial tongue. Model 2 posits that in addition to cell proliferation and interdigital cell death, the overlying epidermal cells need to actively migrate into the interdigital space to form a multi-layered epithelial tongue.

To test these predictions, we constructed a two-dimensional multiscale model of the epithelial invagination between two digits along the XZ axis (dorsal-ventral) to simulate digit separation over time (E13.5-E14.5) (Fig. 5b). We combined a cell-centered model, the Voronoi model, and the sub-cellular element method into a hybrid model where each cell is represented by a single point [1, 2, 6, 8, 9]. To model biomechanical forces relevant for tissue movement, these nodes are connected by generalized Morse potentials that exercise forces on nearby nodes such that the cells move (Fig. S3). To model death of the underlying mesenchymal cells, we randomly removed mesenchymal nodes at constant time intervals. In addition, at constant time intervals one epithelial cell divides randomly. We found that proliferation of epidermal keratinocytes concurrent with mesenchymal interdigital cell death is insufficient to induce IET formation (Fig. 5b). In contrast, when an attractive force was added in the interdigital zone, epidermal cells moved downwards collectively, forming a multi-layered epithelial structure between the digits (Fig. 5c) reminiscent of the IET (Fig. 5d).

In sum, these computational models suggest that collective active migration of epidermal cells, concomitantly with cell proliferation and interdigital cell death, is required to induce the formation of an IET and digit separation.

Collective cell migration of the IET during digit separation

Our mathematical models predict that in addition to epidermal cell proliferation and interdigital cell death, active migration of epidermal cells is required for IET formation. We hypothesized that this happens via collective cell migration where a cohesive group of epithelial cells moves directionally as observed in the development of many organs, including blood vessels, mammary gland, and tracheal branching.

Changes in cell shape, including front-rear cell polarity, and changes in the surrounding extracellular matrix are prototypical features of active cell migration. Thus, we next investigated whether cells at the IET leading edge exhibit migratory characteristics by comparing transmission electron microscopy images of the IET with the surface epidermis (Fig. 6a,b). In the surface epidermis, basal keratinocytes exhibit a cuboidal shape with nuclei oriented mostly perpendicular to the basal lamina (Fig. 6a,c). In contrast, basal keratinocytes in the IET show elongated cell shape with nuclei oriented toward the leading edge, slanting horizontally relative to the basal lamina (Fig. 6b,c,d,e, S4a). These data suggest that the IET represents a collectively migrating, multi-layered epithelial structure.

Consistent with E-cadherin expression in other collectively migrating epithelia (), the IET leader cells downregulate E-cadherin, whereas follower cells maintain strong E-cadherin expression (Fig. S4c). Unlike E-cadherin, P-cadherin is highly expressed in migrating leader cells. P-cadherin activate the small Rho GTPase Cdc42, a promoter of actin polymerization and microtubule re-organization required for front-rear cell polarity (Plutoni et al., 2016). Immunofluorescence staining shows basolateral expression of P-cadherin in basal keratinocytes located distally from the leading edge of the IET, whereas keratinocytes at the leading-edge show increase expression of P-cadherin in the apical membrane adjacent to the basement membrane (Fig. 6f). The increased of P-cadherin at the front of IET leader cells suggests that signaling pathways involved in cell polarity and active migration are activated in IET leading edge.

We also observed signs of IET-extracellular matrix interactions during digit separation. The laminin-1-containing basement membrane is thicker and punctate at the leading edge of the IET (Fig. 6g), whereas it is thinner and continuous more distally, away from the leading edge. These findings suggest active basement membrane remodeling at the IET's leading edge, similar to that found in association with actively migrating epidermal keratinocytes in the migrating wound front. Proteolytic enzymes, including matrix metalloproteinases, degrade the basement membrane and the underlying extracellular matrix to facilitate collective cell migration. Consistent with this notion, the expression of the matrix metalloproteinase Mmp3 is specifically upregulated underneath the IET leading edge in the interdigital mesenchyme (Fig. 6h). These data suggest that in addition to mesenchymal interdigital cell death, the

mesenchymal ECM interacts with the overlying epithelial cells to promote migration of the IET.

Together, these data show that in response to the underlying interdigital mesenchymal cell death, the epidermis invaginates from the dorsal and ventral sides, forming a multilayered interdigital epithelial tongue, the IET, that actively migrates into the underlying mesenchyme to promote digit separation.

Grhl3 is required for normal periderm formation

Having gained understanding of epithelial mechanisms in digit separation, we turned our attention back to the *Grhl3*^{-/-} embryos—to understand how Grhl3 regulates digit separation. At E15.5, the fused digits in *Grhl3*^{-/-} embryos contain an epidermal sheet between them (Fig. 3). Had defective interdigital cell death caused the syndactyly, we would have expected mesenchymal tissue between the digits. In the light of these findings and our data on normal digit separation, we hypothesized that the IET invaginates normally between the digits, but as the IET dives between the digits, the epidermis from the opposing digits fuses, creating an epithelial sheet that fuses the digits. Going back to E14.5 *Grhl3*^{-/-} limbs, when impaired digit separation is first evident, we discovered that the IETs form and migrate normally from the dorsal and ventral side, meeting in the middle (Fig. 7a). But as the IET dives between the digits, the epithelia from adjacent digits adhere to each other, creating extended IETs that appear as epithelial sheets at E15.5 (Fig. 3a).

The adhesion of embryonic surfaces is prevented by the periderm, the outermost layer of the embryonic epidermis (Hammond, Dixon, & Dixon, 2017). We noted that in the IETs in *Grhl3*^{-/-} embryos contained trapped Krt17-positive periderm cells within them, which we never observed in WT embryos (Fig. 7a). This finding suggested that hyperadhesion of periderm cells extended the IETs and fused the digits in *Grhl3*^{-/-} embryos. Consistent with the notion of the opposing digits adhering to each other in *Grhl3*^{-/-} embryos, scanning electron microscopy views of the ventral E14.5 hand pad show a surface cell on a forming digit tightly adhering to a surface cell on the adjacent digit; this phenomenon is not observed in WT embryos (Fig. 7b). These same images also indicate morphological difference of the surface skin in *Grhl3*^{-/-} embryos compared to WT (Fig. 7b); the *Grhl3*^{-/-} epidermal surface is smoother with larger cells than found on the WT surface (Fig. 7b, right panel).

Next, we used immunostaining with Krt17 antibody to test whether periderm forms in the *Grhl3*^{-/-} embryos. Periderm is formed at E13.5 and persists at least to E15.5 (Fig. 7c), indicating that *Grhl3* is not required for specification of periderm. Similar findings were obtained with the late periderm marker Krt6 at several developmental stages (figure S5). The appearance of *Grhl3*^{-/-} periderm cells is clearly abnormal, however, with a spikey cell surface (Fig. 7c; fig. S5). Wholemount Krt17 staining showed that the periderm cells in *Grhl3*^{-/-} embryos are large and irregularly shaped; this abnormality is found across the entire hand surface, including in the interdigital area (Fig. 7d, e). Transmission electron microscopy of the hand pad epidermis at E14.4 indicates that in WT mice, the periderm cells have an endothelial-like shape and are larger than basal and intermediate keratinocytes (Fig. 7f). In contrast, periderm cells in the *Grhl3*^{-/-} epidermis exhibit irregular cell shape, characterized by expansion of the cytoplasm and membrane protrusions (Fig. 7f).

Together, these data indicate that *Grhl3* is dispensable for the formation of periderm cells but required for their normal appearance. These findings could be relevant to the syndactyly in *Grhl3*^{-/-}-embryos because periderm has anti-adhesive properties, preventing pathological epithelial adhesions in the developing embryo.

***Grhl3* is required for asymmetric expression of adhesion complex proteins in digit periderm cells; role in the anti-adhesive function of periderm**

The anti-adhesion function of periderm depends on the exclusion of adhesion complexes from the periderm's apical surface (Fig. S6a). Given the hyper-adhesion observed in the interdigital periderm in *Grhl3*^{-/-}-embryos, we tested whether *Grhl3* is required for normal expression and localization of adhesion complex proteins in the periderm. Immunofluorescence staining of transverse sections in WT E14.5 forelimbs clearly show Dsg1 and E-cadherin expression around intermediate epidermal cells, but no expression on the apical surfaces of periderm cells in the interdigital area (Fig. 8f). In contrast, in *Grhl3*^{-/-}-embryos, Dsg1 and E-cadherin are abnormally expressed on the apical surfaces of interdigital periderm cells (Fig. 8f), mirroring observations from the oral periderm in *Irf6* mutant mice (). Interestingly, the abnormal expression of adhesion proteins in periderm apical surface is not exclusive to the interdigital area, indicated by whole mount staining of *Grhl3*^{-/-}-forelimb epidermis (Figure. S6b). These data indicate that *Grhl3* restricts the localization of adhesion complexes away from the apical surface of the developing periderm in the limb epidermis.

Periderm cell polarity is controlled by the apicolateral expression of tight junctions; which play a key role in restricting adhesion molecule expression from the apical surface. In WT hand epidermis, the tight junction protein ZO-1 is precisely located at the apicolateral junctions, leading to the formation of a highly polarized, endothelial cell-like periderm cells (Fig. 8g). In contrast, *Ghrl3*^{-/-} periderm cells have a punctate expression of ZO-1 that is not restricted to the apicobasal membrane; it is also found in the basolateral side of the cell, where ZO-1 is not normally expressed (Fig. 8a). In addition to the loss of anti-adhesive properties, *Ghrl3*^{-/-} periderm cells also have irregular cell shape.

The combination of these alterations in *Ghrl3*^{-/-} periderm results in the formation of a morphologically abnormal hyper-adhesive periderm that hinders IET bifurcation during digit separation. These data clearly suggest that *Grhl3* in the periderm regulates the expression of genes that are necessary for the restricted expression of adhesion complex proteins from the apical surface, thus preventing pathological adhesion between epithelial surfaces (fig. S6c).

Altogether, these findings highlight the phases of the epithelial mechanism in digit separation. This mechanism is initiated by active cell migration of surface epidermal cells into the interdigital mesenchyme, forming a multilayered-layered epithelial tongue between the developing digits. As the IET invaginate the interdigital zone, periderm cell on one digit repel the periderm cell on the opposing digit due to the lack of adhesion molecules on their apical surfaces. This repelling force leads to IET bifurcation, ultimately digit separation.

Thus, normal periderm development is essential during digit separation, which explains why abnormal periderm formation in *Ghr13*^{-/-}-mice causes syndactyly.

DISCUSSION

Here we uncover epithelial mechanisms required for digit separation in mammals. Our studies indicate that in addition to interdigital mesenchymal cell death, collective migration of an epithelial structure is required for digit separation. Additionally, we identify a key function of the epidermal transcription factor Grainyhead-like 3 (*Ghr13*) in periderm development and function.

For decades, researchers have focused on programmed cell death of the interdigital mesenchyme as a key event in digit separation. Most mouse mutants with soft tissue syndactyly have been ascribed to decreased or altered ICD, work that has identified three main signaling pathways involved in ICD: bone morphogenic proteins (Bmps), fibroblasts growth factors (Fgfs), and retinoic acid (RA). Mice lacking *Bmpr1a* in the epithelia exhibit syndactyly and impaired interdigital cell death of the mesenchyme (Kaltcheva et al., 2016). The high levels of *Bmp2/4* in the interdigital epithelia activates *Bmpr1a*, which results in downregulation of the cell survival factor, fibroblast growth factor-8 (FGF8). The decrease in *Fgf8* levels in the interdigital ectoderm increases retinoic acids (RA) levels in the mesenchyme, triggering ICD.

In *Ghr13*^{-/-}-embryos we observed a mild decrease in activated caspase in the interdigital zone, with normal overall interdigital mesenchymal cell death.

These findings suggested that mechanisms distinct from interdigital cell death are also required for digit separation. Three-dimensional reconstructs of the developing distal limbs at three key stages of digit separation—E13.5, E14.5, and E15.5—characterized epithelial mechanisms important for digit separation. As the interdigital mesenchyme is removed through cell death, the epidermis invaginates from the ventral and the dorsal side. The epithelial leading edge contains a multi-layered epithelial structure, which we refer to as the interdigital epithelial tongue (IET). The IETs from the ventral and dorsal sides eventually meet and separate. As the interdigital cell death that progresses in a distal to proximal direction, the progress of the epithelial invagination also progresses in a distal to proximal direction.

While previous studies have not focused on the role of the epithelium in digit separation, the IET was previously observed in the E15.5 mouse limb where it was described as thickening of the epidermis (YL Wong et.al 2012, Dev Bio). Our ability to create 3D reconstructions of the hand facilitated the definition of the IET.

The epidermal invagination between the digits and the formation of the IET has some similarities with the development of skin appendages, including mammary gland and hair follicles (Fuchs, 2007; Xie, Yao, Han, Huang, & Fu, 2016). Modeling the morphogenetic mechanisms underlying the formation of such epithelial outgrowths, we found that in addition to epithelial cell proliferation and interdigital mesenchymal cell death, a migration force was required for the formation and movement of the IET.

Which led us to study the IET as a collectively migration epithelial front, a developmental phenomenon involved in the formation of many organs during embryogenesis. In

collectively migrating epithelia, cell-cell adhesions are essential for coordinating the collective movement and maintaining the mechanical integrity of the epithelial cohort, and chemotactic cues in the surrounding extracellular matrix are required to guide the directionality of the migration (Ilina & Friedl, 2009; Scarpa & Mayor, 2016). In addition, changes in actin-cytoskeleton and cell polarity of leader cells are required for active migration.

Consistent with this model, keratinocytes at the IET leading edge exhibit morphological features of leader cells with cell elongation and nuclei orientated toward the direction of migration. Downregulation of E-cadherin and up-regulation of P-cadherin at the leading edge, which we observed in the IET, parallels the expression pattern of adhesion molecules during active cell migration in other models. Additionally, modifications of the basement membrane and the mesenchymal extracellular matrix were observed at the IET leading edge compared to surface epidermis.

The formation of the IET brings the epidermis covering opposing digits into close contact. But because the outermost surface of the epidermis is covered by periderm cells, an anti-adhesive layer, adherence of the digits is prevented. Periderm achieves this anti-adhesive function by restricting the expression of adhesion complexes to the basolateral surface. In *Grhl3*^{-/-} embryos, the surface of periderm cells aberrantly expresses adhesion complexes making these cells susceptible to adhesion. Consequently, as the IET moves between the digits the epidermis from opposing digits adhere to each other creating elongated IETs that appear as epithelial sheets between fused digits.

Syndactyly is found in up to 7% of Van der Woude syndrome patients carrying mutations in GRHL3, suggesting that the syndactyly in *Grhl3*^{-/-} mice models this disease. Oral clefts in Van der Woude syndrome of any genetic cause are thought to be due to disrupted oral periderm development. Interestingly, genetic mutations in genes expressed in the periderm such as IRF6, IKKA, SFN, RIPK4 and Jagged 2 (*Jag2*) also result in limb defects (Casey et al., 2006; Richardson, Dixon, Jiang, & Dixon, 2009; Richardson et al., 2014). It will also be of interest in future studies to determine whether syndactyly in mouse mutants for some of the developmental regulators that are expressed in the epidermis could be also involved the epithelial mechanisms we have described here.

Figure 1

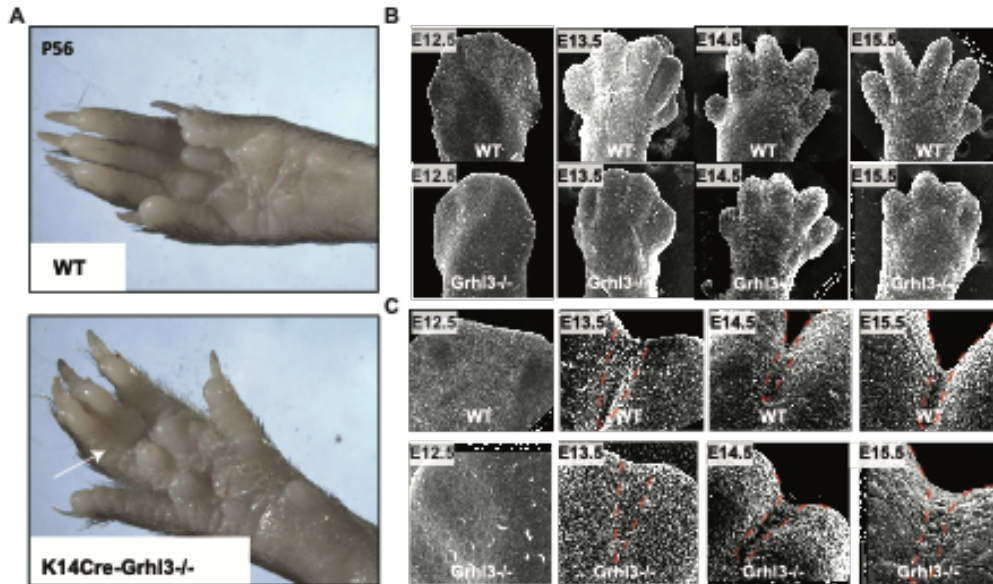


Figure 1. Grhl3 is required for normal digit separation

(A) Forelimbs of wild type mice (top) and mice with epithelial deletion of Grhl3 (bottom) at postnatal day 56. Arrow indicates soft-tissue syndactyly between the third and fourth digit in K14Cre-Grhl3^{-/-} mice. (B) Scanning Electron Microscopy (EM) of wild type and Grhl3^{-/-} forelimbs at E12.5, E13.4, E14.5 and E15.5, showing defective digit separation in Grhl3^{-/-} mice. (C) Higher-magnification scanning EM images of the third and fourth digit in wild-type and Grhl3^{-/-} forelimbs indicate fusion between the digits at E14.5 and E15.5 in Grhl3^{-/-} mice. Dashed lines indicate the interdigital zone.

Figure 2

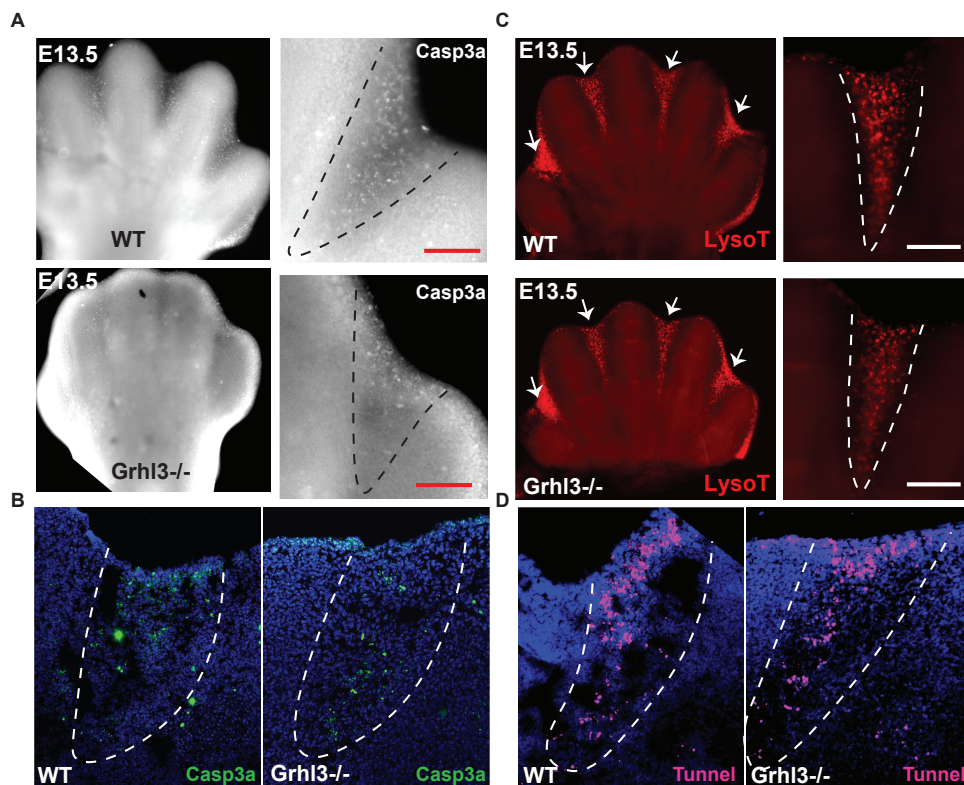


Figure 2. Mesenchymal interdigital cell death progresses normally in *Grhl3*^{-/-} mice

(A) Whole-mount staining of E13.5 forelimb with Cleaved caspase-3 (gray) in both WT and *Grhl3*^{-/-} mice (left panel). Higher-magnification of the interdigital zone indicated by dashed-lines (right panel). (B) Immunofluorescence staining of Cleaved caspase-3 (green) in E13.5 limb sections. Dashed lines indicate interdigital zone. (C) LysoTracker staining of wild-type and *Grhl3*^{-/-} forelimbs at E13.5. Arrows point to the interdigital zone. The right panels are magnified views of the left panels. (D) Tunnel staining (magenta) of E13.5 limb sections from WT and *Grhl3*^{-/-} mice. Dashed lines indicate the interdigital zone.

Figure 3

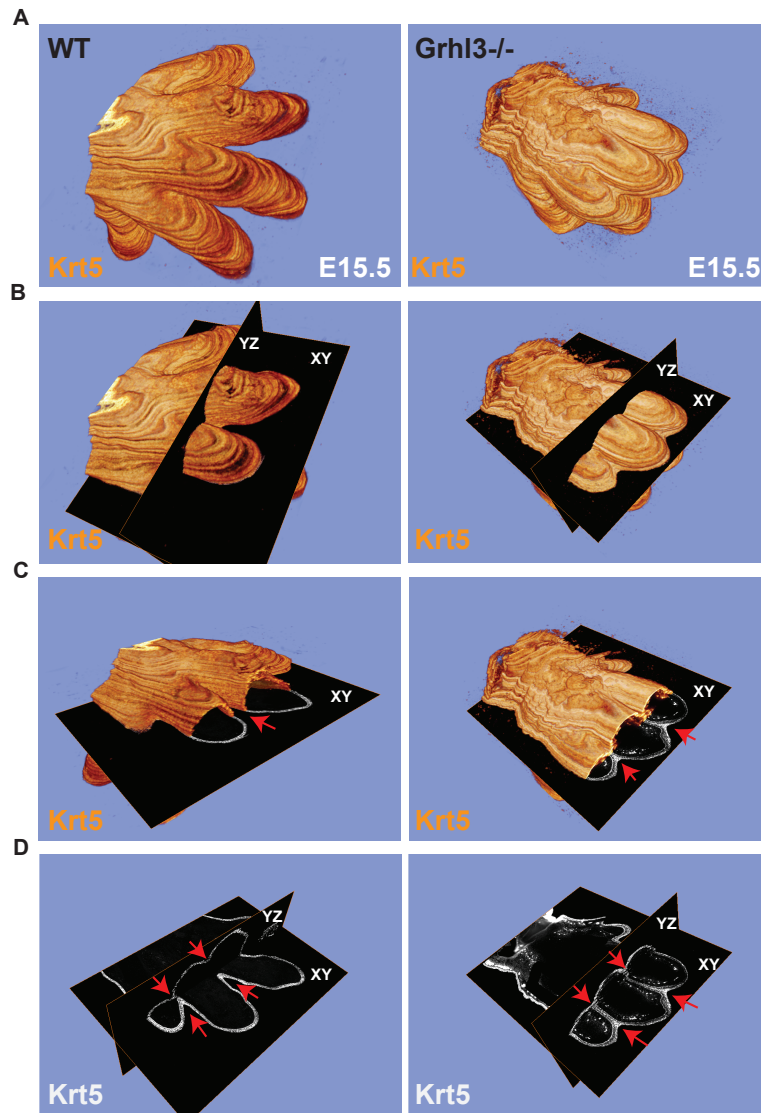


Figure 3. Digits in Grhl3^{-/-} embryos are joined by an epithelial sheet

(A) 3Dl reconstructions of E15.5 whole forelimbs of WT (left panel) and Grhl3^{-/-} (right panel) mice stained with the epithelial marker Keratin-5 (orange). (B) A representation of ortho-slices orientation of the 3D forelimb (YZ: dorsal to ventral, XY: proximal to distal). (C)

Cross-section views of the 3D reconstructs (XY: proximal to distal). Arrows indicate complete separation of the epithelia and the digits in WT (left panel), and epithelial fusion between the unseparated digits in Grhl3 ^{-/-} (right panel). (D) Ortho-slices of the 3D reconstructs showing the epithelia in WT (left panel) and Grhl3 ^{-/-} (right panel) mice in two different planes (YZ: dorsal to ventral, XY: proximal to distal). Arrows indicate the interdigital epithelia in two ortho-slices planes.

Figure 4

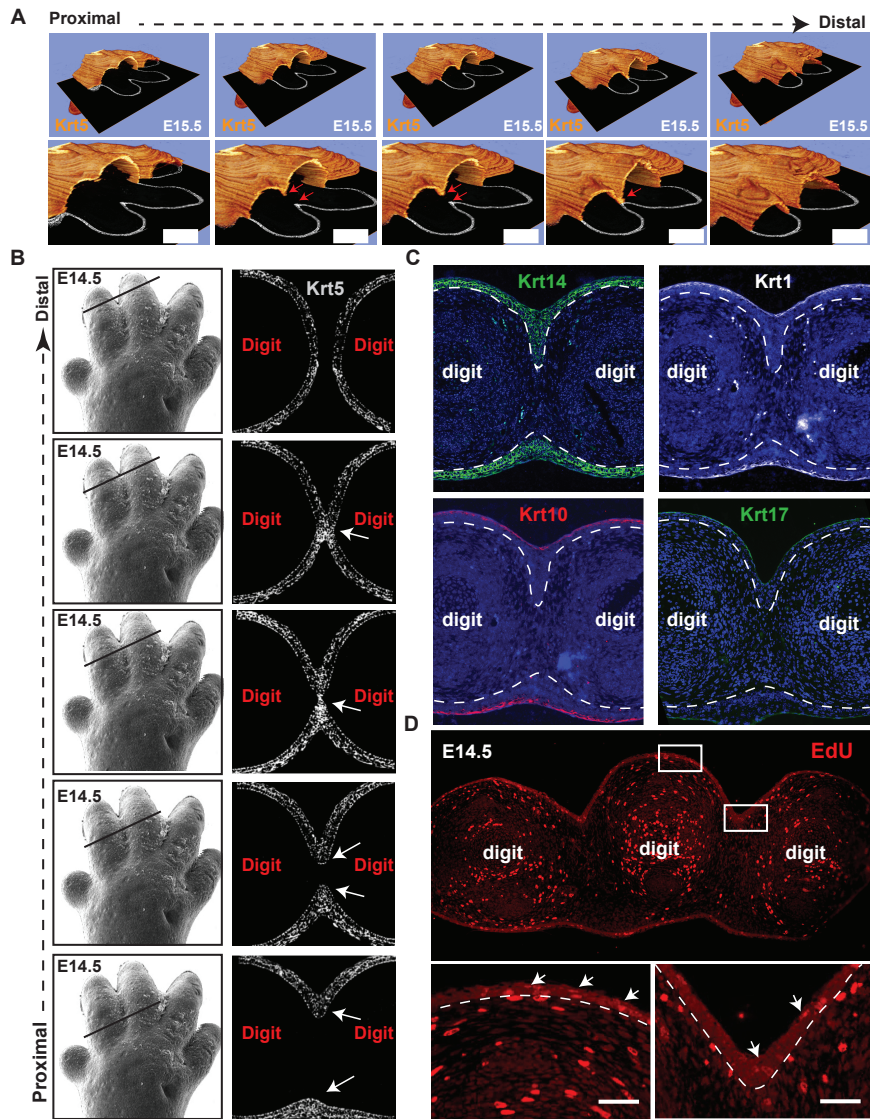


Figure 4. Formation of an interdigital epithelial tongue in normal digit separation

(A) Series of images showing the interdigital epithelia stained with Keratin-5 (orange) in continuous ortho-slices of 3D reconstructions in WT forelimb at E15.5. The lower panel shows higher magnification images. Arrows indicate the interdigital epithelial tongue coming from both axes. (B) Continuous series of (proximal-to-distal) E14.5 mouse

forelimb sections stained with Keratin-5 (gray). Arrows point to the interdigital epithelial tongue (IET). (C) Immunofluorescence staining showing the expression of several epithelial markers Krt14, Krt1, Krt10 and Krt6, respectively, in the forming interdigital epithelial tongue in E14.5 limb. (D) Immunofluorescence staining showing proliferating cells indicated by EdU positive staining in WT forelimb at E14.5. Arrows point to EdU positive cells in the epithelia above the digit and in the interdigital zone.

Figure 5

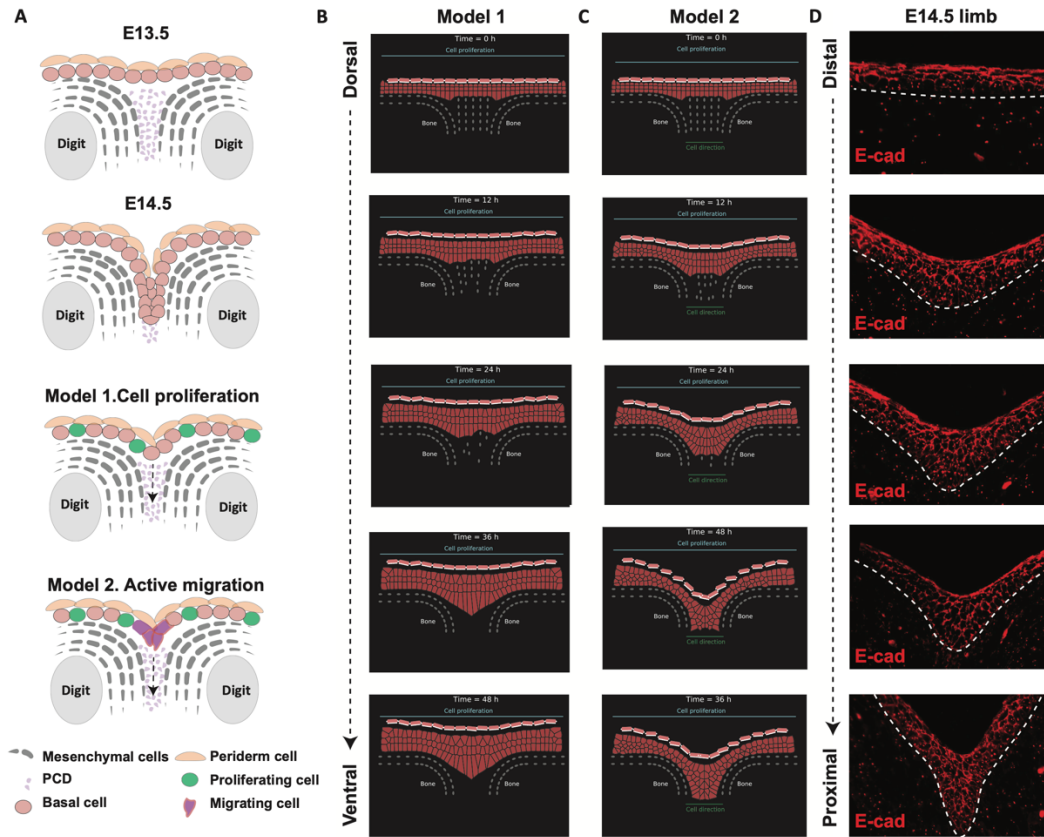


Figure 5. Modeling suggests that directed cell migration plays a role in the formation of the IET

(A) Schematic representations of two proposed models for interdigital epithelial tongue formation during digit separation. (B-C) Cell-centered and Voronoi models represent a time-course (48h) series of events during embryonic limb development. Each cell is represented by a single point. Epithelial cells (pink) and Mesenchymal cells (grey). The biochemical forces inside the tissue are modeled by generalized Morse potentials between all the nodes (green arrows in inset). (B) Proposed model 1: Cell proliferation of the epithelial cells (indicated by the blue line on top) is insufficient to induce IET formation. (C) Proposed model 2: active cell

migration (indicated by the green line at the bottom) is sufficient for the layer of epithelial and periderm cells to invade the cavity between the two bones and lead IET formation. (D) E-cadherin staining of interdigital epithelial in WT forelimb sections at E14.5.

Figure 6

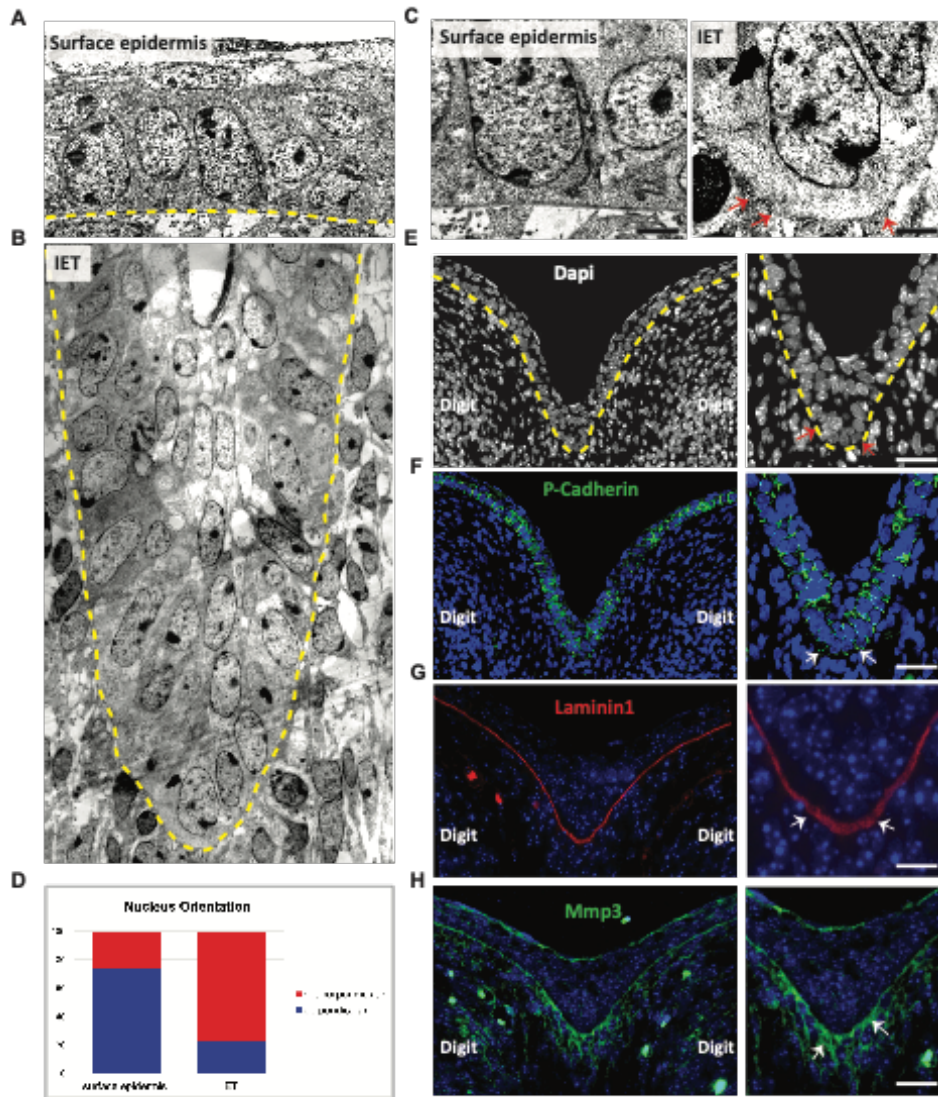


Figure 6. Collective cell migration of the IET during digit separation

(A) Transmission electron microscopy showing the surface epidermis and (B) the interdigital epithelial tongue at E14.5 forelimb in wild-type mice. The dashed line indicates the basement membrane. (C) Higher magnification of cells at the surface and cells at the leading edge of IET. Arrows indicate cellular protrusions and breaks of the basement

membrane. (D) Percentage of cells with nucleus oriented either perpendicular or non-perpendicular to the basement membrane in cells at the surface epidermis and IET leading edge. (E) Immunofluorescence staining of the interdigital epithelial tongue with nuclear marker DAPI (gray), Arrows point to cells at the leading edge. (F) Immunofluorescence staining with adherens junction's marker P-cadherin (green). Arrows indicate the high expression of P-cadherin in basal keratinocytes in the interdigital epithelial tongue. (G) Immunofluorescence staining with the basement membrane marker Laminin1 (red). Arrows indicate punctate expression at the leading edge. (H) Immunofluorescence staining with the extracellular matrix enzyme-matrix metalloproteinase-3 MMP3 (Green). Arrows indicate the cells with high expression of Mmp3. Right panels show Higher-magnification images

Figure 7

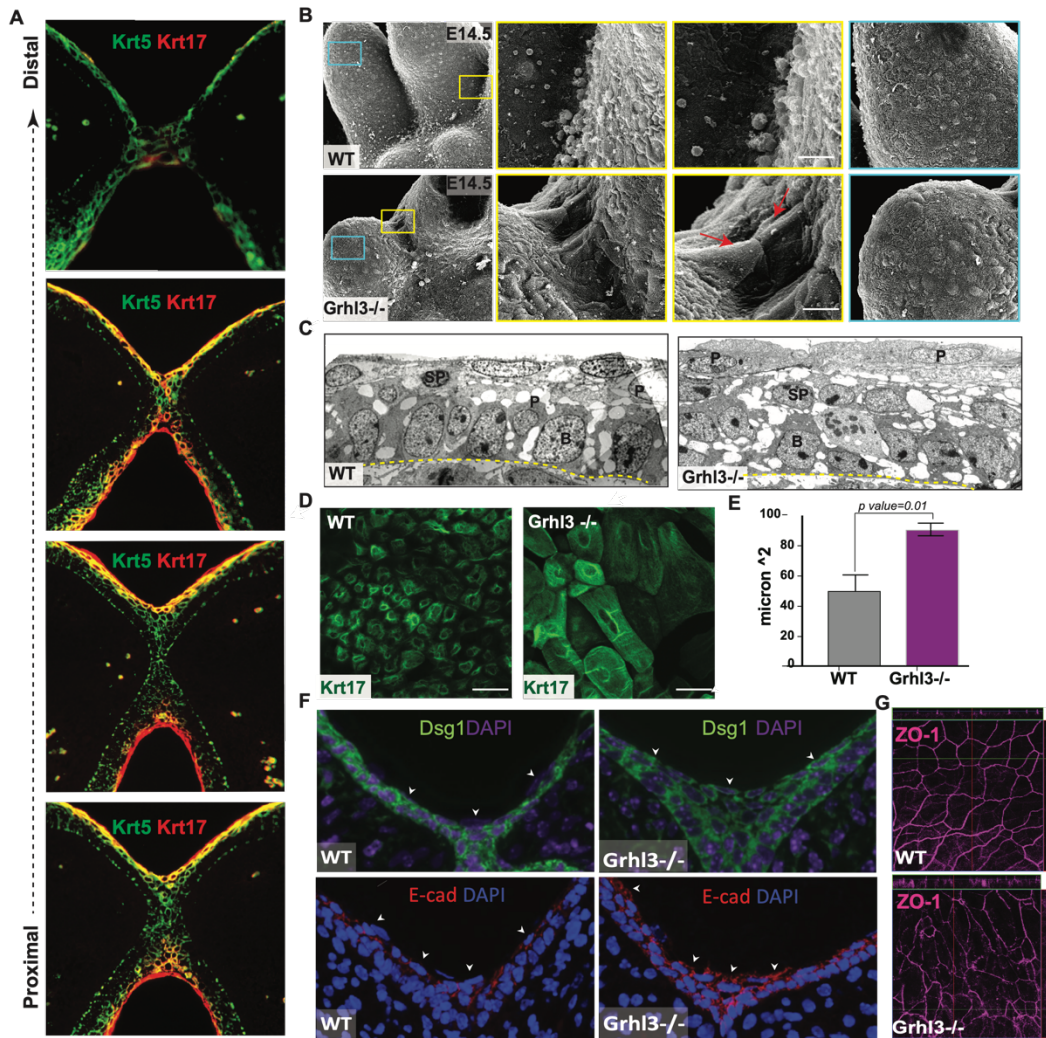


Figure 7. Grhl3 is required for normal periderm formation

(A) Continuous series of E14.5 Grhl3^{-/-} forelimb sections stained with Keratin-5 (green) and Keratin-17 (red). Arrows point to the interdigital epithelial tongue (IET). (B) Scanning Electron microscopy (ventral views) of WT and Grhl3^{-/-} limbs at E14.5. Arrows indicate hyper-adhesion between surface cells between the forming digits. High-magnificent (5020X)

Scanning electron microscopy images of surface cells in (yellow and blue boxes). (C) Transmission Electron microscopy analysis of surface epithelia at E14.5 indicate abnormal periderm cells in Grhl3^{-/-} epidermis compared to periderm cells in WT epidermis. Dashed-line outlines the basement membrane. (D) Whole mount immunofluorescence staining of periderm cells (Keratin-17-green) in WT and Grhl3^{-/-} at E15.5, showing highly disordered periderm cells in Grhl3^{-/-} mice. (E) Average periderm cell size in WT and Grhl3^{-/-} skin at E14.5. (E) Measurements of periderm cell size in WT and Grhl3^{-/-} epidermis. (F) Immunofluorescence staining of Desmoglein-1 (green) and E-cadherin (red) in E14.5 forelimb cross-sections in WT and Grhl3^{-/-}. Arrows indicate the expression of Dsg1 (green) and E-cad (red) on periderm cells surface in Grhl3^{-/-} mice, Purple/Blue indicate nuclear staining. (G) Whole-mount staining of E14.5 limbs showing the expression of the tight junction protein, Zonula occludens-1 ZO-1 (magenta) in WT and Grhl3^{-/-} surface epidermis.

Supplement Figure 1

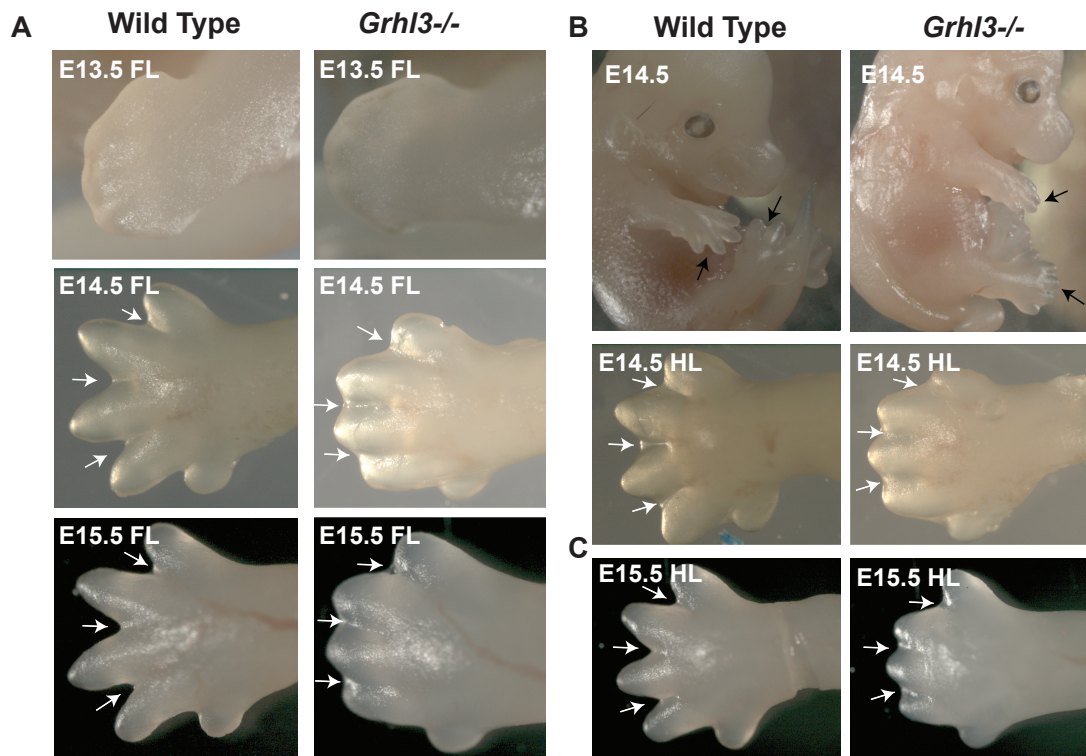


Figure S1, Related to Figure 1- *Grhl3* is required for normal digit separation

(A) Macroscopic images collected via dissecting scope at several developmental stages. Arrows indicate the interdigital zone. (B) *Grhl3*^{-/-} and littermate WT embryos at E14.5. Arrows point to the forelimbs and hindlimbs. (C) Macroscopic images of WT and *Grhl3*^{-/-} hindlimbs collected via dissecting scope at several E14.5 and E15.5. Arrows indicate the interdigital zone.

Supplement figure 2

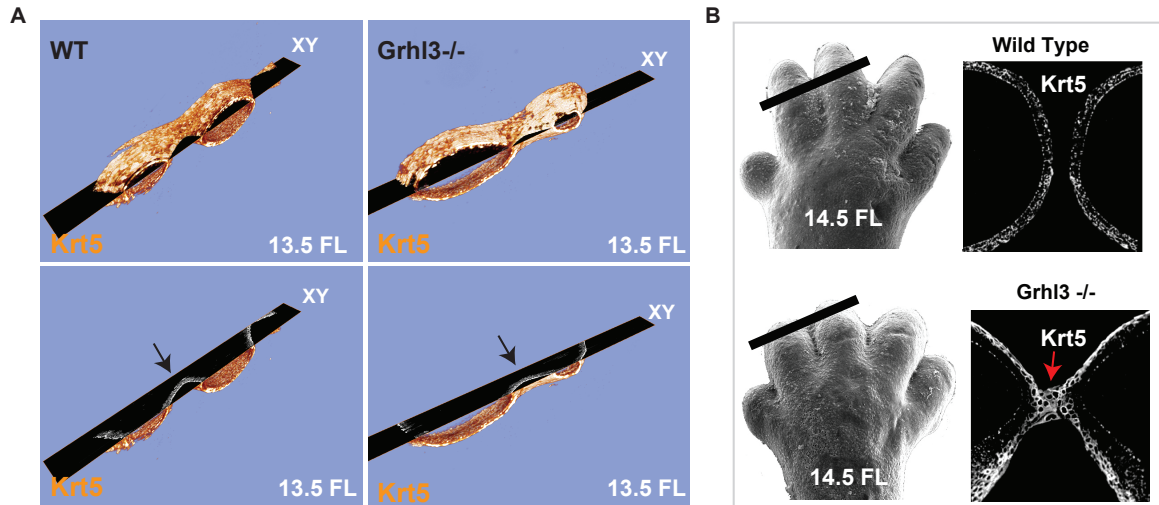


Figure S2, Related to Figure 3- Interdigital fusion of the epithelial results in unseparated digits in Grhl3^{-/-}

(A) Snapshots of 3D reconstructs stained with Keratin-5 (orange) of WT and Grhl3^{-/-} forelimbs at E13.5. Bottom images showing a single plane of the XY axis. Arrows point to the interdigital epithelia, indicated by Keratin-5 staining (gray), in WT and Grhl3^{-/-} mice. (B) Top left: SEM image of WT E14.5 forelimb. The black line indicates the location of the slice. Top right: the indicated slice showing Keratin-5 staining (gray). Bottom left: SEM image of Grhl3^{-/-} E14.5 forelimb. The black line indicates the location of the slice. Bottom right: the indicated slice showing Keratin-5 staining (gray). The red arrow indicates the interdigital epithelial fusion.

Supplement figure 3

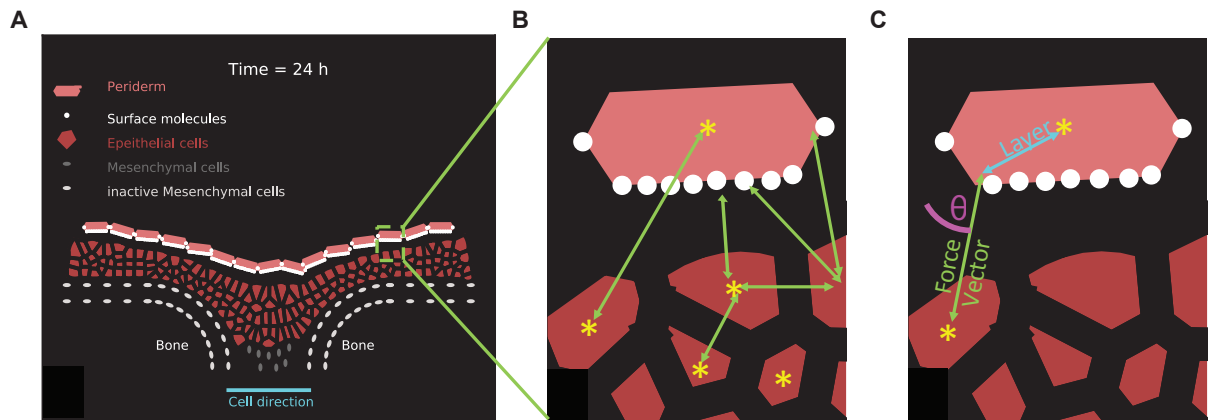


Figure S3, Related to Figure 5- Modeling suggests that directed cell migration plays a role in the formation of the IET

(A) Model of digit separation. (B) The bio-mechanical forces are modeled as generalized Morse potentials between the nodes representing cells. (C) The periderm cells are modeled as rigid elongated hexagons and the sum the forces acting on all nodes lead to a translation and rotation of the cell.

Supplement Figure 4

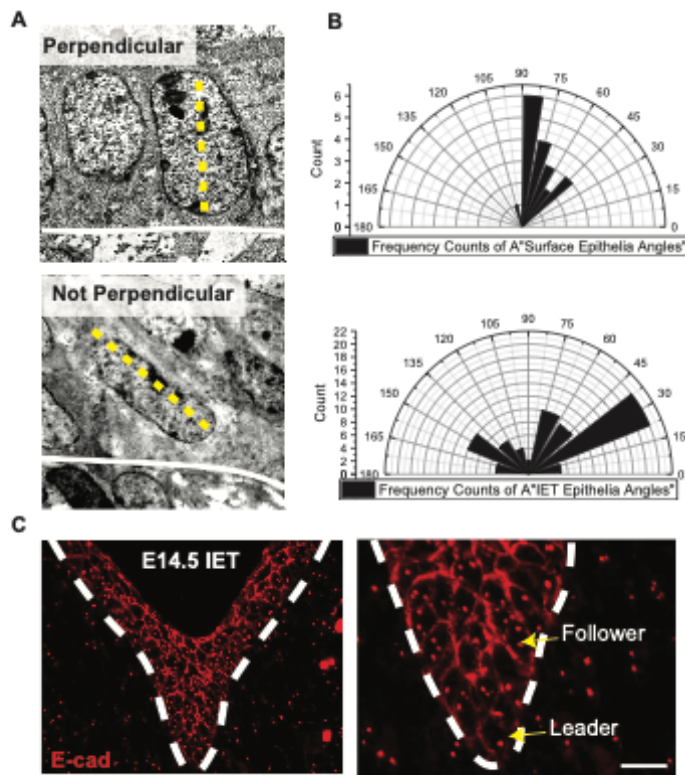


Figure S4, related to Figure 6- Collective cell migration of the IET during digit separation

(A) EM images of a basal keratinocytes in the surface epidermis (top) and IET (bottom). The yellow-dashed lines indicate the orientation of the nucleus. The white solid line indicates the basement membrane. (B) Measurements of the orientation of the nucleus in basal keratinocytes located at the surface epidermis and IET relative to the basement membrane. (C) Left: immunofluorescence staining of E-cadherin (red) at the IET leading edge in WT mice at E14.5. Right: High-magnification of cells at the IET leading edge. White-dashed lines indicate the basement membrane. Yellow Arrows point to follower and leader cells, respectively.

Supplement figure 5

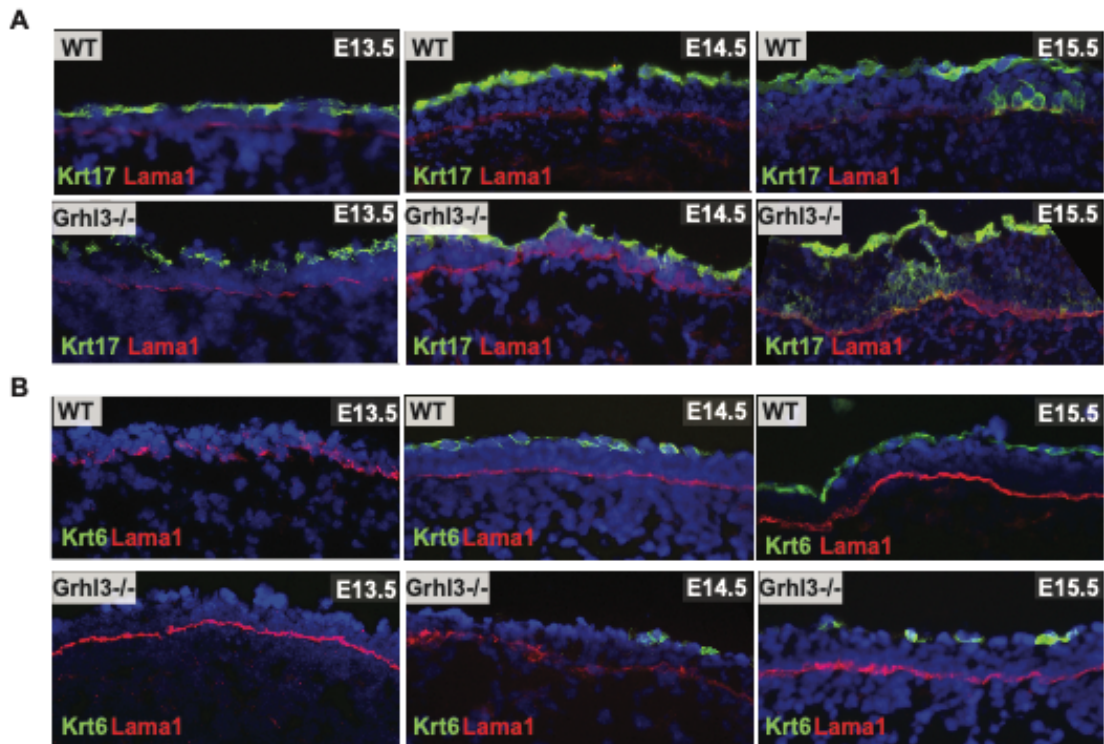


Figure S5, related to Figure 7- Grhl3 is required for normal periderm formation

(A) Immunofluorescence staining of the early periderm marker Keratin-17 (green) and basement membrane marker Laminin-1 (red) in embryonic skin sections collected from WT and Grhl3^{-/-} mice at E13.5, E14.5 and E15.5, respectively. (B) Immunofluorescence staining of the late periderm marker Keratin-6 (green) and basement membrane marker Laminin-1 (red) in embryonic skin sections collected from WT and Grhl3^{-/-} mice at E13.5, E14.5 and E15.5, respectively.

Supplement figure 6

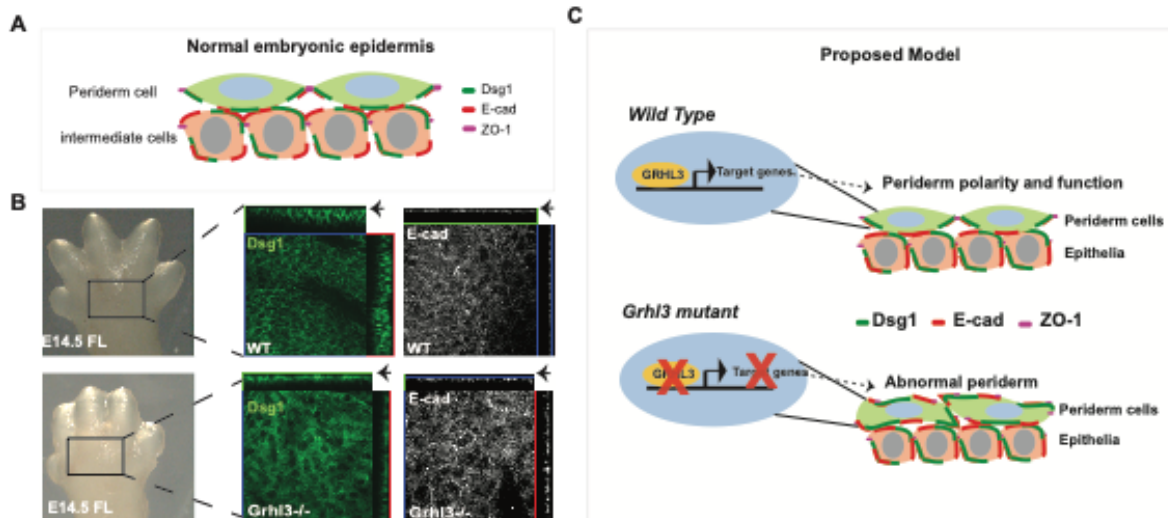


Figure S6, related to Figure 7- Grhl3 is required for normal periderm formation

(A) Schematic representation of adhesion complex proteins expression in intermediate keratinocytes and surface periderm cells in normal embryonic epidermis. (B) Whole-mount staining of adhesion complex proteins Desmoglein-1 (green) and E-cadherin (gray) in E14.5 WT and Grhl3^{-/-} forelimb. Arrows point to the surface cells in the Ortho-slice. (C) Schematic representation of the proposed model of the role of Grhl3 in periderm cells development and function.

CHAPTER 3: TRANSCRIPTIONAL REGULATION OF EPITHELIAL CELL ADHESION REQUIRED FOR COLLECTIVE CELL MIGRATION DURING CUTANEOUS WOUND HEALING

ABSTRACT

In the United States, chronic wounds affect around 6 million patients with a treatment cost reaching 20 billion dollars annually. Despite significant advances, much remains to be understood about the molecular mechanisms that lead to non-healing wounds. Acute wounds heal by three overlapping phases: inflammation, re-epithelization and tissue remodeling. During re-epithelialization, wound-margin keratinocytes migrate via collective cell migration. Changes in the actin-cytoskeleton leads to active migration of leader cells. These cellular changes are distinct from the trailing follower cells, which require a loosening of cell-cell adhesion for effective migration. Yet, the transcriptional regulation of follower cells during collective cell migration is poorly characterized. Grainyhead Like-3 (GRHL3) is an evolutionary conserved transcription factor essential for epidermal development. Grhl3 is upregulated in keratinocytes at the wound front. Mice lacking epidermal Grhl3 exhibit impaired wound healing caused by delayed keratinocyte migration. Microscopic analysis indicated a remarkable decrease of intercellular spaces between follower cells at the wound front coincides with high expression of the adherens junction protein, E-Cadherin. RNA-seq analysis of wounded keratinocytes showed significant downregulation of f-actin-bundling protein-1 (FSCN1), a protein known to bind to the catenin-cadherin complex at the cell membrane. Fscn1 is highly upregulated in migrating follower cells concurrent with high Grhl3 expression and low E-cadherin expression. Motif analysis showed enrichment of Grhl3

motifs in the *Fscn1* gene, suggesting direct binding of Grhl3 to *Fscn1* in follower cells. In addition, ATAC-seq analysis showed a significant decrease of wound-specific peaks near the *Fscn1* gene in the absence of Grhl3. All together, these data elucidate a novel wound-specific mechanism mediated by Grhl3 that is required for cell-cell loosening between follower cells during collective cell migration.

INTRODUCTION

Chronic wounds are a current burden in healthcare that affect millions of patients every year. Chronic wounds are found in the aging population as pressure ulcers and are associated with diabetes and vascular disease (Han & Ceilley, 2017) . Over the past decade, a great amount of research has been conducted identifying several molecules that can improve wound healing, yet the molecular mechanisms required for optimal healing requires further investigations.

In healthy individuals, acute wounds heal by three orchestrated overlapping phases: inflammation, re-epithelization, and tissue remodeling (Mayet et al., 2014). The initiation and regulation of the repair process is mediated by cellular and molecular interactions between the different cell types in the wound environment. Although wounds can heal partially by dermal contraction, re-epithelization of epidermal keratinocytes is a key step for optimal wound healing. During wound re-epithelialization, wound-margin keratinocytes migrate on top of the underlying granulation tissue, ultimately meeting migrating keratinocytes from the opposing margin to close the defect (Bellavia, Fasanaro, Melchionna, Capogrossi, & Napolitano, 2014). The epithelial wound front is an example of collective cell

migration during which a group of cells migrate as a cohesive unit. Several epidermal factors were identified as key players triggering migration of leader cells at the wound edge. Changes in traction forces, the actin-cytoskeleton, and the formation of cytoplasmic projections results in active migration of leader cells at the wound edge (Ilina & Friedl, 2009)(Raja, Sivamani, Garcia, & Isseroff, 2007). These cellular changes are distinct from the trailing follower cells which require a loosening of cell-cell adhesion for effective migration. Such coordination between cells in collective cell migration depends on active cell-cell signaling, however the nature of these signals is poorly understood.

Grainyhead-like 3 (GRHL3) is an evolutionary conserved transcription factor that is required for normal epidermal development (Klein et al., 2017, p. 3; Yu et al., 2006). Mice lacking *Grhl3* exhibit several defects including spina bifida, epidermal barrier defects, and limb malformation. These observations have led to the discovery of the role of *Grhl3* in embryonic development of the epidermis: regulation of the expression of genes essential for barrier formation. In addition to its role in epidermal differentiation, *Grhl3* is also required to promote keratinocyte migration in vitro (Klein et al., 2017). Although dispensable for adult skin homeostasis, *Grhl3* is necessary for barrier recovery during injury suggesting *Grhl3* plays a crucial role in adult skin repair (Gordon et al., 2014, p. 3).

Adult mice lacking epidermal *Grhl3* (*Krt14-Cre-Grhl3*^{-/-}) exhibit a delay in wound closure caused by impaired re-epithelization and defective migration. We found that in response to full thickness wounding, *Grhl3* expression is upregulated at the wound front, specifically in the migrating follower cells at the leading edge. In this study we investigate the role of *Grhl3* in full-thickness wound healing of adult skin and elucidate the *Grhl3*-mediated mechanisms regulating cell-adhesion in follower cells during collective migration.

MATERIALS AND METHOD

Generation of transgenic mice

Transgenic mouse strains used in these studies are Grhl3 floxed mice, K14-Cre/Grhl3^{-/-} mice, and Grhl3-Cre/LacZ reporter mice. C57BL/6J/Grhl3 floxed mice were previously generated and used by the Andersen lab (). Skin-specific deletion of Grhl3 in C57BL/6J/ mice was generated by crossing Grhl3 floxed mice with *Krt14-Cre* mice (purchased from Jackson laboratory). Offspring were bred to produce Wild type, heterozygous and homozygous-Grhl3-flox Cre-positive mice (*Krt14-Cre Grhl3^{-/-}*, *Krt14-Cre Grhl3^{f/f}* and *Krt14-CreGrhl3^{f/f}*, respectively). *Grhl3-Cre/LacZ* reporter mice were purchased from MMRRC (). All mice were housed and maintained in accordance with protocols approved by the University Laboratory Animal Resources (ULAR).

Mouse excisional-wound experiment

Aged matched (8-weeks) *Krt14-Cre Grhl3^{-/-}* and *Krt14-CreGrhl3^{f/f}* littermate mice both males and females were used for wounding. Prior surgery, mice were anesthetized with Ketamine/Xyline according to ULAR approved guidelines. Dorsal back skin was shaved, and hair was removed using Nair cream. Small full-thickness wounds were created using 4 mm biopsy punch on the shaved dorsal back skin. Wounded mice were placed on heating pad and monitored periodically until full recovery. Total of 2-4 wounds per mouse was created in each experiment. For wound closure rate, mice were anesthetized at each indicated time point and pictures of the wounds were collected. For BrdU, mice were injected with 0.5

mg/ml of BrdU (injection volume- 10% of body-weight) and sacrificed after 3 hours post injection for wound tissue collection.

Wound collection, Histology and Immunohistochemistry

Wounded mice were euthanized, and wounds tissues were collected after 1, 3, 5, 7- and 10- days post wounding. For histology, wound tissues were fixed with 10% formalin for 48 hours at 4C, followed by ethanol dehydration. Paraffin-embedded wounds were sectioned (8um thick) using microtome. Hematoxylin and eosin staining were performed as previously described. For Lacz and BrdU staining, wound sections, antigen-retrieval staining method was performed. Primary antibodies used were anti-beta galactosidase (1:100 company) and anti-BrdU (1:100 abcam), respectively overnight at 4C. (cell counting)

For immunofluorescence, fresh-frozen wound tissues were embedded in O.C.T compound and sectioned (8um thick) using Cryostat. Slides were fixed in cold acetone for 10-13 mins at RT. After three washes with 1X PBS slides were fixed with 4% PFA for 10 mins. Slides were then permeabilized with permeabilization buffer (triton-X in PBS) for 10-15 mins and blocked with blocking buffer (1XPBS+ 2%BSA) for 1 hour. For primary antibody, slides were incubated with anti-E-cadherin (1:200 cell signaling), anti-CD45 (1:500 bioscie), anti-cldn1 (abcam), anti-dsg1(cell signaling) and anti-CD31 (Bioscience) overnight at 4C. After several washes with 1XPBS, slides were incubated with secondary antibody (Alexaflora-488/ Alexafloura-594) for 1 hour at RT in dark. Stained slides were mounted with mounting DAPI solution for nuclear staining and imaging. slides were imaged using Keyence BZ-X710 All-in-one fluorescence microscope

Human skin xenograft wound model

A 1 mm of human forehead skin was surgically grafted on the dorsal back skin of immunodeficient mice. The skin was allowed to heal for several days until scab is detached. The wound was created in the middle using 2 mm biopsy punch on the human skin. Wound tissue was collected for analysis after 3 days and embedded in OCT and paraffin for histological analysis.

Transmission electron microscopy

Wound tissues were fixed in 0.25% Gluteraldehyde for 1-2 days. Samples were washed with cacodylate buffer, post-fixed with 1% osmium tetroxide, dehydrated through several ethanol series, and embedded in resin. Sections (1 nm) were contrasted with uranyl acetate and lead citrate and examined on FEI TECNAI SPIRIT transmission electron microscope.

Protein extraction and western-blot

One mm of wound margins was collected and snap-frozen in liquid nitrogen followed by grinding. Grinded tissues were then lysed in RIPA lysis buffer (biorad..) and spun for 15 mins at 4C. Supernatant was collected and purified using Millipore purifying column. Protein concentration was determined using Bradford assay. Equal amount of protein samples (50 ug/ml) from both K14-cre-Grhl3^{+/+} and K14-cre-Grhl3^{-/-} wounds were separated by SDS-page and transferred on nitrocellulose membrane. Blots were blocked with 5% non-fat milk in 1x TBST for 1 hour at RT. Following blocking, blots were incubated with anti-E-cadherin (cell signaling) and anti-GAPDH (cell signaling) antibodies at 4C overnight. after 3 washes

with 1X TBST, blots were incubated with secondary antibody (HRP- 1:1000) for 1 hour at RT. Bands were developed by adding 1ml of westfemto illuminata () and imaged using Genesys.. Band intensities were measured using imageJ. E-cadherin bands measurements were normalized to GAPDH.

Flow cytometry and FAC's sorting

One mm of wound margins (four wounds were pooled per mouse per genotype) and distal unwounded skin were collected, and subcutaneous fat was removed with a scalpel and tissues were placed epidermis facing up on trypsin (GIBCO) at 37 °C for 2 hours on a shaker. Peeled epidermis was diced in 2 ml media (epilife) and the cell suspension was filtered through 70um followed by 40um cell strainers. single-cells were washed with 1X Red-cell lysis buffer followed by 1X PBS then blocked with FACS buffer () for 5 mins on ice. Fluorophore-conjugated antibody staining was performed in dark for 30 mins, on ice. Stained cells were suspended in 400 ul of DAPI/FACS buffer and filtered through 40um strainer before flow cytometry analysis. For wound inflammation analysis, 1 mm of whole-wounds and unwounded skin were collected, diced into small pieces and incubated with 2 ml of collagenase buffer for 2 hours on a rotator at 37C.

Antibodies used are: CD49F-PE (bioscience), CD45-APC (bioscience), CD31-APC (bioscience), TER119-APC (bioscience). Isotype controls of the indicative fluorophore were used as staining controls. Samples were processed using BD LSR II flow cytometer. For FACS sorting, cells were sorted (sorting machine) into 350 ul RLT-BME lysis buffer () followed by RNA extraction using Microelute RNA kit (zymogen). RNA quality was assessed using Agilent

Bioanalyzer and concentration was measured by pico-Chip. Samples with high RIN score <8 were used for sequencing.

RNA-sequencing and analysis

Sequencing library (Single-Read-100) were prepared at the GHIF UCI genomic facility using Illumina ClonTech mRNA sample preparation kit. Libraries were sequenced on Illumina HiSeq 4000 (50 Million reads per sample). Sequencing quality of sequencing data (FastQ files) was determined using FASTQC. Reads were aligned to the mouse genome (mm10 build) using Tophat and Bowtie scripts. Transcript assembly was processed using Klisto and list of differentially expressed genes was generated using DEseq in R. Gene Set Enrichment analysis (GSEA) was applied on differentially expressed genes to determine functional GO categories. HOMER AND meme software were used to identify de novo motifs and enriched Grhl3 motifs in candidate genes, respectively.

ATAC-seq

Wounded and unwounded keratinocytes (100K Cells/sample) were sorted into 300ul of FAC's buffer. Cells were spun at 500 xg for 5 minutes at 4C, then washed with cold 1X PBS. Fifty microliter of cold lysis buffer (10 mM Tris·Cl, 3 mM MgCl₂, 10 mM NaCl, 0.1% MgCl₂ and 10% NP-40) was added to pelleted cells and pipetted up and down to resuspend cells, followed by centrifugation at 500 xg for 10 mins at 4c. Supernatant was discarded and 50 ul of transposition mix (2X TD Buffer, Tn5 Transposase in nuclease-free H₂O) was added to the cell pellet and incubated for 30 mins at 37C. Following transposition, DNA was isolated using Qiagen MinElute Reaction Cleanup kit. DNA was eluted in 10ul of Elution Buffer. DNA quality

was determined using High-Sensitivity DNA assay and PCR amplification. Library generation (Paired-End-100) was performed using (KIT) and then sequenced on Illumina HiSeq 4000 (>70 Million reads per sample). Quality profiling was performed on sequencing files using FASTQC. Adaptors were removed and sequencing were trimmed before alignment with mouse mm10 genome using bowtie2. MACS2 was used for peaks calling. Data were visualized using IGV and R.

Statistical Analysis

One-way ANOVA and Unpaired Students'-T tests were performed in GraphPad Prism 6.0 software. Data were expressed as mean \pm SEM and p values were reported such that *p < 0.05, **p < 0.01, and ***p < 0.001.

RESULTS

Spatiotemporal expression of GRHL3 during stages of wound healing

To study the role of Grhl3 in acute wound healing, we used small wound mouse models on the dorsal back skin (Fig. 1a). In normal mice, re-epithelization of acute wounds starts around the third day post-wounding. Using this model, we were able to characterize epithelial cells located at different zones during re-epithelization, such as the migrating epithelia, proliferating epithelia, and unwounded epithelia (Fig. 1a). To detect the spatiotemporal expression of Grhl3 during all stages of wound healing in adult full-thickness wounds, we applied small wounds on the back skin of LacZ-Grhl3 mice, which were previously used by our lab to detect the expression of Grhl3 in mouse tissues. Wound tissues

were collected after 24 hours, 3, 5-, and 7-days post-wounding. In normal (unwounded) skin, Grhl3 expression was sparse and was detected in the superficial layer of the epidermis (Fig. 1b). Within 24 hours post-wounding, Grhl3 expression increased in keratinocytes at the wound edge (Fig. 1b). During the re-epithelialization phase, Grhl3 was highly upregulated in cells at the migrating leading edge (Fig. 1b). Increased Grhl3 expression in wounded keratinocytes was sustained even after migration was complete in the suprabasal layer (fig. 1b), supporting the role of Grhl3 in restoring the epidermal barrier post injury. The increase of Grhl3 expression at the wound margin suggests a key role of Grhl3 during the early stages of acute wound healing.

Delayed healing of full-thickness wounds in mice lacking epidermal Grhl3

To study the role of Grhl3 during the early stages of wound healing, dorsal skin of mice lacking epidermal Grhl3 (K14-Cre-Grhl3^{-/-}) was challenged to heal full-thickness wounds. Four mm full-thickness wounds were created on the back skin of K14Cre-WT and K14-Cre-Grhl3^{-/-} mice (Fig. 2a). The rate of wound closure was determined by measuring the wound size after 0, 3, 5- and 10-days post-wounding (Fig. 2b). A significant delay in K14-Cre-Grhl3^{-/-} wound closure was detected at both 3- and 5-days post-wounding when compared to control (fig. 2c), suggesting a deficit during the inflammatory and re-epithelialization phases. Although wounds fully closed in both groups and showed no signs of impaired collagen deposition after 10 days (data not shown), the wound scab remained attached to the wound in K14-Cre-Grhl3^{-/-} mice, a phenomenon associated with impaired re-epithelization suggesting impaired full re-epithelization in K14-Cre-Grhl3^{-/-} wounds (data not shown).

Histological analysis of the wound at day 3, a time-point during which K14-Cre-Grhl3^{-/-} mice exhibit a significant delay in wound closure, showed a decrease in the length of the epithelia at the wound edge in K14-Cre-Grhl3^{-/-} mice compared to control mice (Fig. 2e). In addition, the wound edge epithelia in K14-Cre-Grhl3^{-/-} mice is thicker in size than in control mice (fig. 2f). These data clearly indicate a defect in the wound edge epithelia during re-epithelization. Wound re-epithelialization involves two independent processes: proliferation of keratinocytes located distally from the wound edge, and migration of keratinocytes located at the leading edge. Thus, we wanted to determine whether the decrease in the length of the wound edge is a result of altered cell proliferation of keratinocytes. Interestingly, EdU staining of 3- and 5-day wounds indicate no significant differences in the number of proliferative cells at the wound edge in K14Cre-Grhl3^{-/-} compared to control mice (fig. 2g, h). These data strongly suggest that impaired re-epithelization in K14Cre-Grhl3^{-/-} mice is due to altered migration.

Increased cellular-adhesion between follower cells in K14Cre-Grhl3^{-/-} collective cell migration

We then wanted to further characterize keratinocytes at the wound edge during re-epithelization in K14Cre-Grhl3^{-/-} mice. We conducted histological and electron microscopy analysis at day 3 post-wounding (Fig.3). Toluidine blue staining of thin wound sections (100 nm) at day 3 in WT mice show intercellular gaps/spaces between follower cells at the wound

front. These gaps were not found between follower cells in K14Cre-Grhl3^{-/-} wounds (Fig. 3a), but rather follower cells in K14Cre-Grhl3^{-/-} wounds were very close to one another and exhibited a different cell morphology than follower cells in the WT leading edge (Fig3.b). Higher-magnification analysis of follower cells using EM microscopy shows a significant decrease in intercellular spaces between keratinocytes of K14Cre-Grhl3^{-/-} wounds compared to WT mice (fig. 3c, d). These findings suggest that impaired migration in K14Cre-Grhl3^{-/-} mice is caused by increased cellular adhesion between follower cells.

During keratinocyte migration, molecular components of adherens and tight junctions, but not desmosomal junctions, are downregulated at the wound-edge, leading to loosening of adhesion between follower cells required for collective cell migration (Kuwahara, Hatoko, Tada, & Tanaka, 2001). In line with previous findings, no changes in desmosomal junctions were observed in K14Cre-Grhl3^{-/-} wounds compared to WT (Fig. 3e). Interestingly, immunofluorescence analysis of day 3 wound-edges indicates an increase in the cytoplasmic levels of the adherens junction protein E-cadherin in follower cells of K14Cre-Grhl3^{-/-} mice (Fig. 3F). These observations were further supported by western-blot analysis showing a significant increase of E-cadherin protein levels in K14Cre-Grhl3^{-/-} wounds compared to WT (fig. 3G). No significant differences were observed in the expression of tight-junctions at the wound-edge between K14Cre-Grhl3^{-/-} and WT mice (data not shown). These data indicate that the increase in follower cell-cell adhesion is mediated by altered expression of the adherens junction protein, E-cadherin. The phenotype observed in K14-Cre-Grhl3^{-/-} mice after wounding strongly suggest a crucial role of Grhl3 in cell-cell loosening between follower cells during collective cell migration.

Isolation of wound-edge keratinocytes during wound re-epithelization

To understand the Grhl3-mediated mechanism required for cell-cell loosening during collective cell migration, we performed transcriptomic and chromatin accessibility analysis on wound-edge keratinocytes using RNA-sequencing and ATAC-sequencing (Fig.4a). To isolate wound-edge keratinocytes, 1 mm of day 3 wound margin was collected, and the epidermal layer was separated using an enzyme digestion. Fluorescence-activated cell sorting was performed to isolate keratinocytes using the common keratinocytes surface marker alpha-6-integrin (CD49F). Non-keratinocytes such as immune cells, endothelial cells, and hematopoietic cells, were excluded using lineage surface markers (fig.4a). Keratinocytes from the unwounded region of the skin were also collected as a control for the experiment.

Normalized mRNA expression showed high mRNA levels of basal keratinocyte markers, such as Krt14 and Krt5, and superbasal keratinocyte markers, such as Krt1 and Krt10, in both wounded and unwounded samples (fig. 4b). The expression of non-keratinocyte markers was not detected, validating the isolation of epidermal keratinocytes (fig. 4b). In addition, we detected upregulation of wound-associated genes, such as Krt16, Krt17, and Krt6b, in keratinocytes isolated from 1 mm wound margins compared to keratinocytes isolated from unwounded regions (fig.4c). We also found high mRNA expression levels of genes that are known to be expressed exclusively at the wound leading edge such as Itg5a (Fig. 4c). These data validate the isolation of wounded keratinocytes at the leading-edge during re-epithelization.

Transcriptional and chromatin landscape in wound-front keratinocytes during re-epithelization

During acute wound re-epithelialization, 556 genes were differentially expressed (p value <0.05) in wounded keratinocytes at the leading edge compared to keratinocytes at unwounded area (Fig. 5a). Among these genes, 357 genes were upregulated, and 202 genes were downregulated (Fig. 5a) (Table 1, 2). Gene Ontology analysis of the differentially expressed genes showed enrichment of genes involved in several biological processes that have been previously linked to wound healing, including cell adhesion, inflammation, angiogenesis, and wounding (Fig. 5b). Several genes that were previously shown to be upregulated specifically in the wound-leading edge during re-epithelization (*Itg5a*, *Ephb1*, *Mmp13*, *Lama1*, and *Pdgn*) were detected in our analysis (Table 1). These genes are known to promote actin-cytoskeleton organization, cell adhesion, and cell migration. Genes required for wound inflammation angiogenesis (*Plau*, *Il24* and *Hif1a*) were also upregulated at the wound-edge compared to the unwounded region (Table 1). As predicted, genes associated with keratinization, chromatin silencing, and inhibitors of the matrix metalloproteinases, such as *krt1*, *hist1h2ap* and *Timp4*, were downregulated (Table 2).

Genome-wide chromatin accessibility analysis of sorted keratinocytes showed a significant gain of 35,174 ATAC-seq peaks after wounding (Fig. 5c). The majority of the peaks were found at the promoter region, with a slight increase of peaks in the intergenic region of wounded keratinocytes compared to unwounded (Fig. 5d). ATAC-seq signals in both wounded and unwounded keratinocytes showed enrichment of peaks in regions encoding

for basal and suprabasal keratinocyte markers such as Krt14 and Krt1, respectively (Fig. 5e). In wounded keratinocytes, the number of de novo peaks increased in regions encoding for wound specific genes such as Krt6 and leading-edge specific genes such as Itg5a (Fig. 5e).

Additionally, among the differentially expressed genes, 282 genes were enriched with ATAC-peaks at their regulatory region in response to wounding (Fig. 5f). Motif analysis showed significant enrichment of binding motifs for transcription factors associated with epidermal differentiation (Prdm1 and SP1), cell proliferation (Egr1), and cell migration (klf5), all of which are processes required for acute wound healing (Fig. 5f). These data indicate global changes in gene expression and chromatin accessibility in wound-edge keratinocytes during re-epithelization.

Grhl3 promotes collective cell migration via direct regulation of FSCN1 expression in follower cells

We then aimed to identify the Grhl3-mediated transcriptional mechanism required for cell-cell loosening between follower cells during collective cell migration. We performed RNA-seq and ATAC-seq analysis on isolated wounded and unwounded keratinocytes from K14Cre-Grhl3^{-/-} mice. The absence of Grhl3 during wounding negatively affected chromatin accessibility to wound-specific regulatory regions, indicated by the significant loss of peaks in K14Cre-Grhl3^{-/-} wounded keratinocytes compared to WT (Fig. 6a). In addition to changes in chromatin accessibility, 555 genes were differentially mis-regulated (p value >0.05) in

K14Cre-Grhl3^{-/-} wounded keratinocytes (Table 3, 4). Out of the 555 mis-regulated genes, 335 genes were downregulated in K14Cre-Grhl3^{-/-} wounds (Table 4). Gene Ontology analysis of the mis-regulated genes indicates enrichment of genes required for cell-cell adhesion, active migration, response to hypoxia, angiogenesis, and wound healing (fig. 6b) (Table 4).

The majority of genes involved in cell adhesion were downregulated in K14Cre-Grhl3^{-/-} mice opposed to the hyper-adhesion found in follower cells (Fig. 6b). Interestingly, mRNA expression levels of E-cadherin and a previously known downstream target of Grhl3, Arhgef19, were unchanged in K14Cre-Grhl3^{-/-} wounds (Fig. 6c). In contrast, genes that are known to negatively regulate E-cadherin expression, such as Srcin1, Fscn1, and Pdpn, were significantly downregulated in K14Cre-Grhl3^{-/-} wounds (Fig. 6b). These data strongly suggest that Grhl3 negatively regulates cell adhesion in follower cells, resulting in cell-cell loosening required for collective cell migration.

The F-actin bundling protein Fscin-1 (FSCN1) is a known driver of tumor invasiveness due to its ability to downregulate expression of E-cadherin in cancer cells (Hayashi, Osanai, & Lee, 2011; Li et al., 2018). Our previous CHIP-seq data and motif analysis suggest direct binding of Grhl3 to the Fscn1 gene. Although Fscn1 was recently shown to be one of the genes that was significantly upregulated in the wound leading edge, its role in wound healing has not been characterized. Immunofluorescence staining of Fscn1 in day 3 wound sections showed significant up-regulation of Fscn1 in follower cells at the leading edge, which coincides with high Grhl3 expression and low E-cadherin expression (Fig. 6c). In contrast,

Fscn1 was significantly downregulated, nearly absent, in K14Cre-Grhl3^{-/-} wounds (Fig. 6c). In addition, ATAC-seq analysis showed a significant gain of peaks in the Fscn1 regulatory region in WT wounded keratinocytes compared to unwounded (Fig. 6d). No ATAC-peaks in the Fscn1 gene were gained in K14Cre-Grhl3^{-/-} keratinocytes after wounding (Fig. 6d). Altogether, these data strongly suggest that Grhl3 in follower cells regulates the expression and chromatin accessibility of Fscn1 in response to wounding. The high levels of Fscn1 in follower cells negatively regulates E-cadherin expression, resulting in cell-cell loosening required for optimal collective cell migration.

Grhl3-Fscn1 mechanism in human acute wounds

Previous microarray analysis on human wounds indicated a significant increase in Grhl3 mRNA expression levels in skin cells isolated from the wound area during re-epithelization (Nuutila et al., 2012). Although lowly expressed in adult epithelia, Fscn1 is upregulated in human carcinomas (Chen et al., 2019). Therefore, we aimed to investigate the Grhl3-Fscn1 mediated mechanism in collective cell migration during wound healing in humans. Skin samples isolated from the forehead of healthy de-identified patients was xenografted onto the dorsal back of immunodeficient mice (Fig. 7a). Following the surgery, dorsal mouse skin containing human skin was allowed to recover before wounding. A small wound (2-4 mm) was created on the human skin, and wound tissue was collected after 3 days post-wounding, during the period of active re-epithelization.

Immunofluorescence staining showed an increase in Fscn1 expression in the wound leading edge, specifically in follower cells (Fig. 7b), resembling the Fscn1 expression in mouse wounds. Interestingly, E-cadherin expression was nearly absent in follower cells that showed high expression of Fscn1 in human wounds during re-epithelization. These data strongly suggest that Fscn1 negatively downregulates the expression of E-cadherin in follower cells during wound migration in humans, proposing a potential role of Grhl3 in human wound healing.

DISCUSSION

For decades, extensive amounts of research have been conducted to identify key signaling pathways required for normal wound healing. Using mouse wound models, remarkable advances in wound healing research has led to improvement in chronic wound healing, yet chronic non-healing wounds are still a current clinical burden. Despite current advances, a full understanding of the molecular mechanisms that govern specific biological processes, such as cell-migration, is still lacking. Here we identify a novel wound-specific mechanism by which the epidermal transcription factor GRHL3 regulates cell-cell adhesion in follower cells via its downstream target Fscn1 during collective cell migration in adult skin wound healing (Fig. 8).

During the phase of re-epithelization, growth factors such as TGF- β , TNF- α and EGF are produced by both keratinocytes and non-keratinocytes to promote two independent processes required for wound closure: keratinocyte proliferation and migration (Bellavia et al., 2014). Migrating keratinocytes are located in the leading edge of the wound and

physically migrate on top of the underlying wound bed via collective cell migration. During collective cell migration, leader cells at the tip undergo cellular and actin-cytoskeletal changes to facilitate their initial movement on the extracellular matrix. Cells from the migrating tip include follower cells that are linked to leader cells via cell-cell adhesion. The molecular mechanisms regulating leader cell migration have been widely investigated, however, less is known about the molecular mechanisms that regulate follower cells during migration.

Cell-cell adhesion between the trailing follower cells decreases during migration. Ephrin-B1 ligand and its receptor EphB2 are upregulated at the wound leading-edge during re-epithelization (Nunan et al., 2015). Activation of the Ephrin pathway leads to downregulation of the molecular components of adherens junctions leading to loosening between cells at the leading edge enabling collective cell migration. Interestingly, impaired migration of the leading edge in Keratinocyte-Specific KO Grhl3 mice resembles the phenotype found in Keratinocyte-Specific KO of Ephrin-B1/B2, and increases adherens junction molecule E-cadherin in follower cells at the leading edge. Ephrin activation occurs in basal keratinocytes, whereas Grhl3 is expressed in suprabasal keratinocytes, specifically in follower cells at the wound leading edge, suggesting a Grhl3-mediated independent mechanism in superbasal follower cells which regulates adherens junctions during migration.

In vitro, Grhl3 is known to promote migration by directly binding to its downstream targets and by binding to gene regulatory elements such as super-enhancers (). Our ATAC-seq analysis indicated that wound-specific peaks that were gained in control mice were significantly lost in the absence of Grhl3. Interestingly, peaks near genes regulating the

ephrin pathway were also decreased in K14Cre-Grhl3^{-/-} wounds. These data strongly suggest a cell-non autonomous effect of Grhl3 in wounded keratinocytes.

The actin bundling protein, Fscn1, was significantly downregulated in K14Cre-Grhl3^{-/-} wounded keratinocytes. Fscn1 is one of the highly upregulated genes in wound-front keratinocytes, and it physically interacts with β -catenin to modulate the catenin-cadherin adhesion complex on the cell membrane. In cancer metastasis, high Fscn1 expression correlates with low E-cadherin expression. Immunostaining of Fscn1 in mouse wound sections indicate specific upregulation of Fscn1 in follower cells at the leading edge and shows a co-localization with Grhl3 at the wound edge. Fscn1 expression at the wound front was also detected in wounds created on human xenografts. In addition, motif analysis showed enrichment of Grhl3 binding motifs in the Fscn1 gene. All together, these data strongly suggest that Grhl3 regulates the expression of Fscn1 in follower cells, resulting in decreased E-cadherin and cell-cell loosening required for collective cell migration (Fig. 7).

These findings identify a novel wound-specific mechanism that is crucial for acute wound healing in mice and humans. Several chronic wounds such as diabetic ulcers, venous ulcers, and pressure wounds, are associated with impaired wound re-epithelialization. In future studies, determining whether the Grhl3-Fscn1 signaling axis is perturbed in chronic wounds and, ultimately, whether components of this pathway acting downstream of GRHL3 could be a future drug target is worth investigating.

Figure 1

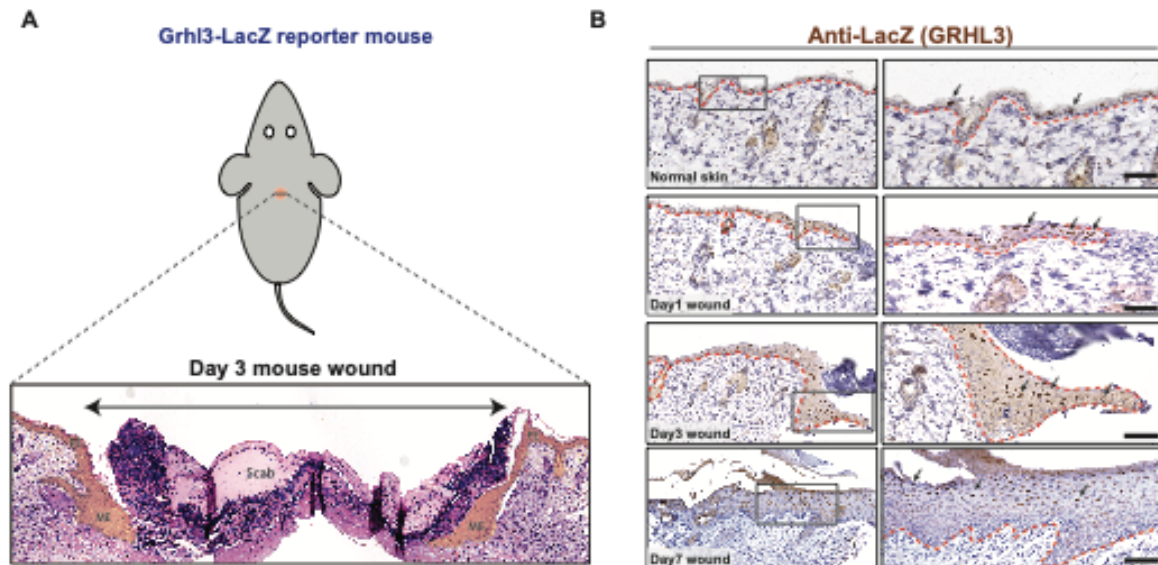


Figure 1. Spatiotemporal expression of GRHL3 during stages of wound healing

(A) Schematic representation of mouse wound model (top). Transverse section of the wound showing three different wound zones PE-proliferating epithelia, ME-migrating epithelia and wound Scab (bottom). (B) Immunohistochemistry analysis of Grhl3 expression in wounded skin sections at several time points post wounding. Sections were stained with Anti-lacZ (brown). The right panel indicates a higher-magnification of the boxed area. Arrows point to positive Grhl3 expression at the wound margin.

Figure 2

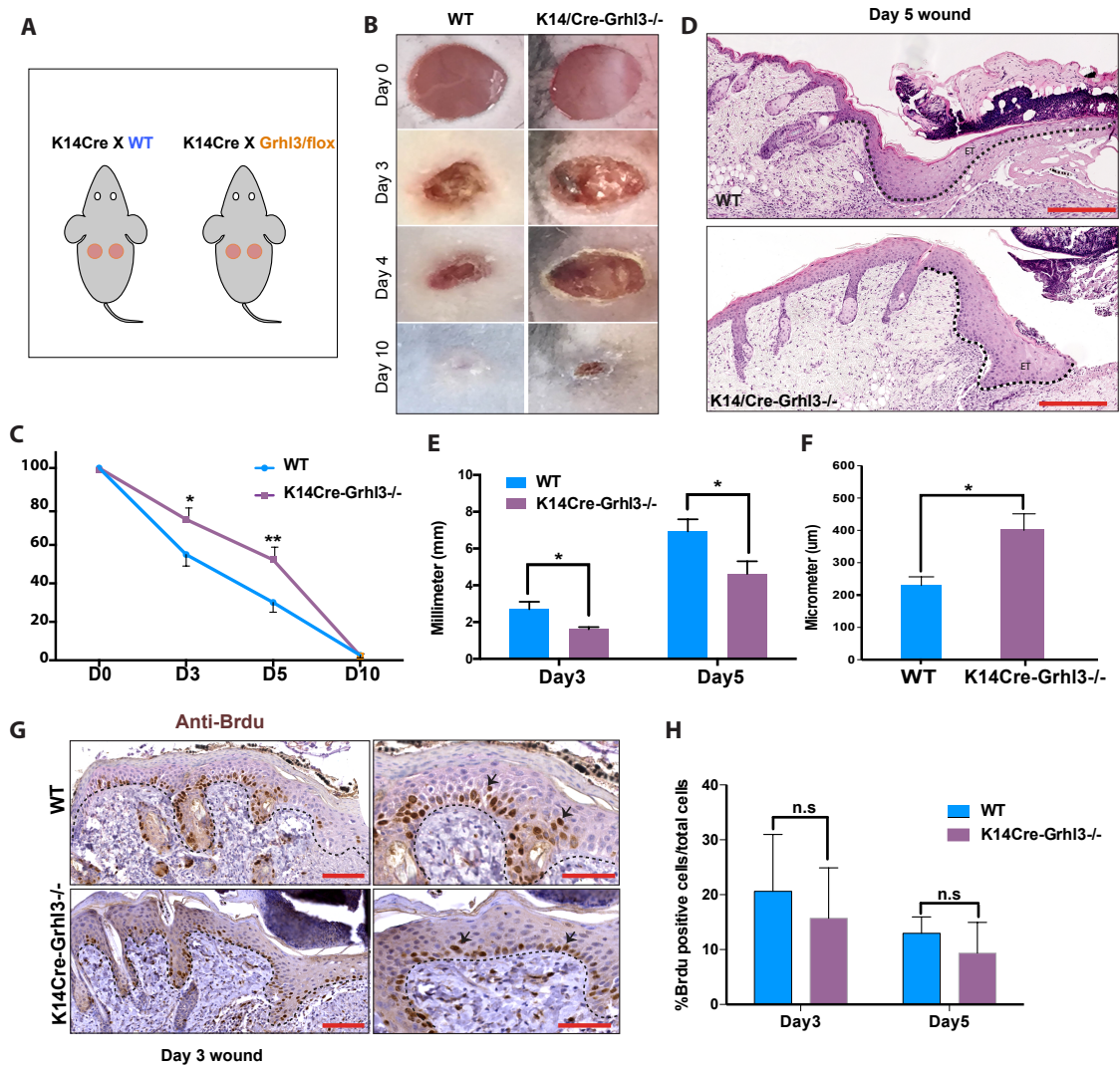


Figure 2. Delayed healing of full-thickness wounds in mice lacking epidermal Grhl3

(A) Schematic representation of mouse wound model (top). (B) Macroscopic images of full-thickness wound at 0, 3, 4 and 10 days in WT and K14Cre-Grhl3^{-/-} mice. (C) Measurements of the wound size over time from the collected macroscopic images in Both WT and K14Cre-

Grhl3^{-/-} mice, N=3-5/time point per genotype (* p value >0.05). (D) H&E staining of wound sections 5 days post wounding. Dotted lines indicate the wound migrating edge. (E) measurements of the wound edge length in WT and K14Cre-Grhl3^{-/-} wound sections 3- and 5-days post wounding, N=3-5/time point per genotype (* p value >0.05). (F) Measurements of the wound edge thickness in WT and K14Cre-Grhl3^{-/-} wound sections 5 days post wounding, N=3-5/time point per genotype (* p value >0.05). (G) EdU staining of WT and K14Cre-Grhl3^{-/-} wound sections 5 days post wounding, N=3-5/ genotype (* p value >0.05). Dotted lines indicate the epidermal layer. Right panel shows higher magnification. Arrows point to positive EdU cells. (H) quantification of the number of EdU positive cells in WT and K14Cre-Grhl3^{-/-} wound sections 5 days post wounding, N=3/ genotype.

Figure 3

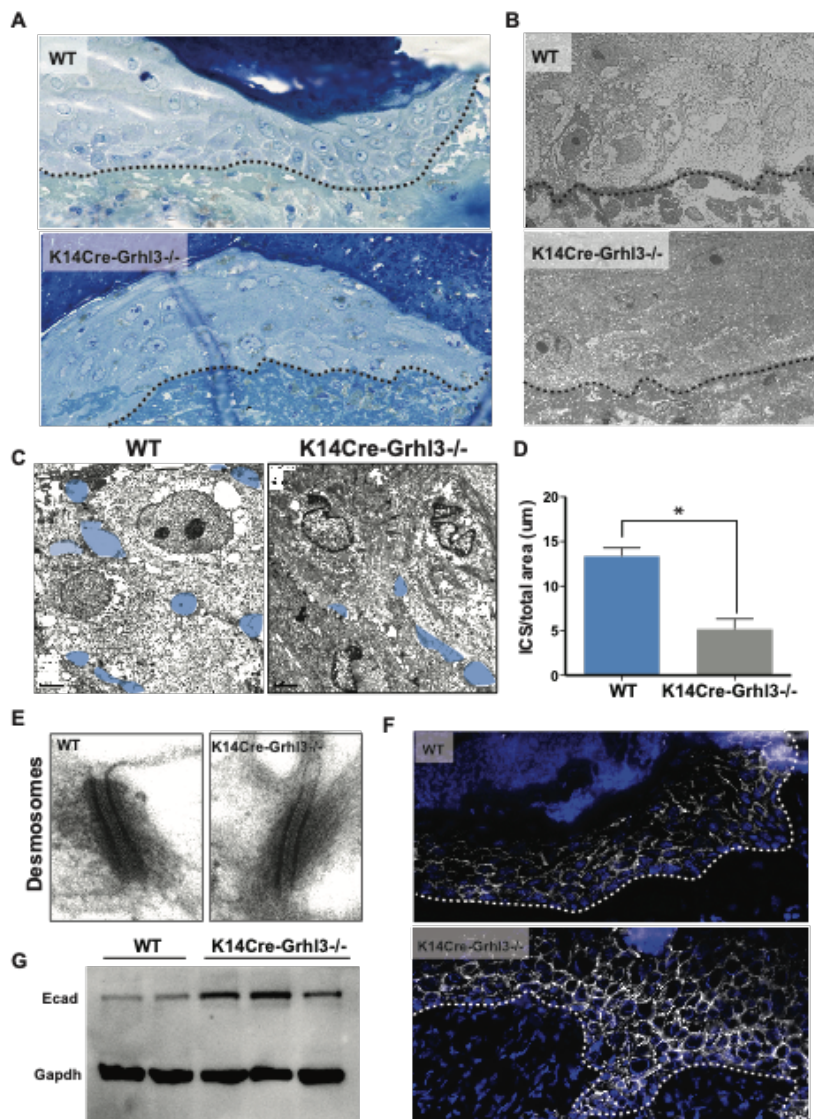


Figure 3. Increased cellular-adhesion between follower cells in K14Cre-Grhl3^{-/-} migrating wound tongue

(A) Bright-field images of the wound edge stained with Semi-resin blue staining at day 3. Dotted line indicates the basement membrane. (B) Transmission Electron Microscopy of the

wound- edge at Day 3 in WT and K14Cre-Grhl3^{-/-} mice. Dotted lines indicate the basement membrane. (C) Higher-magnification of Transmission Electron microscopy images showing two individual cells at the wound edge in WT and K14Cre-Grhl3^{-/-} wounds at Day 3. Light blue filling indicate the intercellular spaces between two epidermal cells. (D) measurements of the intercellular spaces between epidermal cells at the wound edge collected from TEM imaging analysis, N=2 /genotype (* p value >0.05). (D) High-magnification EM images showing desmosomal junctions between epidermal cells at the wound edge. (F) Immunofluorescence analysis of E-cadherin in wound sections collected from WT and K14Cre-Grhl3^{-/-} mice 3 days post wounding. Dotted line indicate the basement membrane. (G) Westren-blot analysis of protein lysate isolated from the wound margin 3 days post wounding. Bands indicate the expression of E-cadherin and the loading control (Gapdh) in 3 WT and 3 K14Cre-Grhl3^{-/-} mice.

Figure 4

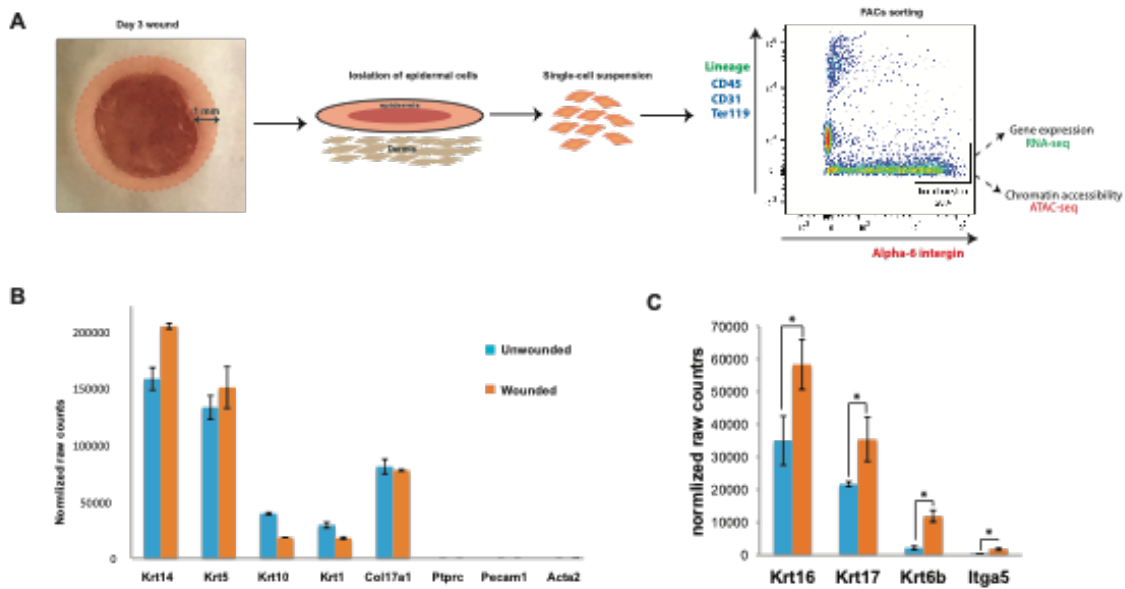


Figure 4. Isolation of wound-edge keratinocytes during wound re-epithelialization

(A) Schematic representation of isolation of wound-edge keratinocytes 3 days post wounding. (B) Normalized raw transcript counts of keratinocytes and non-keratinocytes markers in unwounded and wounded WT samples. (C) Normalized raw transcript counts of wound-specific markers in unwounded and wounded WT samples.

Figure 5

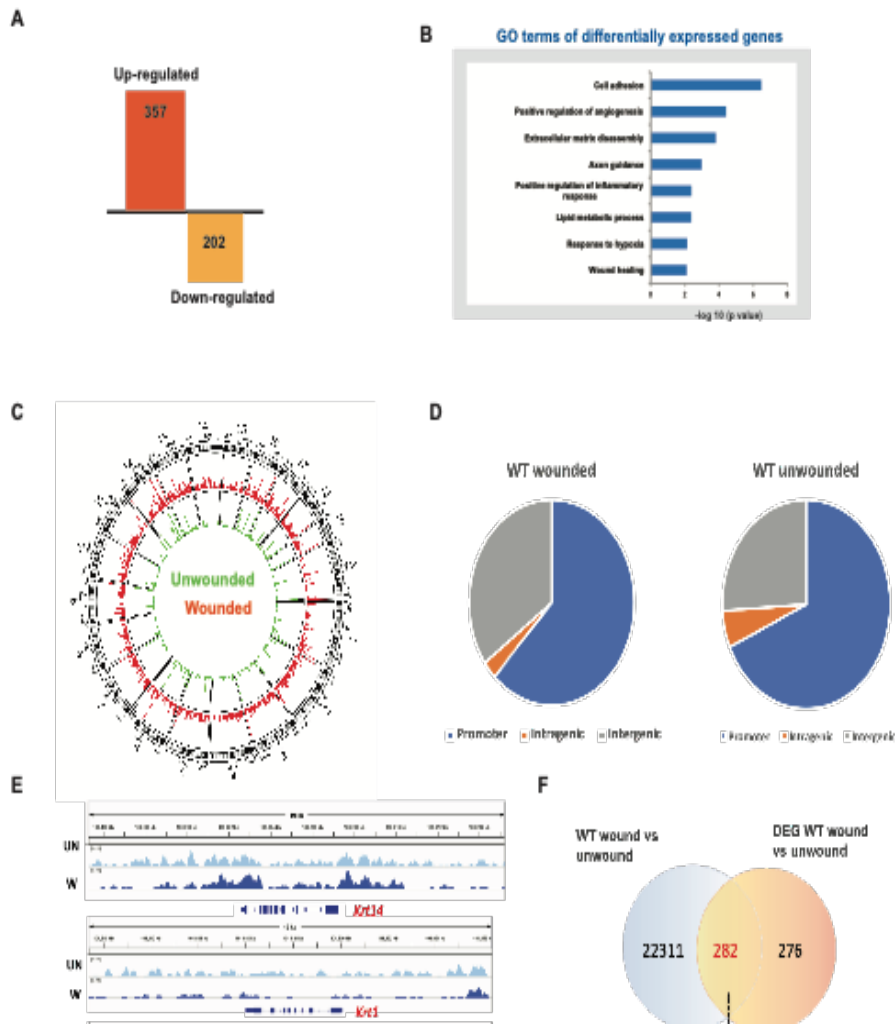


Figure 5. Transcriptional and chromatin landscape in wound-front keratinocytes during re-epithelization

(A) Heat-maps showing the differentially expressed genes in unwounded and wounded sorted keratinocytes in WT mice 3 days post wounding. (B) a graph showing number of up-regulated and down-regulated genes in wounded-keratinocytes. (C) GO functional category

of differentially expressed in wounded-keratinocytes 3 days post wounding. (D) Global ATAC-seq peaks in sorted unwounded and day 3 wounded keratinocytes in WT mice. (E) Pie chart showing the genomic distribution of ATAC-peaks in unwounded and wounded keratinocytes. (F) IGV analysis showing ATAC-peaks found in the regulatory region of Krt14, Krt1, Krt6 and Itg5a genes, respectively. (G) Pie chart showing genes that are differentially regulated in wounded keratinocytes and gained wounded-ATAC peaks. Motif analysis on overlap genes indicate enrichment of binding motifs of the indicated transcription factors.

Figure 6

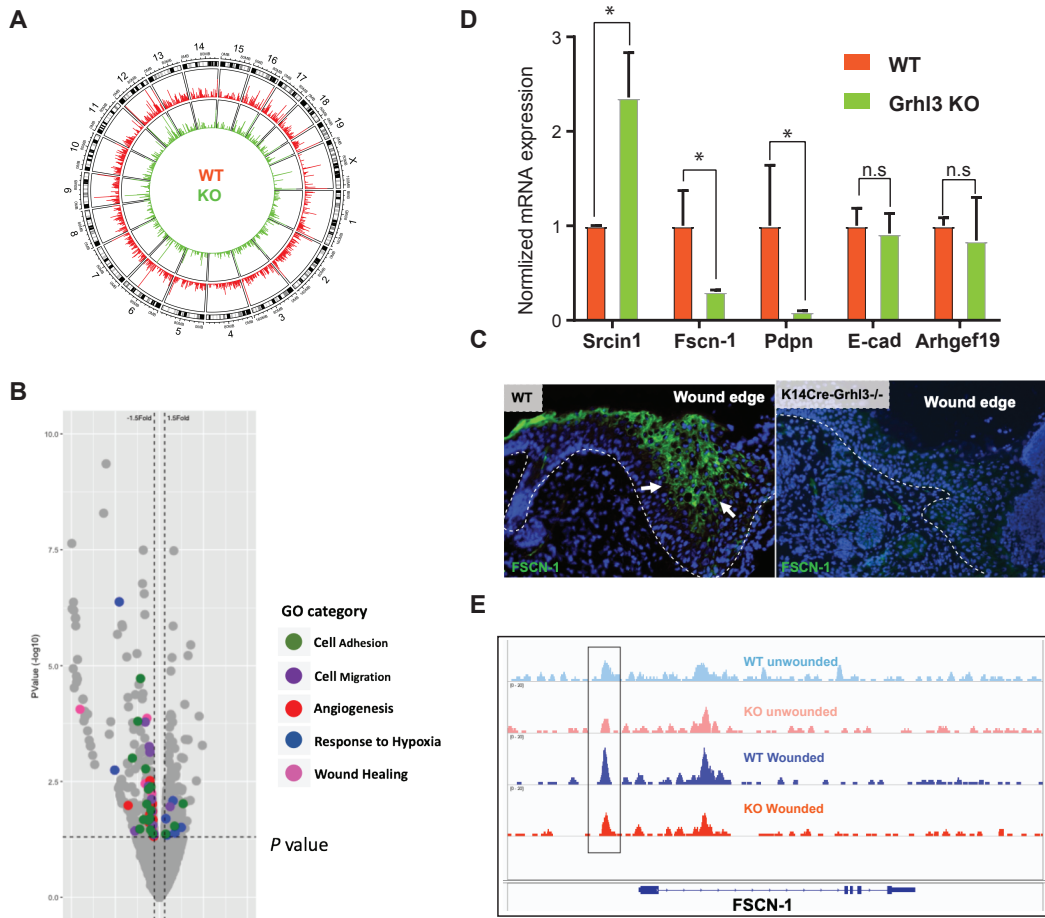


Figure 6. Grhl3 promote collective cell migration via direct regulation of FSCN1 expression in follower cells

(A) Global ATAC-seq peaks in sorted wounded keratinocytes in WT and K14Cre-Grhl3^{-/-} mice 3 days post wounding. (B) Volcano plot showing GO functional category of mis-regulated genes in wounded-keratinocytes isolated from K14Cre-Grhl3^{-/-} 3 days post wounding. (C) Normalized transcript expression levels of mis-regulated genes in WT and K14Cre-Grhl3^{-/-} mice 3 days post wounding, N=2/genotype (* p value >0.05). (D)

Immunofluorescence staining of FSCN1 in WT and K14Cre-Grhl3^{-/-} wound sections at Day 3. Dotted line indicates the basement membrane. (E) IGV analysis showing ATAC-peaks found in the regulatory region of Fscn1 gene in WT and K14Cre-Grhl3^{-/-} unwounded and wounded keratinocytes.

Figure 7

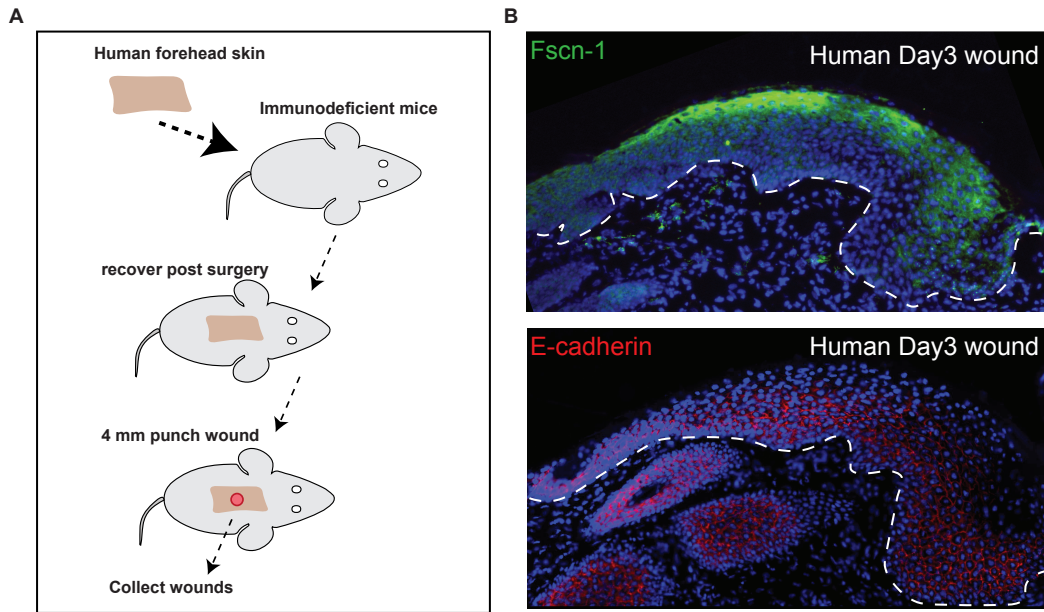


Figure 7. Grhl3-Fscn1 mechanism in human acute wounds

(A) Schematic representation of human skin xenograft and wound model. (B) Immunofluorescence staining with Fscn1 (green) and E-cadherin (red) in human day 3 wound sections. Dotted lines indicate the basement membrane.

Figure 8

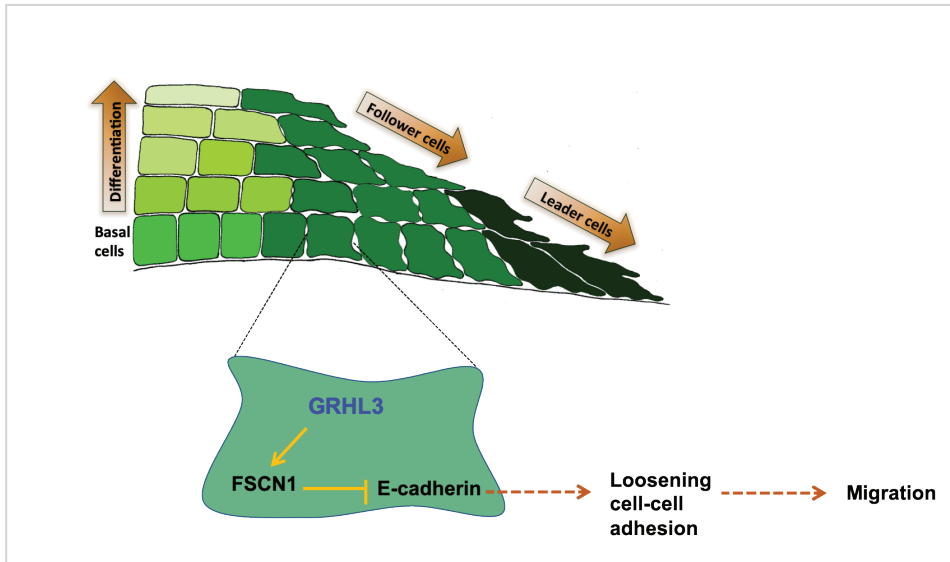


Figure 8. Proposed model of Grhl3-Fscn1 signaling pathway during collective cell migration in wounding

Schematic representation of wound-edge keratinocytes. GRHL3 in follower cells directly bind and increase the expression of Fscn1. Fscn1 in follower cells negatively regulate E-cadherin expression, resulting in cell-cell loosening, promoting for collective cell migration.

Table 2.1 Up-regulated genes in WT wounded-keratinocytes 3 days post wounding

genes	logFC	logCPM	LR	PValue	FDR
Mmp9	11.7431165	3.4878557	74.5711953	5.85E-18	6.74E-14
Col5a3	10.0049519	1.77924769	52.9115046	3.49E-13	1.57E-09
Gm20683	9.20479806	1.00672705	33.1956749	8.33E-09	2.81E-05
Sparcl1	9.04266213	0.85894624	31.0868179	2.47E-08	4.16E-05
Xlr	8.25732974	0.11961799	22.5338737	2.06E-06	0.00163938
Rtp4	5.79861697	0.02284101	18.0944317	2.10E-05	0.01289766
Notch4	5.7308183	-0.0415625	17.6498916	2.66E-05	0.01493387
Pglyrp2	5.3126704	-0.4015895	14.9790466	0.00010871	0.03762537
Acmsd	5.2176133	0.32223434	16.9728285	3.79E-05	0.01827948
Arg1	4.65494879	1.13317661	16.9837598	3.77E-05	0.01827948
Oas1a	4.5176158	0.37643601	12.0815713	0.00050923	0.12576256
Gm6733	4.44992773	0.47923357	16.0297448	6.24E-05	0.02550513
Sema6d	4.3721002	1.70955833	23.0412247	1.59E-06	0.00133769
Cmpk2	4.3461595	-0.5054111	11.3986079	0.00073499	0.15031693
Rusc2	4.31192883	2.91915897	15.463405	8.41E-05	0.03070569
Gm10719	4.1287892	0.53519984	9.71900489	0.00182372	0.25377942
Gm21833	4.10716735	0.78558525	9.60295314	0.00194265	0.25707695
Fndc1	4.00129706	2.32011431	14.8768134	0.00011476	0.03778287
Rps6-ps4	3.85872727	5.09985671	73.5139033	9.99E-18	6.74E-14
Bmpr1b	3.81493769	1.42250612	18.1206051	2.07E-05	0.01289766

Entpd1	3.77895345	-0.1851208	8.97010198	0.00274433	0.33372076
Uncx	3.76033319	0.36348696	11.2172725	0.0008104	0.15626733
Pde2a	3.68389008	-0.239386	10.0438586	0.00152857	0.23226862
Oasl2	3.62637629	1.68524561	18.427803	1.76E-05	0.01190958
Nxpe5	3.59955808	0.62739192	10.1464997	0.00144575	0.23226862
Ptprb	3.58906503	1.72311314	17.4047997	3.02E-05	0.01630894
Acta2	3.58563327	2.5200026	27.1088964	1.92E-07	0.00021632
Aph1c	3.55040688	0.58743063	9.6063627	0.00193904	0.25707695
Ifit1bl2	3.48821039	-0.4207279	7.75033038	0.00537027	0.48005249
Dchs2	3.47933128	0.6401799	11.5920776	0.00066233	0.13754125
Cdh5	3.44244477	1.5550702	9.7389489	0.00180404	0.25365558
Morn2	3.42393117	0.01920547	7.49731537	0.0061791	0.52866059
Olfra459	3.38120639	-0.4961385	7.36623521	0.00664599	0.54368251
Cd14	3.37916685	0.74598612	5.71245246	0.01684499	0.90227652
Oas1g	3.37343027	0.3822429	8.68715301	0.00320461	0.35748594
Olfra397	3.33627921	0.35114049	10.5482459	0.00116298	0.19870834
Pdpr	3.2021993	3.10987377	16.2857554	5.45E-05	0.02450873

Table 2.2 Down-regulated genes in WT wounded-keratinocytes 3 days post wounding

Gene	logFC	logCPM	LR	PValue	FDR
Gm10175	- 9.5719498	1.37004807	31.9226523	1.60E-08	3.09E-05
Gm6158	- 9.0491072	0.87083752	30.769404	2.91E-08	4.36E-05
AW822252	- 8.3157363	9.25001567	16.4668983	4.95E-05	0.02304291
A930009A15Rik	- 5.4921637	-0.2431275	15.6082219	7.79E-05	0.0300485
Gm10163	- 5.1140105	4.31681635	5.06892987	0.02435842	0.99633305
Gm6710	- 4.9442653	0.57461996	16.2225824	5.63E-05	0.02452228
Gm7353	- 4.1380561	0.82244017	11.7918513	0.00059491	0.12951668
AC132586.6	- 4.1380561	0.82244017	11.7918513	0.00059491	0.12951668
6430571L13Rik	- 3.9165953	0.41230946	11.8826761	0.00056658	0.12951668
Qrich2	- 3.8855263	1.17104068	15.4622681	8.42E-05	0.03070569
Mef2c	- 3.4529884	0.47606697	9.65876371	0.0018845	0.25693975
Timp4	- 3.2505213	-0.2743921	8.83324862	0.00295791	0.34710244
Itm2a	- 3.2469575	-0.575507	6.79109638	0.00916136	0.64072577
Gulo	- 3.1970668	0.05075964	6.3676254	0.0116221	0.73075189
Panx3	- 3.1933815	0.36309554	5.97127196	0.01454079	0.83519815
Wfdc3	- 3.1349814	0.72015578	9.82912013	0.0017177	0.24665513
Syng1	- 3.1252745	0.17332741	7.62123955	0.00576848	0.50890835
Ptrhd1	- 3.0476334	0.21681315	7.28053715	0.00697057	0.56003725
H2-T-ps	- 3.0294103	0.41733326	8.63898058	0.00329045	0.36109399
Frg2f1	- 2.9861218	-0.0941366	7.44816422	0.00635012	0.52866059

Kif27	-	0.28429015	5.0900454	0.02406356	0.99509474
	2.9262024				
Gm7367	-	0.1100309	5.10986074	0.02379023	0.99509474
	2.9107043				
Slc9a3r2	-	0.93571649	8.83682202	0.00295213	0.34710244
	2.8388886				
Gm10031	-	2.62818568	10.8843199	0.00096982	0.17454135
	2.8337427				
Notum	-2.803095	-0.0494067	7.44872243	0.00634815	0.52866059
Zfp85	-	1.26577706	9.6736008	0.00186935	0.25693975
	2.7581509				
Rpl10-ps5	-	5.55583014	7.8230165	0.0051585	0.47046939
	2.7378668				
Fam25c	-	1.13147017	4.36500513	0.03668437	0.99958683
	2.5507038				
Serpinb3a	-	0.28073164	4.36486783	0.03668733	0.99958683
	2.4834928				
1700030J22Rik	-2.41616	0.24564274	5.49704072	0.01904868	0.92544623
1190005I06Rik	-	0.7890082	4.59379742	0.03208785	0.99958683
	2.3534298				
Zfp580	-2.318628	0.90498986	6.7299708	0.00948062	0.65177257
Map3k21	-	0.87644091	6.57566615	0.01033823	0.69255377
	2.2930728				
Hoxa9	-	2.44444055	8.20485375	0.00417785	0.42400442
	2.2610083				
Kcnj13	-	0.08947263	5.3243693	0.02102922	0.94933908
	2.2574206				
Icam2	-	1.1348675	5.71453196	0.01682505	0.90227652
	2.2538929				
Sgpp2	-	1.06157175	6.87144797	0.00875837	0.63094266
	2.2004488				
Arnt2	-	1.07985227	5.04746452	0.024662	0.99808695
	2.1332735				
AC073947.2	-	-0.1638263	4.44636922	0.03497553	0.99958683
	2.1327918				

Table 2.3 Up-regulated genes in K14Cre-Grhl3 wounded-keratinocytes 3 days post wounding

genes	logFC	logCPM	LR	PValue	FDR
C330021F23Rik	5.03583022	3.14172583	49.1652333	2.35E-12	2.10E-09
Gm9493	4.87337709	5.62024345	12.0179069	0.00052692	0.07437315
Gm13301	4.50931921	2.35814558	14.7350599	0.00012372	0.02370022
Gm45234	4.19665163	5.05469145	8.76607866	0.00306885	0.27617548
Gm5148	3.68818469	8.41498405	146.605858	9.57E-34	4.28E-30
Gm11361	3.55056725	2.4317597	21.4825438	3.57E-06	0.00113997
Mmrn1	3.49635087	1.30274084	7.00924863	0.00810897	0.54366593
AC099934.3	3.25429755	2.81705259	12.5483201	0.00039656	0.05974729
Gm6641	3.24909011	2.52489615	20.4717214	6.05E-06	0.00184431
Rex2	3.12119379	1.288173	5.19014346	0.02271534	0.93460956
Gm2237	3.03783041	1.06046811	6.89833445	0.00862761	0.56159034
Enpp2	2.93358587	1.97229308	12.5727658	0.00039141	0.05964093
Rybp-ps	2.91151435	0.99870412	4.5638634	0.03265333	0.99944176
Spag16	2.87985008	2.42903365	15.8590503	6.82E-05	0.01475842
Slitrk2	2.71949463	1.95952347	10.8171636	0.00100563	0.11958183
Sele	2.6850183	1.3455111	6.71166006	0.00957845	0.58116497
AC162934.3	2.6591551	1.17133924	4.66423744	0.0307971	0.99944176
Rps6-ps4	2.57105045	7.41173995	53.9360908	2.07E-13	1.98E-10
Gapt	2.56206665	1.19576251	6.5935	0.01023518	0.59443861

Gm21188	2.56020593	1.62822744	8.05848743	0.0045291	0.3614921
Caps2	2.51665419	1.22750725	6.06618938	0.01377939	0.69983484
Kxd1	2.51550261	6.53902789	54.9356361	1.25E-13	1.39E-10
Ankrd31	2.51545735	1.23918865	5.74531721	0.01653267	0.77984434
Slc26a7	2.5132395	1.6671459	7.875026	0.00501222	0.38186814
Twist2	2.49710394	2.37532944	10.8946505	0.00096442	0.11756327
Gm10036	2.4754452	5.94790912	64.4136034	1.01E-15	1.50E-12
Ryr1	2.47285505	2.17246717	4.64592386	0.03112738	0.99944176
Ces5a	2.47131933	1.67885549	4.23456706	0.03960872	0.99944176
Lekr1	2.42590336	1.64232105	5.48441454	0.01918674	0.86624598
Slc26a3	2.42394704	0.68846938	3.95169829	0.04682409	0.99944176
Olfr243	2.36251062	1.53811441	6.59256818	0.01024053	0.59443861
Mab2112	2.2853611	0.94955795	4.93159452	0.02636997	0.99324436
Olfr1277	2.26425551	0.87698882	4.30281369	0.03804937	0.99944176
Ramp3	2.26065432	1.3221257	4.65571439	0.03095035	0.99944176
Cd300lg	2.24836285	1.95108054	6.05962205	0.01383073	0.69983484
Fam151b	2.23439393	1.09554251	4.76758196	0.02900053	0.99944176
Scd4	2.22694846	1.57570791	4.96080038	0.0259282	0.98212227
Olfr1167	2.20839531	0.766339	4.2218216	0.0399073	0.99944176

Table 2.4 Down-regulated genes in K14Cre-Grhl3 wounded-keratinocytes 3 days post wounding

genes	logFC	logCPM	LR	PValue	FDR
Gm28661	-14.100145	6.30674489	167.632301	2.43E-38	3.26E-34
Rpl10-ps1	-13.202662	5.41098252	110.127459	9.19E-26	3.08E-22
Pgam1-ps2	-12.587803	4.79817016	97.83754	4.54E-23	1.22E-19
Zdbf2	-4.473931	0.09417476	7.55176845	0.00599512	0.43219666
Neu2	-4.4558358	0.07614601	7.41539047	0.00646683	0.45638787
Tagap	-4.3833772	0.76594516	8.84376903	0.00294091	0.26826318
AC123954.1	-3.4219989	1.92584973	9.51111318	0.00204231	0.2043684
Serpinf1	-3.3094096	0.78533353	5.90212972	0.01512259	0.73470575
Casq2	-3.2771597	1.05534492	6.61093496	0.01013544	0.59443861
E130208F15Rik	-3.2376442	1.36910242	6.73742807	0.00944106	0.58050735
Morn2	-2.8553346	0.39137302	4.45353937	0.03482899	0.99944176
Slc5a8	-2.8455937	0.67313993	4.75195218	0.02926508	0.99944176
Mmp9	-2.8442785	4.00754751	12.113758	0.00050051	0.07216517
Trnp1	-2.8103915	2.13365507	6.14767027	0.01315853	0.68388669
Matk	-2.7916016	0.62900532	4.34017001	0.03722321	0.99944176
Ndufs6	-2.7832779	2.5116346	4.97924988	0.0256531	0.98212227
Rbpsuh-rs3	-2.766899	2.50263995	9.8585408	0.00169045	0.17848721
Serpina3f	-2.7538196	0.85052062	4.64879399	0.03107537	0.99944176
B930094E09Rik	-2.413266	1.08151065	4.05475979	0.04404699	0.99944176

Tnfrsf23	-2.4041245	2.77794081	4.85164675	0.02761975	0.99944176
Rplp1	-2.3929865	8.55841681	10.8132964	0.00100774	0.11958183
Dchs2	-2.3838162	1.05620312	3.92171813	0.04766614	0.99944176
Acta2	-2.3558052	2.95843154	10.510389	0.00118705	0.13375789
Ncapb	-1.1272935	4.65224883	6.84657305	0.00888115	0.56979566
Ddit4	-1.1272472	4.16606929	5.26091431	0.02180956	0.92021778
Myadm	-1.1233091	5.03052791	8.26668026	0.00403793	0.33592589
S100a11	-1.1214017	7.31267736	10.9590912	0.00093145	0.11458604
Grem1	-1.1187439	4.65985796	5.74075162	0.0165757	0.77984434
Fmnl2	-1.1101087	5.20735841	8.74948823	0.00309689	0.27630875
Atf5	-1.0955711	4.72769686	5.8730176	0.01537468	0.73892123
Pdp2	-1.0926174	3.84675862	4.48384808	0.0342166	0.99944176
Fscn1	-1.0890411	6.55203512	11.3989296	0.00073486	0.09566792
Ptgs2	-1.0824022	6.9862172	8.7903539	0.00302827	0.2743658
Mt2	-1.072796	6.82305706	11.3628453	0.00074928	0.09660662
Ass1	-1.0713077	5.95401778	4.63210613	0.03137902	0.99944176
Dock10	-1.0676586	3.82725642	4.0392904	0.04445251	0.99944176
Scd2	-1.0640478	6.60678613	10.6110114	0.00112416	0.13111353
Eif3j2	-1.0628184	5.30943685	8.2544327	0.00406526	0.33592589

CHAPTER 4: GRHL3-MEDIATED VASODILATION IN CUTANEOUS WOUND HEALING

ABSTRACT

Diseases such as Diabetes and vascular diseases affect signaling pathways involved in normal wound healing, leading to chronic non-healing wounds. Despite the current advances in wound healing research, full understanding of cellular interactions required for complete wound closure is still lacking. Normal wounds heal over three overlapping phases: Inflammation, re-epithelization, and tissue remodeling. During the first phase of healing, neurogenic vasodilation of dermal blood vessels in the wound area is essential for the inflammatory response, oxygenation and immune cell recruitment. Mice with targeted deletion of the epidermal transcription factor GRHL3 exhibit a delay in wound healing during the early phases. In K14Cre-Grhl3^{-/-} mice, we observed a significant decrease in venous vasodilation, which resulted in a decrease in blood flow after wounding. Transcriptomic analysis of wound margin keratinocytes indicates a significant decrease in the expression of prostaglandin E2-producing enzymes Cox-2 and PTGE synthase in K14Cre-Grhl3^{-/-} mice. These data strongly suggest that in response to wounding, Grhl3 in the epidermis regulate the expression of enzymes required for Prostaglandin E2 biosynthesis and secretion to the dermis, activating neurogenic vasodilation. These data reveal a novel epidermal-dermal signaling pathway required for optimal wound healing.

INTRODUCTION

Non-healing wounds are associated with several disease factors such as diabetes, vascular diseases, neuropathies and edema (Han & Ceilley, 2017). The cellular mechanism of wound healing has been widely investigated, identifying three main overlapping phases: inflammation, re-epithelization and tissue remodeling (Han & Ceilley, 2017; Mayet et al., 2014). During all phases, damaged skin cells including keratinocytes, dermal fibroblasts, immune cells, dermal nerve fibers, and endothelial cells molecularly interact to orchestrating the healing process. Despite the current advances in wound healing research, less is known

about the epidermal-dermal cellular interaction and their molecular signaling pathways required for normal wound healing.

Right after injury, injured blood vessels are sealed via fibrin clot formation. Once the blood is stopped, pro-inflammatory mediators such as growth factors, cytokines and neurotransmitters are released by injured skin cells to initiate the inflammatory response (Ashrafi, Baguneid, & Bayat, 2016). The recruitment of immune cells to the wound site is mediated by vasodilation of the local dermal blood vessels. During inflammation, dilation of the local blood vessels is mediated via neurogenic vasodilation. Neurogenic vasodilation is activated by the release of neuromodulators such as histamine, bradykinin, and prostaglandin from wounded keratinocytes in the epidermis. The release of neurotransmitters sensitizes the innervated afferent axon terminals in the central nervous system (CNS) releasing several neuropeptides such as substance P and CGRP from the peripheral terminals of C fibers that directly acts on the dermal blood vessel mediating vasodilation (Steinhoff & Luger, 2012).

Prostaglandin E2 is a vasodilatory factor known to regulate blood flow and stimulate angiogenesis. In wounding, epidermal keratinocytes produce large amounts of PGE2 that is secreted to the underlying dermis (Park, Pillinger, & Abramson, 2006; Pentland & Mahoney, 1990; Syeda et al., 2012). PGE2 production depends on oxygenation of Arachidonic acid by the cyclooxygenase enzyme and PGE synthase. In wounded keratinocytes, PGE2 biosynthesis is mediated by the induced COX-2 enzyme that is highly expressed in wounded epidermis (Kämpfer, Bräutigam, Geisslinger, Pfeilschifter, & Frank, 2003).

Grainyhead-like 3 is an epidermal transcription factor that is required for development. Embryonic deletion of *grhl3* in mice is lethal, resulting in defective neural tube closure and epidermal barrier formation (Yu et al., 2006). Mice with conditional deletion of *Grhl3* in the epidermis exhibit delayed wound healing. The impaired wound healing is associated with a defect in neurogenic vasodilation and decreased blood flow after wounding. These observations are intriguing since *Grhl3* expression is exclusive to the epidermis, an epidermal-dermal cross-talk required for optimal vascular response. In this study, we investigate *Grhl3*-mediated mechanism required for dermal vasodilation during wound healing.

MATERIALS AND METHODS

Generation of transgenic mice

Transgenic mouse strains used in these studies are Grhl3 floxed mice, K14-Cre/Grhl3^{-/-} mice, and Grhl3-Cre/LacZ reporter mice. C57BL/6J/Grhl3 floxed mice were previously generated and used by the Andersen lab (). Skin-specific deletion of Grhl3 in C57BL/6J/ mice was generated by crossing Grhl3 floxed mice with *Krt14-Cre* mice (purchased from Jackson laboratory). Offsprings were bred to produce Wild type, heterozygous and homozygous-Grhl3-flox Cre-positive mice (*Krt14-Cre Grhl3^{-/-}*, *Krt14-Cre Grhl3^{f/f}* and *Krt14-CreGrhl3^{f/f}*, respectively). All mice were housed and maintained in accordance with protocols approved by the University Laboratory Animal Resources (ULAR).

Mouse excisional-wound experiment

Aged matched (8-weeks) *Krt14-Cre Grhl3^{-/-}* and *Krt14-CreGrhl3^{f/f}* littermate mice both males and females were used for wounding. Prior surgery, mice were anesthetized with Ketamine/Xyline according to ULAR approved guidelines. Dorsal back skin was shaved, and hair was removed using Nair cream. Small full-thickness wounds were created using 4 mm biopsy punch on the shaved dorsal back skin. Wounded mice were placed on heating pad and monitored periodically until full recovery. Total of 2-4 wounds per mouse was created in each experiment. For wound closure rate, mice were anesthetized at each indicated time point and pictures of the wounds were collected. For ear wound model, 2 mm biopsy punch was used to create a small wound in the middle of the ear.

Measurement of Vasodilation

Macroscopic images of wounded skin flaps were taken using dissecting scope at day 3 and Day 5 post wounding. Dilation was determined by measuring the width of the large vein was using Imagej.

Immunofluorescence and whole mount staining

Wounded mice were euthanized, and wound tissues were collected after 24 hrs post wounding.

For immunofluorescence, fresh-frozen wound tissues were embedded in O.C.T compound and sectioned (8µm thick) using Cryostat. Slides were fixed in cold acetone for 10-13 mins at RT. After three washes with 1X PBS slides were fixed with 4% PFA for 10 mins. Slides were then permeabilized with permeabilization buffer (triton-X in PBS) for 10-15 mins and blocked with blocking buffer for 1 hour. For primary antibody, slides were incubated with anti-CD45 (1:500 bioscience) overnight at 4C. After several washes with 1XPBS, slides were incubated with secondary antibody (Alexaflora-488/ Alexafloura-594) for 1 hour at RT in dark. Stained slides were mounted with DAPI for nuclear staining and imaging. Slides were imaged using Keyence BZ-X710 All-in-one fluorescence microscope.

For ear whole mount staining, whole wounded ear was dissected and skin (top layer) was separated from the cartilage. The ear skin was fixed in 4%PFA for one day, followed by 20 mins washes with 1XPBS. Samples were permeabilized with permeabilization buffer (triton-X in PBS) for 1 hour and blocked with blocking buffer overnight at 4c. Primary antibody anti-CD31 (1:100) was incubated for 1-2 days at 4C. Following several 20 mins washes with 1X PBS, samples were incubated with secondary antibody (Alexaflora-488 1:500) for 1-2 hours in the dark. Ear skin was mounted on a glass slide and imaged using Keyence BZ-X710 All-in-one fluorescence microscope.

Window chamber and measurement of the relative blood flow

Window chambers were surgically sutured to the dorsal back skin of the mouse, and a wound/window was created on one of the sides. The mouse's dorsal window chamber was transilluminated with a 633 nm red helium neon laser. A Chameleon-3 camera by Point Grey was used to acquire 10 .tif images each at exposure times of 10, 100, and 1000 ms. The acquired images were then processed in Matlab to form SFI maps. The raw speckle images were spatially processed with a 7x7 sliding window to calculate $K = \frac{\sigma}{\langle I \rangle}$ for each pixel. The resulting speckle contrast image is then converted into a Speckle Flow Index (SFI) map via the formula $SFI = \frac{1}{2K^2T}$. A region of interest (viz. the length of the main venule) is selected,

and Matlab was used to calculate the mean intensity, the standard deviation, and the number of pixels. This process was repeated on approximately 2-3-day intervals for up to a 10-day period for each mouse. The acquired means were plotted against time to compare the changes in relative blood flow over time between the K14Cre-Grhl3^{-/-} and wild type mice

Flow cytometry and FAC's sorting

One mm of wound margins (four wounds were pooled per mouse per genotype) and distal unwounded skin were collected, and subcutaneous fat was removed with a scalpel and tissues were placed epidermis facing up on trypsin (GIBCO) at 37 °C for 2 hours on a shaker. Peeled epidermis was diced in 2 ml media (epilife) and the cell suspension was filtered through 70um followed by 40um cell strainers. single-cells were washed with 1X Red-cell lysis buffer followed by 1X PBS then blocked with FACS buffer () for 5 mins on ice. Fluorophore-conjugated antibody staining was performed in dark for 30 mins, on ice. Stained cells were suspended in 400 ul of DAPI/FACS buffer and filtered through 40um strainer before flow cytometry analysis. For wound inflammation analysis, 1 mm of whole-wounds and unwounded skin were collected, diced into small pieces and incubated with 2 ml of collagenase buffer () for 2 hours on a rotator at 37C.

Antibodies used are: CD49F-PE(), CD45-APC(), CD31-APC(), TER119-APC(). Isotype controls of the indicative fluorophore were used as staining controls. Samples were processed using BD LSR II flow cytometer. For FACS sorting, cells were sorted (sorting machine) into 350 ul RLT-BME lysis buffer () followed by RNA extraction using Microelute RNA kit (zymogen). RNA quality was assessed using Agilent Bioanalyzer and concentration was measured by pico-Chip. Samples with high RIN score <8 were used for sequencing.

RNA-sequencing and analysis

Sequencing library (Single-Read-100) were prepared at the GHIF UCI genomic facility using Illumina ClonTech mRNA sample preparation kit (). Libraries were sequenced on Illumina HiSeq 4000 (50 Million reads per sample). Sequencing quality of sequencing data (FastQ files) was determined using FASTQC. Reads were aligned to the mouse genome (mm10 build) using Tophat and Bowtie scripts. Transcript assembly was processed using Klisto and list of differentially expressed genes was generated using DEseq in R . Gene Set Enrichment

analysis (GSEA) was applied on differentially expressed genes to determine functional GO categories. HOMER AND meme software were used to identify de novo motifs and enriched Grhl3 motifs in candidate genes, respectively.

Statistical Analysis

One-way ANOVA and Unpaired Students'-T tests were performed in GraphPad Prism 6.0 software. Data were expressed as mean \pm SEM and p values were reported such that *p < 0.05, **p < 0.01, and ***p < 0.001.

RESULTS

Defective vasodilation in mice lacking epidermal Grhl3

Grainyhead like-3 expression is up-regulated at the wound edge as early as 24 hours after wounding. Through our work, we show that keratinocyte-specific deletion of Grhl3 (K14Cre-Grhl3^{-/-}) in adult skin results in impaired healing of full-thickness wounds (Chapter 3). Interestingly, macroscopic views of wounded dorsal skin flaps after 3 days show a vascular defect in K14Cre-Grhl3^{-/-} mice characterized by a remarkable reduction in blood venous dilation compared to WT (Fig. 1a). In normal mice, vasodilation of dermal blood vessels is macroscopically detected in wound skin flaps within 24 hours post-wounding and increases in the first three days, during the inflammatory phase (data not shown). Macroscopic images of wounded skin flaps in K14Cre-Grhl3^{-/-} mice show a decrease in the width of the dermal vein at several time points in wounding (Fig. 1b), indicating that the defective vasodilation persist during later stages of wound healing. The decreased venous dilation in the K14Cre-Grhl3^{-/-} mice is general, extending well beyond where an epidermally-secreted molecule would be expected to work, suggesting a defect neurogenic vasodilation.

Since mouse ears are highly vascularized, we performed a small ear wound model on K14Cre-Grhl3^{-/-} and WT mice to detect the vascular defect. Whole-mount staining with the vascular endothelial marker CD31 on Day 3 wounded ears show a remarkable decrease in the blood vessel width in K14Cre-Grhl3^{-/-} wounded ear compared to WT (Fig. 1c). These data clearly indicate that mice lacking epidermal Grhl3 exhibit vascular defect in response to

wounding. Intriguingly, Grhl3 is not expressed in dermal endothelial cells, which suggests an indirect role of Grhl3 on the neuronal pathway required for wound vasodilation.

Decreased relative blood flow in K14Cre-Grhl3^{-/-} mice during wound healing

Dermal vasodilation increases blood flow to the wound site, facilitating immune cell entry to supply the wound bed with oxygen and nutrients required for optimal repair. Thus, we sought to investigate the effect of defective vasodilation in K14Cre-Grhl3^{-/-} mice on relative blood flow in response to wounding. We performed window chamber wound model on the dorsal skin in WT and K14Cre-Grhl3^{-/-} mice. The window chamber was surgically implemented on the dorsal skin and a circular piece of the skin was excised creating a wound (Fig. 2a). The dorsal window chambers were transilluminated with a 633 nm red helium neon laser and a Chameleon-3 camera by Point Grey was used to acquire images each at several exposure times. The acquired images were then processed using Matlab to form heat maps of the relative blood flow. Speckle Flow Index maps of window chambers from WT mice show an increase in the relative blood flow after 3 days post-wounding (Fig. 2b, c). The increase in blood flow was accompanied with an increase in blood vessel size and vascular branching, both of which persisted and significantly increased until 8 days post-wounding (Fig. b2). In contrast, window chambers in K14Cre-Grhl3^{-/-} mice clearly indicate a defect in the vascular response after wounding, showing minimal changes in vascular size and branching (Fig. 2b). The relative blood flow rate is significantly decreased in K14Cre-Grhl3^{-/-} mice at Day3 and Day8 compared to WT (Fig. 2b, c). These data strongly indicate that the defective vasodilation observed in K14Cre-Grhl3^{-/-} mice result in decreased blood flow and vascularization in response to wounding.

Unaltered inflammatory response in K14Cre-Grhl3^{-/-} mice

Immune cells at the wound site such as macrophages, neutrophils and mast cells produce high amounts of vascular-endothelial growth factors and other vasoactive mediators to promote neurogenic vasodilation. Our previous work showed that Grhl3 is required to regulate inflammation in Psoriatic skin. Thus, we wanted to determine if the defective vasodilation in K14Cre-Grhl3^{-/-} mice is caused by defective inflammation. Immunofluorescence staining of CD45, a common marker to detect all immune cells, indicate

no difference in CD45 expression between K14Cre-Grhl3^{-/-} and WT wounds after 24 hours (Fig. 3a). In addition, infiltration of immune cells to the epidermis was normal in K14Cre-Grhl3^{-/-} mice after 24 hours post-wounding compared to its unwounded region (Fig. 3b). Neutrophils are the first type of immune cells recruited to the wound site and are the most predominant in the first few days of the inflammatory phase. Neutrophils, as well as macrophages, secrete several cytokines and factors such as IL-17 and VEGF-A that increases vasodilation and vascular permeability. Flow cytometry analysis investigating different immune cell populations at the wound site clearly show high percentage of neutrophils in both WT and K14Cre-Grhl3^{-/-} out of all immune cells after 24 hours post-wounding (Fig.3 c). In addition, the ratio of immune cell populations in K14Cre-Grhl3^{-/-} mice was relatively similar to the ratio of immune cell populations WT mice (Fig.3 c), indicating no alteration in immune cell number and type recruited to the wound site in K14Cre-Grhl3^{-/-} mice. Altogether, these data clearly indicate that loss of Grhl3 in the epidermis does not affect the epidermal and dermal inflammatory response during wound healing.

Grhl3 mediates Prostaglandin E2 production in the epidermis during wound healing

To identify the vasodilatory role of Grhl3, we performed transcriptomic analysis on sorted wound-margin keratinocytes (1mm) 24 hours post-wounding from both K14Cre-Grhl3^{-/-} and WT mice. In K14Cre-Grhl3^{-/-} mice, 475 genes were significantly mis-regulated in K14Cre-Grhl3^{-/-} wounded keratinocytes 24 hours post-wounding (Table1). Gene ontology analysis on the mis-regulated genes show enrichment of genes involved in angiogenesis, response to hypoxia, prostaglandin metabolic process, cell migration and adhesion and wound healing (Fig. 4a). The majority of the genes involved in indicated GO categories were significantly down-regulated in K14Cre-Grhl3^{-/-} wounded-keratinocytes compared to WT mice (Fig. 4a, Table1).

We were interested in genes involved in prostaglandin metabolic processes given that Prostaglandin E2 (PGE2) is a known mediator of neurogenic vasodilation. In wounding, keratinocytes produce a great amount of PGE2 that is secreted to the underlying dermis, acting on the adjacent nerve endings to activating neurogenic vasodilation. Epidermal PGE2 synthesis depends on the metabolism of arachidonic acid by key processing enzymes such as cyclooxygenase 2 (Cox-2), also called Ptg2, and PTGE synthase. Interestingly, transcript

levels of both COX-2 and Ptge synthase were significantly downregulated in K14Cre-Grh3^{-/-} wounded keratinocytes compared to WT 24 hours post-wounding (Fig. 4b, c). These data strongly suggest a potential decrease in PGE2 production in wounded-keratinocytes lacking Grhl3.

DISCUSSION

Our analysis of the defective vasodilation phenotype in keratinocyte-specific deleted Grhl3 mice has revealed highly interesting findings. Our data reveal a novel role of Grhl3 in the epidermis regulating a pathway required for dermal tissue function during skin repair.

Grainyhead-like 3 is an evolutionary conserved transcription factor that is essential during embryonic development of the epidermis. Although dispensable for adult skin hemostasis, Grhl3 expression increases in response to injury. In acute wound healing, Grhl3 is highly up-regulated at the wound margin within 24 hours post-wounding. Mice lacking epidermal Grhl3 (K14Cre-Grhl3^{-/-}) exhibit delayed wound closure during the early phases. In the previous chapter (chapter 3), we described a Grhl3-mediated mechanism regulating keratinocyte migration during wound re-epithelialization. Here, we describe another Grhl3-mediated mechanism that occurs during the early responses of wound healing.

The K14Cre-Grhl3^{-/-} mice exhibited a defect in the vascular response after wounding. This defect is associated with decreased venous dilation, decrease relative blood flow and decreased vascular branching compared to wild-type mice. The observed decrease in venous dilation in the Grhl3 cko mice extend well beyond where an epidermally-secreted molecule is expected to work. This observation suggests that the secreted molecule acts on sensory neurons that send signals to the CNS that are then relayed via efferent autonomic nerves mediating vasodilation.

Keratinocytes secrete large amounts of neurotransmitters such as prostaglandins during injury. Prostaglandin is a key vasodilator that is produced by skin cells during injury. The biosynthesis of PGE2 in the epidermis is mediated by arachidonic acid oxygenation via cyclooxygenase (COX) enzyme. Unlike COX-1, COX2 isoform is induced by peripheral inflammation. Oxygenation of arachidonic acid by COX-2 generates prostaglandin H₂ that is further processed by prostaglandin E synthase to produce Prostaglandin E₂ (PGE₂). Our

transcriptomic analysis on wound-margin keratinocytes 24 hours post-wounding indicate mis-regulation of several genes required for PGE2 biosynthesis such as COX-2 and PGE synthase. Both Cox-2 and PGE synthase were significantly downregulated in K14Cre-Grhl3^{-/-} mice 24 hours post-wounding. These data strongly suggest that PGE2 production in K14Cre-Grhl3^{-/-} mice is decreased, causing the defective vasodilation in the wound area. Our future direction is to detect the levels of PGE2 production and neurotransmitters produced by activated neurogenic vasodilation such as CGRP in Grhl3 cKO skin. If PGE2 levels are indeed affected, then topical application with PGE2 on mouse dorsal skin may rescue the defective vasodilation in K14Cre-Grhl3^{-/-} mice. These data highlight a novel mechanism by which an epidermal transcription factor regulate the expression of genes required for vasoactive factor secretion to the dermis required for normal neurogenic vasodilation. This study highlights a new mechanism of epidermal communication with the neuronal pathway in the skin.

Figure 1

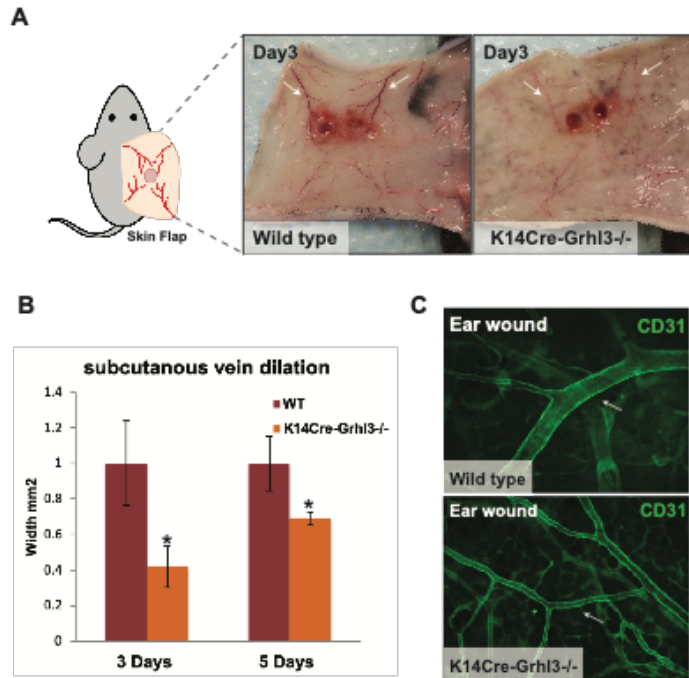


Figure 1. Defective vasodilation in mice lacking epidermal Grhl3

(A) Macroscopic images of dorsal skin flaps in WT and K14Cre-Grhl3^{-/-} mice 3 days post wounding. Arrows point to the two main subcutaneous veins. (B) Measurements of subcutaneous venous width in skin flaps collected 3- and 5-days post wounding, N=3/genotype (* p value > 0.05). (C) Whole-mount staining of blood vessels with anti- CD31 (green) in ears 3 days post wounding. Arrows point to the width of blood vessel in WT and K14Cre-Grhl3^{-/-} mice.

Figure 2

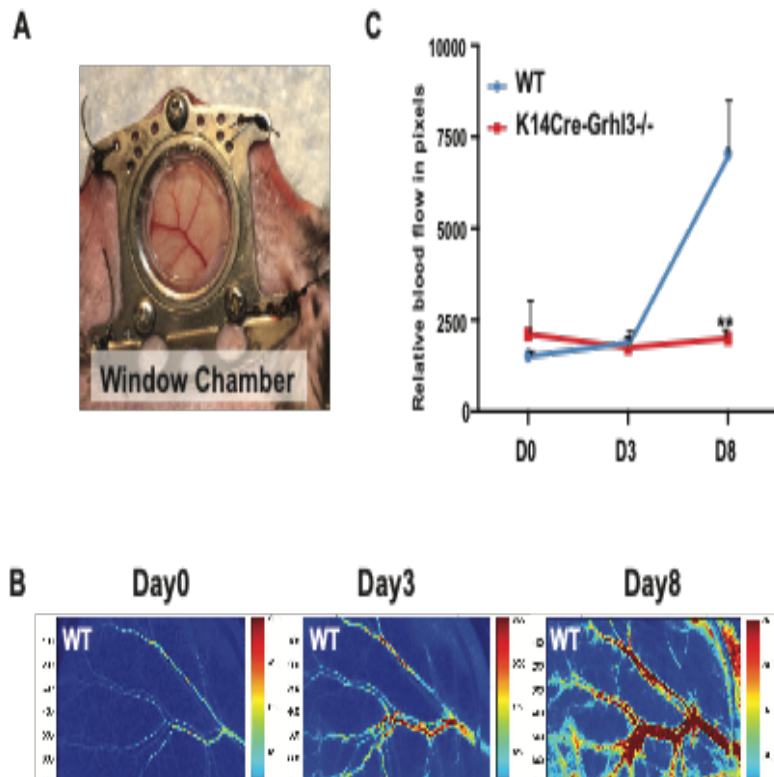


Figure 2. Decreased relative blood flow in K14Cre-Grhl3-/- mice during wound healing

(A) Macroscopic image of window chamber wound model on mouse dorsal skin. (B) Speckle Flow Index maps of WT and K14Cre-Grhl3-/- window chambers at several time points (day 0, day 3 and day 8) post wounding. (C) Measurements of the relative blood flow determined by Speckle Flow Index in WT and K14Cre-Grhl3-/- window chambers at the indicated time points. The mean intensity and the number of pixels were calculated from the SFI maps, then acquired means were plotted against time, N=3/genotype (* p value >0.05).

Figure 3

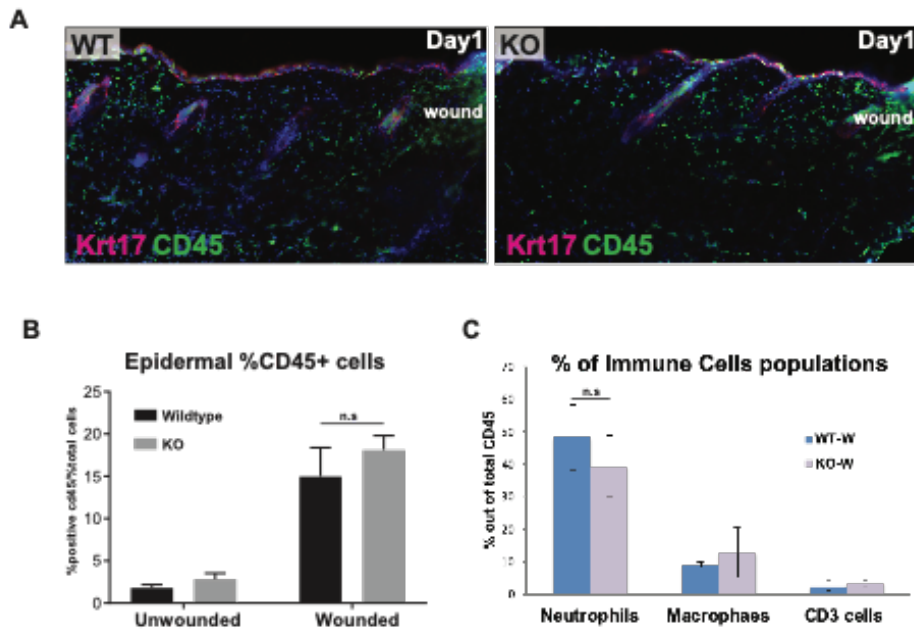


Figure 3. Unaltered inflammatory response in K14Cre-Grhl3^{-/-} mice

(A) Immunofluorescence staining of CD45 (green) and Krt17 (red) in sections collected 24 hrs post wounding. (B) Flow cytometry analysis indicate the percentage of CD45+ cells out of total cells in WT and K14Cre-Grhl3^{-/-} in unwounded and 24hrs wounded epidermis, N=3/genotype (n.s -not significant). (C) Flow cytometry analysis indicate the percentage of Neutrophils, macrophages and T-cells (CD3) out of total CD45+ cells collected from whole skin 24hrs post wounding, N=3/genotype (n.s-not significant).

Figure 4

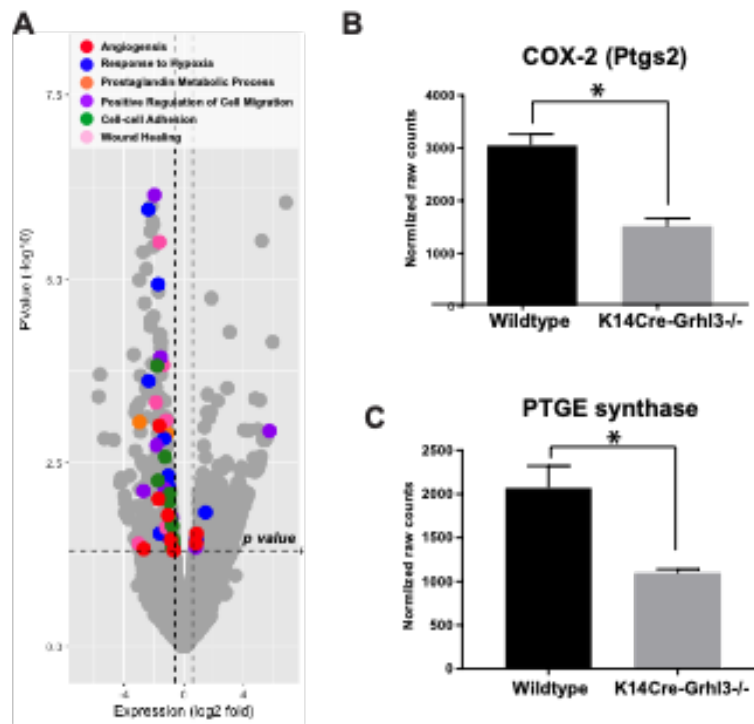


Figure 4. Grhl3 mediates Prostaglandin E2 production in the epidermis during wound healing

(A)Volcano plot showing GO functional category of mis-regulated genes in wounded-keratinocytes isolated from K14Cre-Grhl3-/- 24 hrs post wounding. (B) Normalized transcript expression levels of COX-2 wounded-keratinocytes isolated from WT and K14Cre-Grhl3-/- mice 24hrs post wounding, N=2/genotype (* p value>0.05). (C) Normalized transcript expression levels of PTGE synthase in wounded-keratinocytes isolated from WT and K14Cre-Grhl3-/- mice 24hrs post wounding, N=2/genotype (* p value>0.05)

Figure 5

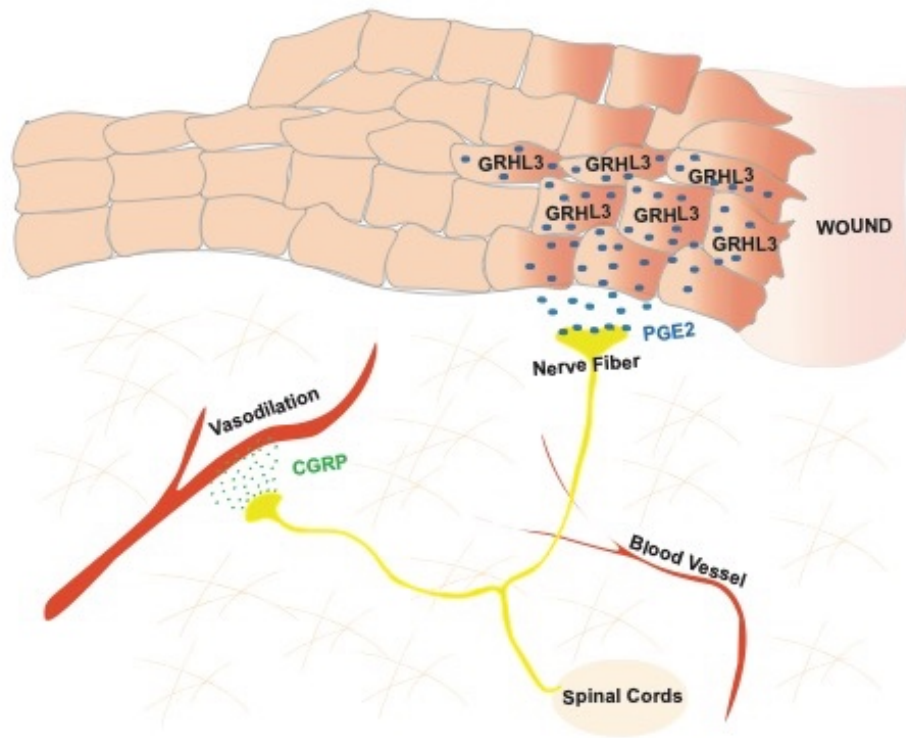


Figure 5. Grhl3-mediated Vasodilation in cutaneous wound healing

(A) Schematic representation of Grhl3-mediated regulation of PGE2 production in the epidermis required for neurogenic vasodilation during wound healing.

Table 3-1 Differentially expressed genes in K14Cre-Grhl3^{-/-} wounded-keratinocytes 24 hrs post wounding

genes	logFC	logCPM	LR	PValue	FDR
Rps23-ps1	14.4971385	6.56484202	148.068054	4.58E-34	6.26E-30
Gm14036	11.7324679	3.81581843	100.494586	1.19E-23	8.10E-20
Oaz1-ps	-11.051929	3.14308747	61.1785084	5.21E-15	2.37E-11
Ndufb4	4.57001145	4.4171206	49.6029229	1.88E-12	6.42E-09
Gm28539	-10.739909	2.8363608	48.8504766	2.76E-12	7.54E-09
Gjb2	-2.4929959	8.85700401	38.6273335	5.13E-10	1.17E-06
Krt6b	-2.210653	9.68925814	36.3239347	1.67E-09	3.26E-06
Gm10136	9.72979674	1.83873705	28.6642654	8.61E-08	0.00013153
Ube2n-ps1	9.64223001	1.75348207	28.6497131	8.67E-08	0.00013153
Gm2961	7.77428022	6.42795893	25.2975671	4.91E-07	0.00067061
Itga5	-1.9776007	6.50389534	24.5457011	7.26E-07	0.00090044
Hist1h4a	6.83915301	1.94777158	24.0921471	9.18E-07	0.00104454
Prdm1	-2.1845681	5.97807325	23.8753138	1.03E-06	0.00107913
Nppb	-2.3747319	4.82579345	23.6720648	1.14E-06	0.00111365
Endou	-2.1007265	5.47451829	22.9409756	1.67E-06	0.00152007
Tinagl1	-2.0493474	5.6650662	22.7604027	1.84E-06	0.00156544
Hist1h4h	9.12571812	1.25608743	22.515984	2.08E-06	0.00167323
Kxd1	-2.2345467	6.75257554	22.3568301	2.26E-06	0.00171679
Gm10093	5.20531373	3.53945025	21.787459	3.05E-06	0.00216782
Krt6a	-1.6304848	12.1070924	21.7068632	3.18E-06	0.00216782

Procr	-2.0486443	5.48875055	21.4439789	3.64E-06	0.0023679
Mmp13	-2.7364746	6.84441997	21.1066451	4.34E-06	0.00264695
Gm10175	8.95801058	1.09603177	21.0447121	4.49E-06	0.00264695
Olf155	9.22254774	1.347121	20.9745218	4.65E-06	0.00264695
Gm18445	-2.5047966	5.32258103	20.1062089	7.33E-06	0.00399962
Inhba	-2.97592	5.04729344	19.4455608	1.04E-05	0.00543378
Plau	-1.7193134	6.47500046	19.1774793	1.19E-05	0.00602125
Tgm1	-1.6965563	6.15429538	18.7369569	1.50E-05	0.00731421
Zfp46	1.84816931	6.08543246	18.3455011	1.84E-05	0.00867199
Tnfrsf23	-2.637175	3.77538388	18.054087	2.15E-05	0.00976892
Glp2r	8.47737396	0.64380068	17.9751589	2.24E-05	0.00985399
Klk10	-2.0356492	4.70662687	17.263572	3.25E-05	0.01387784
Spr2h	-2.2339625	4.44880378	17.0094157	3.72E-05	0.01538404
Cdk5r1	-2.2168838	5.22117695	16.6600185	4.47E-05	0.01794985
Rbpjl	3.06590698	3.18868815	16.3325152	5.31E-05	0.01996376
Gm20521	-8.395263	0.60339826	16.3040791	5.39E-05	0.01996376
Hist1h2ai	8.15840914	0.3504923	16.2981	5.41E-05	0.01996376
BC100530	-1.5743651	7.18801802	16.2009051	5.70E-05	0.02046161
Ptgs2	-1.1050138	7.3607033	10.3782341	0.0012751	0.16734408
Ptges	-0.9878307	6.63031953	7.30528666	0.0068752	0.51278493

REFERENCES

Aberdam D, Gambaro K, Rostagno P, Aberdam E, de la Forest Divonne S, and Rouleau M (2007) Key role of p63 in BMP-4-induced epidermal commitment of embryonic stem cells. *Cell Cycle* 6: 291–294. <https://doi.org/10.4161/cc.6.3.3800>.

Adameyko I, Lallemand F, Aquino JB, Pereira JA, Topilko P, Müller T, Fritz N, Beljajeva A, Mochii M, Liste I, Usoskin D, Suter U, Birchmeier C, and Ernfors P (2009) Schwann cell precursors from nerve innervation are a cellular origin of melanocytes in skin. *Cell* 139: 366–379. <https://doi.org/10.1016/j.cell.2009.07.049>.

Andersen B, Schonemann MD, Flynn SE, Pearse RV, Singh H, and Rosenfeld MG (1993) Skn-1a and Skn-1i: Two functionally distinct Oct-2-related factors expressed in epidermis. *Science* 260: 78–82.

Andersen B, Hariri A, Pittelkow MR, and Rosenfeld MG (1997a) Characterization of Skn-1a/i POU domain factors and linkage to papillomavirus gene expression. *The Journal of Biological Chemistry* 272: 15905–15913.

Andersen B, Weinberg WC, Rennekampff O, McEvelly RJ, Bermingham JR, Hooshmand F, Vasilyev V, Hansbrough JF, Pittelkow MR, Yuspa SH, and Rosenfeld MG (1997b) Functions of the POU domain genes Skn-1a/i and Tst-1/Oct-6/SCIP in epidermal differentiation. *Genes & Development* 11: 1873–1884.

Anderson MJ, Schimmang T, and Lewandoski M (2016) An FGF3-BMP signaling axis regulates caudal neural tube closure, neural crest specification and anterior-posterior axis extension. *PLoS Genetics* 12. <https://doi.org/10.1371/journal.pgen.1006018>.

Aoki Y, Saint-Germain N, Gyda M, Magner-Fink E, Lee Y-H, Credidio C, and Saint-Jeannet J-P (2003) Sox10 regulates the development of neural crest-derived melanocytes in *Xenopus*. *Developmental Biology* 259: 19–33.

Bakkers J, Hild M, Kramer C, Furutani-Seiki M, and Hammerschmidt M (2002) Zebrafish DNp63 is a direct target of Bmp signaling and encodes a transcriptional repressor blocking neural specification in the ventral ectoderm. *Developmental Cell* 2: 617–627. [https://doi.org/10.1016/S1534-5807\(02\)00163-6](https://doi.org/10.1016/S1534-5807(02)00163-6).

Bardot ES, Valdes VJ, Zhang J, Perdigoto CN, Nicolis S, Hearn SA, Silva JM, and Ezhkova E (2013) Polycomb subunits Ezh1 and Ezh2 regulate the Merkel cell differentiation program in skin stem cells. *The EMBO Journal* 32: 1990–2000. <https://doi.org/10.1038/emboj.2013.110>.

Bäsler K and Brandner JM (2017) Tight junctions in skin inflammation. *Pflügers Archiv* 469: 3–14. <https://doi.org/10.1007/s00424-016-1903-9>.

Bickenbach JR, Greer JM, Bundman DS, Rothnagel JA, and Roop DR (1995) Loricrin expression is coordinated with other epidermal proteins and the appearance of lipid lamellar granules in development. *The Journal of Investigative Dermatology* 104: 405–410.

Bikle DD, Xie Z, and Tu C-L (2012) Calcium regulation of keratinocyte differentiation. *Expert Review of Endocrinology and Metabolism* 7: 461–472. <https://doi.org/10.1586/eem.12.34>.

Blanpain C, Lowry WE, Pasolli HA, and Fuchs E (2006) Canonical notch signaling functions as a commitment switch in the epidermal lineage. *Genes & Development* 20: 3022–3035. <https://doi.org/10.1101/gad.1477606>.

Blanpain C and Fuchs E (2009) Epidermal homeostasis: A balancing act of stem cells in the skin. *Nature Reviews. Molecular Cell Biology* 10: 207–217. <https://doi.org/10.1038/nrm2636>.

Botchkarev VA (2015) Epigenetic regulation of epidermal development and keratinocyte differentiation. *The Journal of Investigative Dermatology. Symposium Proceedings* 17: 18–19. <https://doi.org/10.1038/jidsymp.2015.15>.

Bergstralh DT, Haack T, and St Johnston D (2013) Epithelial polarity and spindle orientation: Intersecting pathways. *Philosophical Transactions of the Royal Society B: Biological Sciences* 368. <https://doi.org/10.1098/rstb.2013.0291>.

Byrne C, Tainsky M, and Fuchs E (1994) Programming gene expression in developing epidermis. *Development (Cambridge, England)* 120: 2369–2383.

Candi E, Schmidt R, and Melino G (2005) The cornified envelope: A model of cell death in the skin. *Nature Reviews. Molecular Cell Biology* 6: 328–340. <https://doi.org/10.1038/nrm1619>.

Candi E, Rufini A, Terrinoni A, Dinsdale D, Ranalli M, Paradisi A, De Laurenzi V, Spagnoli LG, Catani MV, Ramadan S, Knight RA, and Melino G (2006) Differential roles of p63 isoforms in epidermal development: Selective genetic complementation in p63 null mice. *Cell Death and Differentiation* 13: 1037–1047. <https://doi.org/10.1038/sj.cdd.4401926>. Cangkrama M, Ting SB, and Darido C (2013) Stem cells behind the barrier. *International Journal of Molecular Sciences* 14: 13670–13686. <https://doi.org/10.3390/ijms140713670>. Casey LM, Lan Y, Cho E-S, Maltby KM, Gridley T, and Jiang R (2006) Jag2-Notch1 signaling regulates oral epithelial differentiation and palate development. *Developmental Dynamics* 235: 1830–1844. <https://doi.org/10.1002/dvdy.20821>.

Chan A, Godoy-Gijon E, Nuno-Gonzalez A, Crumrine D, Hupe M, Choi E-H, Gruber R, Williams ML, Choate K, Fleckman PH, and Elias PM (2015) Cellular basis of secondary infections and impaired desquamation in certain inherited ichthyoses. *JAMA Dermatology* 151: 285–292. <https://doi.org/10.1001/jamadermatol.2014.3369>.

Chang HY, Chi J-T, Dudoit S, Bondre C, van de Rijn M, Botstein D, and Brown PO (2002) Diversity, topographic differentiation, and positional memory in human fibroblasts. *Proceedings of the National Academy of Sciences* 99: 12877–12882. <https://doi.org/10.1073/pnas.162488599>.

Chew YC, Adhikary G, Xu W, Wilson GM, and Eckert RL (2013) Protein kinase C δ increases Kruppel-like factor 4 protein, which drives involucrin gene transcription in differentiating keratinocytes. *The Journal of Biological Chemistry* 288: 17759–17768. <https://doi.org/10.1074/jbc.M113.477133>.

Cichorek M, Wachulska M, Stasiewicz A, and Tyminska A (2013) Skin melanocytes: Biology and development. *Advances in Dermatology and Allergology* 30: 30–41. <https://doi.org/10.5114/pdia.2013.33376>.

Clevers H and Nusse R (2012) Wnt/b-catenin signaling and disease. *Cell* 149: 1192–1205. <https://doi.org/10.1016/j.cell.2012.05.012>.

Cohen MA, Itsykson P, and Reubinoff BE (2010) The role of FGF-signaling in early neural specification of human embryonic stem cells. *Developmental Biology* 340: 450–458. <https://doi.org/10.1016/j.ydbio.2010.01.030>.

Costanzo A, Fausti F, Spallone G, Moretti F, Narcisi A, and Botti E (2015) Programmed cell death in the skin. *The International Journal of Developmental Biology* 59: 73–78. <https://doi.org/10.1016/j.ijdb.2015.01.001>.

org/10.1387/ijdb.150050ac.

Dale BA, Holbrook KA, Kimball JR, Hoff M, and Sun TT (1985) Expression of epidermal keratins and filaggrin during human fetal skin development. *The Journal of Cell Biology* 101: 1257–1269. <https://doi.org/10.1083/jcb.101.4.1257>.

De Castro SCP, Hirst CS, Savery D, Rolo A, Lickert H, Andersen B, Copp AJ, and Greene NDE (2018) Neural tube closure depends on expression of Grainyhead-like 3 in multiple tissues. *Developmental Biology* 435(2): 130–137. <https://doi.org/10.1016/j.ydbio.2018.01.016>.

De Groote P, Tran HT, Franssen M, Tanghe G, Urwyler C, De Craene B, Leurs K, Gilbert B, Van Imschoot G, De Rycke R, Guérin CJ, Holland P, Berx G, Vandenabeele P, Lippens S, Vleminckx K, and Declercq W (2015) A novel RIPK4-IRF6 connection is required to prevent epithelial fusions characteristic for popliteal pterygium syndromes. *Cell Death and Differentiation* 22: 1012–1024. <https://doi.org/10.1038/cdd.2014.191>.

De la Garza G, Schleiffarth JR, Dunnwald M, Mankad A, Weirather JL, Bonde G, Butcher S, Mansour TA, Kousa YA, Fukazawa CF, Houston DW, Manak JR, Schutte BC, Wagner D, and Cornell RA (2013) Interferon regulatory factor 6 promotes differentiation of the periderm by activating expression of Grainyhead-like 3. *The Journal of Investigative Dermatology* 133: 68–77. <https://doi.org/10.1038/jid.2012.269>.

Denning MF (2010) Protein kinase C/mitogen-activated protein kinase signaling in keratinocyte differentiation control. *The Journal of Investigative Dermatology* 130: 1968–1970. <https://doi.org/10.1038/jid.2010.194>.

Descargues P, Sil AK, and Karin M (2008) IKK α , a critical regulator of epidermal differentiation and a suppressor of skin cancer. *The EMBO Journal* 27: 2639–2647.

<https://doi.org/10.1038/emboj.2008.196>.

[org/10.1038/emboj.2008.196](https://doi.org/10.1038/emboj.2008.196).

Ding X, Bloch W, Iden S, Rüegg MA, Hall MN, Leptin M, Partridge L, and Eming SA (2016) mTORC1 and mTORC2 regulate skin morphogenesis and epidermal barrier formation.

Nature

Communications 7: 13226. <https://doi.org/10.1038/ncomms13226>.

Długosz AA and Yuspa SH (1994) Protein kinase C regulates keratinocyte transglutaminase (TGK) gene expression in cultured primary mouse epidermal keratinocytes induced to terminally differentiate by calcium. *The Journal of Investigative Dermatology* 102: 409–414.

Eckert RL, Adhikary G, Young CA, Jans R, Crish JF, Xu W, and Rorke EA (2013) AP1 transcription factors in epidermal differentiation and skin cancer [WWW Document].

Journal of

Skin Cancer 2013: 537028. <https://doi.org/10.1155/2013/537028>.

Elias PM, Williams ML, Holleran WM, Jiang YJ, and Schmuth M (2008) Pathogenesis of permeability barrier abnormalities in the ichthyoses: Inherited disorders of lipid metabolism.

Journal of Lipid Research 49: 697–714. <https://doi.org/10.1194/jlr.R800002-JLR200>.

Elias PM, Gruber R, Crumrine D, Menon G, Williams ML, Wakefield JS, Holleran WM, and Uchida Y (2014) Formation and functions of the corneocyte lipid envelope (CLE). *Biochimica et*

Biophysica Acta 1841: 314–318. <https://doi.org/10.1016/j.bbalip.2013.09.011>.

Ernfors P (2010) Cellular origin and developmental mechanisms during the formation of skin melanocytes. *Experimental Cell Research* 316: 1397–1407. <https://doi.org/10.1016/j.yexcr.2010.02.042>.

Ezhkova E, Pasolli HA, Parker JS, Stokes N, Su IH, Hannon G, Tarakhovsky A, and Fuchs E (2009) Ezh2 orchestrates gene expression for the stepwise differentiation of tissue-specific stem cells. *Cell* 136: 1122–1135. <https://doi.org/10.1016/j.cell.2008.12.043>.

Fessing MY, Mardaryev AN, Gdula MR, Sharov AA, Sharova TY, Rapisarda V, Gordon KB, Smorodchenko AD, Poterlowicz K, Ferone G, Kohwi Y, Missero C, Kohwi-Shigematsu T, and Botchkarev VA (2011) p63 regulates Satb1 to control tissue-specific chromatin remodeling during development of the epidermis. *The Journal of Cell Biology* 194: 825–839. <https://doi.org/10.1083/jcb.201101148>.

Fischer H, Scherz J, Szabo S, Mildner M, Benarafa C, Torriglia A, Tschachler E, and Eckhart L (2011) DNase 2 is the main DNA-degrading enzyme of the stratum corneum. *PLoS One* 6(3): e17581. <https://doi.org/10.1371/journal.pone.0017581>.

Foley J, Dann P, Hong J, Cosgrove J, Dreyer B, Rimm D, Dunbar M, Philbrick W, and Wysolmerski J (2001) Parathyroid hormone-related protein maintains mammary epithelial fate and triggers nipple skin differentiation during embryonic breast development. *Development* 128: 513–525.

Fu DJ, Thomson C, Lunny DP, Dopping-Hepenstal PJ, McGrath JA, Smith FJD, Irwin McLean WH, and Leslie Pedrioli DM (2014) Keratin 9 is required for the structural integrity and terminal differentiation of the palmoplantar epidermis. *The Journal of Investigative Dermatology* 134: 754–763. <https://doi.org/10.1038/jid.2013.356>.

Fuchs E (2007) Scratching the surface of skin development. *Nature* 445: 834–842.
<https://doi.org/10.1038/nature05659>.

Fujita M, Furukawa F, Fujii K, Horiguchi Y, Takeichi M, and Imamura S (1992) Expression of cadherin cell adhesion molecules during human skin development: Morphogenesis of epidermis, hair follicles and eccrine sweat ducts. *Archives of Dermatological Research* 284: 159–166.

Gandarillas A and Watt FM (1997) C-Myc promotes differentiation of human epidermal stemcells. *Genes & Development* 11: 2869–2882.

Gebhardt T, Whitney PG, Zaid A, Mackay LK, Brooks AG, Heath WR, Carbone FR, and Mueller SN (2011) Different patterns of peripheral migration by memory CD4⁺ and CD8⁺ T cells. *Nature* 477: 216–219. <https://doi.org/10.1038/nature10339>.

Ghosh K, O’Neil K, and Capell BC (2018) Histone modifiers: Dynamic regulators of the cutaneous transcriptome. *Journal of Dermatological Science* 89: 226–232. <https://doi.org/10.1016/j.jdermsci.2017.12.006>.

Ahmed Ahmed, H., Akbari, H., Emami, A., & Akbari, M. R. (2017). Genetic Overview of Syndactyly and Polydactyly. *Plastic and Reconstructive Surgery Global Open*, 5(11).
<https://doi.org/10.1097/GOX.0000000000001549>

Bellavia, G., Fasanaro, P., Melchionna, R., Capogrossi, M. C., & Napolitano, M. (2014). Transcriptional control of skin reepithelialization. *Journal of Dermatological Science*, 73(1), 3–9. <https://doi.org/10.1016/j.jdermsci.2013.08.007>

Casey, L. M., Lan, Y., Cho, E.-S., Maltby, K. M., Gridley, T., & Jiang, R. (2006). Jag2-Notch1 signaling regulates oral epithelial differentiation and palate development.

- Developmental Dynamics: An Official Publication of the American Association of Anatomists*, 235(7), 1830–1844. <https://doi.org/10.1002/dvdy.20821>
- Chen, Y., Tian, T., Li, Z.-Y., Wang, C.-Y., Deng, R., Deng, W.-Y., ... Li, H. (2019). FSCN1 is an effective marker of poor prognosis and a potential therapeutic target in human tongue squamous cell carcinoma. *Cell Death & Disease*, 10(5), 356. <https://doi.org/10.1038/s41419-019-1574-5>
- Fallon, J. F., & Cameron, J. A. (1977). Interdigital cell death during limb development of the turtle and lizard with an interpretation of evolutionary significance. *Development*, 40(1), 285–289.
- Fuchs, E. (2007). Scratching the surface of skin development. *Nature*, 445(7130), 834. <https://doi.org/10.1038/nature05659>
- Gordon, W. M., Zeller, M. D., Klein, R. H., Swindell, W. R., Ho, H., Espetia, F., ... Andersen, B. (2014). A GRHL3-regulated repair pathway suppresses immune-mediated epidermal hyperplasia. *The Journal of Clinical Investigation*, 124(12), 5205–5218. <https://doi.org/10.1172/JCI77138>
- Hammond, N. L., Dixon, J., & Dixon, M. J. (2017). Periderm: Life-cycle and function during orofacial and epidermal development. *Seminars in Cell & Developmental Biology*. <https://doi.org/10.1016/j.semcd.2017.08.021>
- Han, G., & Ceilley, R. (2017). Chronic Wound Healing: A Review of Current Management and Treatments. *Advances in Therapy*, 34(3), 599–610. <https://doi.org/10.1007/s12325-017-0478-y>
- Hayashi, Y., Osanai, M., & Lee, G.-H. (2011). Fascin-1 expression correlates with repression of E-cadherin expression in hepatocellular carcinoma cells and augments their

- invasiveness in combination with matrix metalloproteinases. *Cancer Science*, *102*(6), 1228–1235. <https://doi.org/10.1111/j.1349-7006.2011.01910.x>
- Hernández-Martínez, R., & Covarrubias, L. (2011). Interdigital cell death function and regulation: New insights on an old programmed cell death model. *Development, Growth & Differentiation*, *53*(2), 245–258. <https://doi.org/10.1111/j.1440-169X.2010.01246.x>
- Iliina, O., & Friedl, P. (2009). Mechanisms of collective cell migration at a glance. *Journal of Cell Science*, *122*(18), 3203–3208. <https://doi.org/10.1242/jcs.036525>
- Kaltcheva, M. M., Anderson, M. J., Harfe, B. D., & Lewandoski, M. (2016). BMPs are direct triggers of interdigital programmed cell death. *Developmental Biology*, *411*(2), 266–276. <https://doi.org/10.1016/j.ydbio.2015.12.016>
- Klein, R. H., Lin, Z., Hopkin, A. S., Gordon, W., Tsoi, L. C., Liang, Y., ... Andersen, B. (2017). GRHL3 binding and enhancers rearrange as epidermal keratinocytes transition between functional states. *PLoS Genetics*, *13*(4), e1006745. <https://doi.org/10.1371/journal.pgen.1006745>
- Kondo, S., Schutte, B. C., Richardson, R. J., Bjork, B. C., Knight, A. S., Watanabe, Y., ... Murray, J. C. (2002). Mutations in IRF6 cause Van der Woude and popliteal pterygium syndromes. *Nature Genetics*, *32*(2), 285–289. <https://doi.org/10.1038/ng985>
- Kuwahara, M., Hatoko, M., Tada, H., & Tanaka, A. (2001). E-cadherin expression in wound healing of mouse skin. *Journal of Cutaneous Pathology*, *28*(4), 191–199.
- Li, J., Zhang, S., Pei, M., Wu, L., Liu, Y., Li, H., ... Li, X. (2018). FSCN1 Promotes Epithelial-Mesenchymal Transition Through Increasing Snail1 in Ovarian Cancer Cells. *Cellular*

Physiology and Biochemistry, 49(5), 1766–1777.

<https://doi.org/10.1159/000493622>

Lorda-Diez, C. I., Montero, J. A., Garcia-Porrero, J. A., & Hurle, J. M. (2015). Interdigital tissue regression in the developing limb of vertebrates. *International Journal of Developmental Biology*, 59(1-2-3), 55–62. <https://doi.org/10.1387/ijdb.150065jh>

Mayet, N., Choonara, Y. E., Kumar, P., Tomar, L. K., Tyagi, C., Du Toit, L. C., & Pillay, V. (2014). A Comprehensive Review of Advanced Biopolymeric Wound Healing Systems. *Journal of Pharmaceutical Sciences*, 103(8), 2211–2230.

<https://doi.org/10.1002/jps.24068>

Montero, J. A., & Hurlé, J. M. (2010). Sculpturing digit shape by cell death. *Apoptosis*, 15(3), 365–375. <https://doi.org/10.1007/s10495-009-0444-5>

Nunan, R., Campbell, J., Mori, R., Pitulescu, M. E., Jiang, W. G., Harding, K. G., ... Martin, P. (2015). Ephrin-Bs Drive Junctional Downregulation and Actin Stress Fiber Disassembly to Enable Wound Re-epithelialization. *Cell Reports*, 13(7), 1380–1395. <https://doi.org/10.1016/j.celrep.2015.09.085>

Nuutila, K., Siltanen, A., Peura, M., Bizik, J., Kaartinen, I., Kuokkanen, H., ... Kankuri, E. (2012). Human skin transcriptome during superficial cutaneous wound healing. *Wound Repair and Regeneration*, 20(6), 830–839. <https://doi.org/10.1111/j.1524-475X.2012.00831.x>

Pajni-Underwood, S., Wilson, C. P., Elder, C., Mishina, Y., & Lewandoski, M. (2007). BMP signals control limb bud interdigital programmed cell death by regulating FGF signaling. *Development (Cambridge, England)*, 134(12), 2359–2368.

<https://doi.org/10.1242/dev.001677>

- Peyrard-Janvid, M., Leslie, E. J., Kousa, Y. A., Smith, T. L., Dunnwald, M., Magnusson, M., ... Schutte, B. C. (2014). Dominant mutations in GRHL3 cause Van der Woude Syndrome and disrupt oral periderm development. *American Journal of Human Genetics*, *94*(1), 23–32. <https://doi.org/10.1016/j.ajhg.2013.11.009>
- Plutoni, C., Bazellieres, E., Borgne-Rochet, M. L., Comunale, F., Bruges, A., Séveno, M., ... Gauthier-Rouvière, C. (2016). P-cadherin promotes collective cell migration via a Cdc42-mediated increase in mechanical forces. *The Journal of Cell Biology*, *212*(2), 199–217. <https://doi.org/10.1083/jcb.201505105>
- Raja, null, Sivamani, K., Garcia, M. S., & Isseroff, R. R. (2007). Wound re-epithelialization: modulating keratinocyte migration in wound healing. *Frontiers in Bioscience: A Journal and Virtual Library*, *12*, 2849–2868.
- Richardson, R. J., Dixon, J., Jiang, R., & Dixon, M. J. (2009). Integration of IRF6 and Jagged2 signalling is essential for controlling palatal adhesion and fusion competence. *Human Molecular Genetics*, *18*(14), 2632–2642. <https://doi.org/10.1093/hmg/ddp201>
- Richardson, R. J., Hammond, N. L., Coulombe, P. A., Saloranta, C., Nousiainen, H. O., Salonen, R., ... Dixon, M. J. (2014). Periderm prevents pathological epithelial adhesions during embryogenesis. *The Journal of Clinical Investigation*, *124*(9), 3891–3900. <https://doi.org/10.1172/JCI71946>
- Salas-Vidal, E., Lomelí, H., Castro-Obregón, S., Cuervo, R., Escalante-Alcalde, D., & Covarrubias, L. (1998). Reactive oxygen species participate in the control of mouse embryonic cell death. *Experimental Cell Research*, *238*(1), 136–147.

- Salas-Vidal, E., Valencia, C., & Covarrubias, L. (2001). Differential tissue growth and patterns of cell death in mouse limb autopod morphogenesis. *Developmental Dynamics*, 220(4), 295–306. <https://doi.org/10.1002/dvdy.1108>
- Scarpa, E., & Mayor, R. (2016). Collective cell migration in development. *The Journal of Cell Biology*, 212(2), 143–155. <https://doi.org/10.1083/jcb.201508047>
- Xie, J., Yao, B., Han, Y., Huang, S., & Fu, X. (2016). Skin appendage-derived stem cells: cell biology and potential for wound repair. *Burns & Trauma*, 4. <https://doi.org/10.1186/s41038-016-0064-6>
- Yu, Z., Lin, K. K., Bhandari, A., Spencer, J. A., Xu, X., Wang, N., ... Andersen, B. (2006). The Grainyhead-like epithelial transactivator Get-1/Grhl3 regulates epidermal terminal differentiation and interacts functionally with LMO4. *Developmental Biology*, 299(1), 122–136. <https://doi.org/10.1016/j.ydbio.2006.07.015>
- Ahmed, H., Akbari, H., Emami, A., & Akbari, M. R. (2017). Genetic Overview of Syndactyly and Polydactyly. *Plastic and Reconstructive Surgery Global Open*, 5(11). <https://doi.org/10.1097/GOX.0000000000001549>
- Bellavia, G., Fasanaro, P., Melchionna, R., Capogrossi, M. C., & Napolitano, M. (2014). Transcriptional control of skin reepithelialization. *Journal of Dermatological Science*, 73(1), 3–9. <https://doi.org/10.1016/j.jdermsci.2013.08.007>
- Casey, L. M., Lan, Y., Cho, E.-S., Maltby, K. M., Gridley, T., & Jiang, R. (2006). Jag2-Notch1 signaling regulates oral epithelial differentiation and palate development. *Developmental Dynamics: An Official Publication of the American Association of Anatomists*, 235(7), 1830–1844. <https://doi.org/10.1002/dvdy.20821>

- Chen, Y., Tian, T., Li, Z.-Y., Wang, C.-Y., Deng, R., Deng, W.-Y., ... Li, H. (2019). FSCN1 is an effective marker of poor prognosis and a potential therapeutic target in human tongue squamous cell carcinoma. *Cell Death & Disease, 10*(5), 356.
<https://doi.org/10.1038/s41419-019-1574-5>
- Fallon, J. F., & Cameron, J. A. (1977). Interdigital cell death during limb development of the turtle and lizard with an interpretation of evolutionary significance. *Development, 40*(1), 285–289.
- Fuchs, E. (2007). Scratching the surface of skin development. *Nature, 445*(7130), 834.
<https://doi.org/10.1038/nature05659>
- Gordon, W. M., Zeller, M. D., Klein, R. H., Swindell, W. R., Ho, H., Espetia, F., ... Andersen, B. (2014). A GRHL3-regulated repair pathway suppresses immune-mediated epidermal hyperplasia. *The Journal of Clinical Investigation, 124*(12), 5205–5218.
<https://doi.org/10.1172/JCI77138>
- Hammond, N. L., Dixon, J., & Dixon, M. J. (2017). Periderm: Life-cycle and function during orofacial and epidermal development. *Seminars in Cell & Developmental Biology.*
<https://doi.org/10.1016/j.semcd.2017.08.021>
- Han, G., & Ceilley, R. (2017). Chronic Wound Healing: A Review of Current Management and Treatments. *Advances in Therapy, 34*(3), 599–610.
<https://doi.org/10.1007/s12325-017-0478-y>
- Hayashi, Y., Osanai, M., & Lee, G.-H. (2011). Fascin-1 expression correlates with repression of E-cadherin expression in hepatocellular carcinoma cells and augments their invasiveness in combination with matrix metalloproteinases. *Cancer Science, 102*(6), 1228–1235. <https://doi.org/10.1111/j.1349-7006.2011.01910.x>

- Hernández-Martínez, R., & Covarrubias, L. (2011). Interdigital cell death function and regulation: New insights on an old programmed cell death model. *Development, Growth & Differentiation*, *53*(2), 245–258. <https://doi.org/10.1111/j.1440-169X.2010.01246.x>
- Ilina, O., & Friedl, P. (2009). Mechanisms of collective cell migration at a glance. *Journal of Cell Science*, *122*(18), 3203–3208. <https://doi.org/10.1242/jcs.036525>
- Kaltcheva, M. M., Anderson, M. J., Harfe, B. D., & Lewandoski, M. (2016). BMPs are direct triggers of interdigital programmed cell death. *Developmental Biology*, *411*(2), 266–276. <https://doi.org/10.1016/j.ydbio.2015.12.016>
- Klein, R. H., Lin, Z., Hopkin, A. S., Gordon, W., Tsoi, L. C., Liang, Y., ... Andersen, B. (2017). GRHL3 binding and enhancers rearrange as epidermal keratinocytes transition between functional states. *PLoS Genetics*, *13*(4), e1006745. <https://doi.org/10.1371/journal.pgen.1006745>
- Kondo, S., Schutte, B. C., Richardson, R. J., Bjork, B. C., Knight, A. S., Watanabe, Y., ... Murray, J. C. (2002). Mutations in IRF6 cause Van der Woude and popliteal pterygium syndromes. *Nature Genetics*, *32*(2), 285–289. <https://doi.org/10.1038/ng985>
- Kuwahara, M., Hatoko, M., Tada, H., & Tanaka, A. (2001). E-cadherin expression in wound healing of mouse skin. *Journal of Cutaneous Pathology*, *28*(4), 191–199.
- Li, J., Zhang, S., Pei, M., Wu, L., Liu, Y., Li, H., ... Li, X. (2018). FSCN1 Promotes Epithelial-Mesenchymal Transition Through Increasing Snail1 in Ovarian Cancer Cells. *Cellular Physiology and Biochemistry*, *49*(5), 1766–1777. <https://doi.org/10.1159/000493622>

- Lorda-Diez, C. I., Montero, J. A., Garcia-Porrero, J. A., & Hurle, J. M. (2015). Interdigital tissue regression in the developing limb of vertebrates. *International Journal of Developmental Biology*, 59(1-2-3), 55–62. <https://doi.org/10.1387/ijdb.150065jh>
- Mayet, N., Choonara, Y. E., Kumar, P., Tomar, L. K., Tyagi, C., Du Toit, L. C., & Pillay, V. (2014). A Comprehensive Review of Advanced Biopolymeric Wound Healing Systems. *Journal of Pharmaceutical Sciences*, 103(8), 2211–2230. <https://doi.org/10.1002/jps.24068>
- Montero, J. A., & Hurlé, J. M. (2010). Sculpturing digit shape by cell death. *Apoptosis*, 15(3), 365–375. <https://doi.org/10.1007/s10495-009-0444-5>
- Nunan, R., Campbell, J., Mori, R., Pitulescu, M. E., Jiang, W. G., Harding, K. G., ... Martin, P. (2015). Ephrin-Bs Drive Junctional Downregulation and Actin Stress Fiber Disassembly to Enable Wound Re-epithelialization. *Cell Reports*, 13(7), 1380–1395. <https://doi.org/10.1016/j.celrep.2015.09.085>
- Nuutila, K., Siltanen, A., Peura, M., Bizik, J., Kaartinen, I., Kuokkanen, H., ... Kankuri, E. (2012). Human skin transcriptome during superficial cutaneous wound healing. *Wound Repair and Regeneration*, 20(6), 830–839. <https://doi.org/10.1111/j.1524-475X.2012.00831.x>
- Pajni-Underwood, S., Wilson, C. P., Elder, C., Mishina, Y., & Lewandoski, M. (2007). BMP signals control limb bud interdigital programmed cell death by regulating FGF signaling. *Development (Cambridge, England)*, 134(12), 2359–2368. <https://doi.org/10.1242/dev.001677>
- Peyrard-Janvid, M., Leslie, E. J., Kousa, Y. A., Smith, T. L., Dunnwald, M., Magnusson, M., ... Schutte, B. C. (2014). Dominant mutations in GRHL3 cause Van der Woude

- Syndrome and disrupt oral periderm development. *American Journal of Human Genetics*, 94(1), 23–32. <https://doi.org/10.1016/j.ajhg.2013.11.009>
- Plutoni, C., Bazellieres, E., Borgne-Rochet, M. L., Comunale, F., Brugues, A., Séveno, M., ... Gauthier-Rouvière, C. (2016). P-cadherin promotes collective cell migration via a Cdc42-mediated increase in mechanical forces. *The Journal of Cell Biology*, 212(2), 199–217. <https://doi.org/10.1083/jcb.201505105>
- Raja, null, Sivamani, K., Garcia, M. S., & Isseroff, R. R. (2007). Wound re-epithelialization: modulating keratinocyte migration in wound healing. *Frontiers in Bioscience: A Journal and Virtual Library*, 12, 2849–2868.
- Richardson, R. J., Dixon, J., Jiang, R., & Dixon, M. J. (2009). Integration of IRF6 and Jagged2 signalling is essential for controlling palatal adhesion and fusion competence. *Human Molecular Genetics*, 18(14), 2632–2642. <https://doi.org/10.1093/hmg/ddp201>
- Richardson, R. J., Hammond, N. L., Coulombe, P. A., Saloranta, C., Nousiainen, H. O., Salonen, R., ... Dixon, M. J. (2014). Periderm prevents pathological epithelial adhesions during embryogenesis. *The Journal of Clinical Investigation*, 124(9), 3891–3900. <https://doi.org/10.1172/JCI71946>
- Salas-Vidal, E., Lomelí, H., Castro-Obregón, S., Cuervo, R., Escalante-Alcalde, D., & Covarrubias, L. (1998). Reactive oxygen species participate in the control of mouse embryonic cell death. *Experimental Cell Research*, 238(1), 136–147.
- Salas-Vidal, E., Valencia, C., & Covarrubias, L. (2001). Differential tissue growth and patterns of cell death in mouse limb autopod morphogenesis. *Developmental Dynamics*, 220(4), 295–306. <https://doi.org/10.1002/dvdy.1108>

- Scarpa, E., & Mayor, R. (2016). Collective cell migration in development. *The Journal of Cell Biology*, 212(2), 143–155. <https://doi.org/10.1083/jcb.201508047>
- Xie, J., Yao, B., Han, Y., Huang, S., & Fu, X. (2016). Skin appendage-derived stem cells: cell biology and potential for wound repair. *Burns & Trauma*, 4. <https://doi.org/10.1186/s41038-016-0064-6>
- Yu, Z., Lin, K. K., Bhandari, A., Spencer, J. A., Xu, X., Wang, N., ... Andersen, B. (2006). The Grainyhead-like epithelial transactivator Get-1/Grhl3 regulates epidermal terminal differentiation and interacts functionally with LMO4. *Developmental Biology*, 299(1), 122–136. <https://doi.org/10.1016/j.ydbio.2006.07.015>
- Ahmed, H., Akbari, H., Emami, A., & Akbari, M. R. (2017). Genetic Overview of Syndactyly and Polydactyly. *Plastic and Reconstructive Surgery Global Open*, 5(11). <https://doi.org/10.1097/GOX.0000000000001549>
- Bellavia, G., Fasanaro, P., Melchionna, R., Capogrossi, M. C., & Napolitano, M. (2014). Transcriptional control of skin reepithelialization. *Journal of Dermatological Science*, 73(1), 3–9. <https://doi.org/10.1016/j.jdermsci.2013.08.007>
- Casey, L. M., Lan, Y., Cho, E.-S., Maltby, K. M., Gridley, T., & Jiang, R. (2006). Jag2-Notch1 signaling regulates oral epithelial differentiation and palate development. *Developmental Dynamics: An Official Publication of the American Association of Anatomists*, 235(7), 1830–1844. <https://doi.org/10.1002/dvdy.20821>
- Chen, Y., Tian, T., Li, Z.-Y., Wang, C.-Y., Deng, R., Deng, W.-Y., ... Li, H. (2019). FSCN1 is an effective marker of poor prognosis and a potential therapeutic target in human tongue squamous cell carcinoma. *Cell Death & Disease*, 10(5), 356. <https://doi.org/10.1038/s41419-019-1574-5>

- Fallon, J. F., & Cameron, J. A. (1977). Interdigital cell death during limb development of the turtle and lizard with an interpretation of evolutionary significance. *Development*, *40*(1), 285–289.
- Fuchs, E. (2007). Scratching the surface of skin development. *Nature*, *445*(7130), 834.
<https://doi.org/10.1038/nature05659>
- Gordon, W. M., Zeller, M. D., Klein, R. H., Swindell, W. R., Ho, H., Espetia, F., ... Andersen, B. (2014). A GRHL3-regulated repair pathway suppresses immune-mediated epidermal hyperplasia. *The Journal of Clinical Investigation*, *124*(12), 5205–5218.
<https://doi.org/10.1172/JCI77138>
- Hammond, N. L., Dixon, J., & Dixon, M. J. (2017). Periderm: Life-cycle and function during orofacial and epidermal development. *Seminars in Cell & Developmental Biology*.
<https://doi.org/10.1016/j.semcdb.2017.08.021>
- Han, G., & Ceilley, R. (2017). Chronic Wound Healing: A Review of Current Management and Treatments. *Advances in Therapy*, *34*(3), 599–610.
<https://doi.org/10.1007/s12325-017-0478-y>
- Hayashi, Y., Osanai, M., & Lee, G.-H. (2011). Fascin-1 expression correlates with repression of E-cadherin expression in hepatocellular carcinoma cells and augments their invasiveness in combination with matrix metalloproteinases. *Cancer Science*, *102*(6), 1228–1235. <https://doi.org/10.1111/j.1349-7006.2011.01910.x>
- Hernández-Martínez, R., & Covarrubias, L. (2011). Interdigital cell death function and regulation: New insights on an old programmed cell death model. *Development, Growth & Differentiation*, *53*(2), 245–258. <https://doi.org/10.1111/j.1440-169X.2010.01246.x>

- Irina, O., & Friedl, P. (2009). Mechanisms of collective cell migration at a glance. *Journal of Cell Science*, 122(18), 3203–3208. <https://doi.org/10.1242/jcs.036525>
- Kaltcheva, M. M., Anderson, M. J., Harfe, B. D., & Lewandoski, M. (2016). BMPs are direct triggers of interdigital programmed cell death. *Developmental Biology*, 411(2), 266–276. <https://doi.org/10.1016/j.ydbio.2015.12.016>
- Klein, R. H., Lin, Z., Hopkin, A. S., Gordon, W., Tsoi, L. C., Liang, Y., ... Andersen, B. (2017). GRHL3 binding and enhancers rearrange as epidermal keratinocytes transition between functional states. *PLoS Genetics*, 13(4), e1006745. <https://doi.org/10.1371/journal.pgen.1006745>
- Kondo, S., Schutte, B. C., Richardson, R. J., Bjork, B. C., Knight, A. S., Watanabe, Y., ... Murray, J. C. (2002). Mutations in IRF6 cause Van der Woude and popliteal pterygium syndromes. *Nature Genetics*, 32(2), 285–289. <https://doi.org/10.1038/ng985>
- Kuwahara, M., Hatoko, M., Tada, H., & Tanaka, A. (2001). E-cadherin expression in wound healing of mouse skin. *Journal of Cutaneous Pathology*, 28(4), 191–199.
- Li, J., Zhang, S., Pei, M., Wu, L., Liu, Y., Li, H., ... Li, X. (2018). FSCN1 Promotes Epithelial-Mesenchymal Transition Through Increasing Snail1 in Ovarian Cancer Cells. *Cellular Physiology and Biochemistry*, 49(5), 1766–1777. <https://doi.org/10.1159/000493622>
- Lorda-Diez, C. I., Montero, J. A., Garcia-Porrero, J. A., & Hurle, J. M. (2015). Interdigital tissue regression in the developing limb of vertebrates. *International Journal of Developmental Biology*, 59(1-2-3), 55–62. <https://doi.org/10.1387/ijdb.150065jh>
- Mayet, N., Choonara, Y. E., Kumar, P., Tomar, L. K., Tyagi, C., Du Toit, L. C., & Pillay, V. (2014). A Comprehensive Review of Advanced Biopolymeric Wound Healing Systems.

- Journal of Pharmaceutical Sciences*, 103(8), 2211–2230.
<https://doi.org/10.1002/jps.24068>
- Montero, J. A., & Hurlé, J. M. (2010). Sculpturing digit shape by cell death. *Apoptosis*, 15(3), 365–375. <https://doi.org/10.1007/s10495-009-0444-5>
- Nunan, R., Campbell, J., Mori, R., Pitulescu, M. E., Jiang, W. G., Harding, K. G., ... Martin, P. (2015). Ephrin-Bs Drive Junctional Downregulation and Actin Stress Fiber Disassembly to Enable Wound Re-epithelialization. *Cell Reports*, 13(7), 1380–1395. <https://doi.org/10.1016/j.celrep.2015.09.085>
- Nuutila, K., Siltanen, A., Peura, M., Bizik, J., Kaartinen, I., Kuokkanen, H., ... Kankuri, E. (2012). Human skin transcriptome during superficial cutaneous wound healing. *Wound Repair and Regeneration*, 20(6), 830–839. <https://doi.org/10.1111/j.1524-475X.2012.00831.x>
- Pajni-Underwood, S., Wilson, C. P., Elder, C., Mishina, Y., & Lewandoski, M. (2007). BMP signals control limb bud interdigital programmed cell death by regulating FGF signaling. *Development (Cambridge, England)*, 134(12), 2359–2368. <https://doi.org/10.1242/dev.001677>
- Peyrard-Janvid, M., Leslie, E. J., Kousa, Y. A., Smith, T. L., Dunnwald, M., Magnusson, M., ... Schutte, B. C. (2014). Dominant mutations in GRHL3 cause Van der Woude Syndrome and disrupt oral periderm development. *American Journal of Human Genetics*, 94(1), 23–32. <https://doi.org/10.1016/j.ajhg.2013.11.009>
- Plutoni, C., Bazellieres, E., Borgne-Rochet, M. L., Comunale, F., Brugues, A., Séveno, M., ... Gauthier-Rouvière, C. (2016). P-cadherin promotes collective cell migration via a

- Cdc42-mediated increase in mechanical forces. *The Journal of Cell Biology*, 212(2), 199–217. <https://doi.org/10.1083/jcb.201505105>
- Raja, null, Sivamani, K., Garcia, M. S., & Isseroff, R. R. (2007). Wound re-epithelialization: modulating keratinocyte migration in wound healing. *Frontiers in Bioscience: A Journal and Virtual Library*, 12, 2849–2868.
- Richardson, R. J., Dixon, J., Jiang, R., & Dixon, M. J. (2009). Integration of IRF6 and Jagged2 signalling is essential for controlling palatal adhesion and fusion competence. *Human Molecular Genetics*, 18(14), 2632–2642. <https://doi.org/10.1093/hmg/ddp201>
- Richardson, R. J., Hammond, N. L., Coulombe, P. A., Saloranta, C., Nousiainen, H. O., Salonen, R., ... Dixon, M. J. (2014). Periderm prevents pathological epithelial adhesions during embryogenesis. *The Journal of Clinical Investigation*, 124(9), 3891–3900. <https://doi.org/10.1172/JCI71946>
- Salas-Vidal, E., Lomelí, H., Castro-Obregón, S., Cuervo, R., Escalante-Alcalde, D., & Covarrubias, L. (1998). Reactive oxygen species participate in the control of mouse embryonic cell death. *Experimental Cell Research*, 238(1), 136–147.
- Salas-Vidal, E., Valencia, C., & Covarrubias, L. (2001). Differential tissue growth and patterns of cell death in mouse limb autopod morphogenesis. *Developmental Dynamics*, 220(4), 295–306. <https://doi.org/10.1002/dvdy.1108>
- Scarpa, E., & Mayor, R. (2016). Collective cell migration in development. *The Journal of Cell Biology*, 212(2), 143–155. <https://doi.org/10.1083/jcb.201508047>

Xie, J., Yao, B., Han, Y., Huang, S., & Fu, X. (2016). Skin appendage-derived stem cells: cell biology and potential for wound repair. *Burns & Trauma*, 4.

<https://doi.org/10.1186/s41038-016-0064-6>

Yu, Z., Lin, K. K., Bhandari, A., Spencer, J. A., Xu, X., Wang, N., ... Andersen, B. (2006). The Grainyhead-like epithelial transactivator Get-1/Grhl3 regulates epidermal terminal differentiation and interacts functionally with LMO4. *Developmental Biology*, 299(1),

122–136. <https://doi.org/10.1016/j.ydbio.2006.07.015>